PRETREATMENT OF COAL MINING SLUDGE THROUGH SULFATION ROASTING AND WATER LEACHING FOR ALUMINIUM EXTRACTION

LEW CHIA XIN

UNIVERSITI TUNKU ABDUL RAHMAN

PRETREATMENT OF COAL MINING SLUDGE THROUGH SULFATION ROASTING AND WATER LEACHING FOR ALUMINIUM EXTRACTION

LEW CHIA XIN

A project report submitted in partial fulfilment of the requirements for the award of Bachelor of Chemical Engineering with Honours

Lee Kong Chian Faculty of Engineering and Science
Universiti Tunku Abdul Rahman

May 2024

DECLARATION

I hereby declare that this project report is based on my original work except for citations and quotations which have been duly acknowledged. I also declare that it has not been previously and concurrently submitted for any other degree or award at UTAR or other institutions.

Signature : *lcx*

Name : Lew Chia Xin

ID No. : 19UEB02457

Date : 13 May 2024

APPROVAL FOR SUBMISSION

I certify that this project report entitled **"PRETREATMENT OF COAL MINING SLUDGE THROUGH SULFATION ROASTING AND WATER LEACHING FOR ALUMINIUM EXTRACTION"** was prepared by **LEW CHIA XIN** has met the required standard for submission in partial fulfilment of the requirements for the award of Bachelor of Chemical Engineering with Honours at Universiti Tunku Abdul Rahman.

Approved by,

Signature : steven

Supervisor : Dr. Steven Lim

Date : 15.5.2024

Signature : -

Co-Supervisor : -

Date : -

ACKNOWLEDGEMENTS

I would like to express my gratitude to everyone who helped me complete this project with success. First and foremost, I would like to express my deepest appreciation to my project supervisor, Dr. Steven Lim, for all of his invaluable advice, guidance, and patience throughout the study progressed.

Next, I would like to thank Universiti Tunku Abdul Rahman (UTAR) for providing the opportunity and platform for me to learn from this final year project. Besides, thanks should also go to all the laboratory officers from the Department of Laboratory Management and Safety Administration (DLMSA) at Lee Kong Chian Faculty of Engineering and Science (LKC FES), who offered technical assistance and guidance as needed.

Following this, a special thanks goes to the postgraduate student, Mr. Lee Sean Jun for his precious advice and assistance in operating the instruments. Last but not least, I would be remiss in not mentioning my loving parents and friends for their moral support and encouragement during this journey.

ABSTRACT

The current sludge management plan was ineffective and a waste of valuable substances for coal mining sludge. So, the study aimed to examine the characteristics of raw coal mining sludge and propose a suitable purification method for it. Several analytical techniques were used for the characterisation. Thermogravimetric Analysis (TGA) revealed the sludge was thermally stable after 700 ℃ while Brunauer-Emmett-Teller (BET) determined its surface area, pore sizes, and volumes were 44.97 m^2/g, 12.42 nm, and 0.09 cm^3/g, respectively. Scanning Electron Microscopy (SEM) further showed that the sludge's surface morphology had a slightly porous irregular structure with an uneven flake-like appearance at the outside borders. Corresponding to Energy Dispersive X-ray spectroscopy (EDX) results, which indicated that oxygen, silicon, and aluminium were the major elements present, the flaky structure was identified as silica oxide. Quartz, kaolinite, muscovite, and magnetite were also discovered to be the primary minerals in the sludge via X-ray diffraction (XRD). Moreover, Fourier Transform Infrared (FTIR) identified silicon and aluminium-related functional groups in the sludge. As such, sulfation roasting and water leaching approach was proposed as the separation method to extract the aluminium from coal mining sludge. Six groups of parameter studies were conducted and EDX was used to assess the extraction efficiency. The ideal conditions were defined as 500 °C roasting temperature, 1:2 sludge to ammonium sulphate mass ratio, 90-minute roasting period, 80 °C leaching temperature, 1:10 solid-liquid ratio, and 90-minute leaching time, yielding 93.2 % extraction efficiency of aluminium from sludge. Afterward, SEM-EDX, XRD, and FTIR were used again to characterise the treated coal mining sludge. The sludge's surface morphology got smoother and the flake-like appearance region was much more visible. The primary element also changed to solely silicon and oxygen based on the EDX test. Furthermore, no kaolinite and aluminium-related bond was found in the XRD and FTIR results compared to the previous, suggesting the proposed separation method was effective. As silica oxide is currently the primary constituent in coal mining sludge, it is possible to infer that the treated sludge can be utilised as an active product for other purposes like glass and ceramic ingredients.

TABLE OF CONTENTS

LIST OF TABLES

LIST OF FIGURES

LIST OF SYMBOLS / ABBREVIATIONS

η	aluminium extraction efficiency, %
w_B	weightage of aluminium in the sludge before experiment, wt.%
w_A	weightage of aluminium in the sludge after experiment, wt.%
AMCSD	American Mineralogist Crystal Structure Database
AMD	acid mine drainage
BET	brunauer-emmett-teller
CA	citric acid
CHX	cyclohexane
CMS	coal mine sludge
EDTA	ethylenediamine tetraacetic acid
FTIR	fourier transform infrared
GLDA	glutamic acid
HPAM	hydrolysed polyacrylamide
ICP-OES	Inductively Coupled Plasma Optical Emission Spectroscopy
IUPAC	International Union of Pure and Applied Chemistry
KBr	potassium bromide
PAHs	polycyclic aromatic hydrocarbons
SDGs	sustainable development goals
SEM-EDX	scanning electron microscopy with energy dispersive x-ray spectroscopy
TGA	thermogravimetric analysis
WAS	waste activated sludge
XRD	x-ray diffraction
Al	aluminium
Cd	cadmium
Cs	cesium
Cu	copper
Fe	iron
Mg	magnesium
Mn	manganese

Ni	nickel
O	oxygen
Pb	lead
Si	silicon
Sn	tin

LIST OF APPENDICES

CHAPTER 1

INTRODUCTION

1.1 General Introduction

1.1.1 Coal Mining Industry

The coal mining industry is recognised as one of the key players shaping the global energy landscape. The mining process usually involves the surface or underground extraction of coal deposits from the Earth's crust. For centuries, coal has been a vital fuel source in human life because of its high energy content, affordability, and abundant reserves. Referring to Figure 1.1, coal mining has been a reliable source of energy for the growth of industry, heating, and the production of electricity (Government of Canada, 2023).

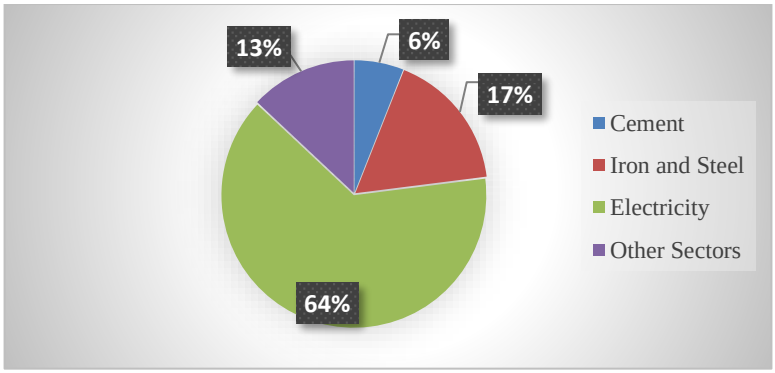

Figure 1.1: Global Coal Demand by Sector in 2020 (Government of Canada, 2023).

With the rise of the human population and the development of technology, more urban areas and industries are being built up, indicating more energy demands around the world. According to the Government of Canada (2023), a total of 7.8 billion tonnes of coal were produced globally in 2012. It then increased, reaching a peak of 8.1 billion tonnes in 2013, before declining for a few years. But in 2019, the coal production climbed again to 8.2 billion tonnes. Therefore, it is impossible to overstate coal's significance in supplying energy needs.

1.1.2 Coal Mining Sludge Production

When a mining area is in operation, wastewater is generated along with coal. To further illustrate, coal mining activities can produce a lot of dust, especially during excavation and transportation. At this time, water is often sprayed onto coal stockpiles or mining sites to control dust. As a result, the water used for dust suppression is contaminated with things like coal and soil and is known as wastewater. In another instance, surface water or rainfall may come into contact with exposed coal or mining sites, causing runoff that contains silt, contaminants, and suspended particles, forming wastewater. So, in order to keep the mine dry and facilitate mining operations, this wastewater must be pumped out of the mine (United States Environmental Protection Agency, 2023). The authority also claims that this wastewater must be treated before discharge to other water bodies. At the moment of wastewater processing in the treatment plant, its by-product, known as sludge, is formed. To make it more specific, it is defined as coal mining sludge and is used to describe mud-like materials that are made up primarily of water and solid particles (Safeopedia, n.d.).

Based on past statistics shown in Figure 1.2, the market for water and wastewater management in the mining sector including the coal mining industry, was attained at USD 4730.2 million in 2018 and is anticipated to reach USD 7973.7 million in 2023.

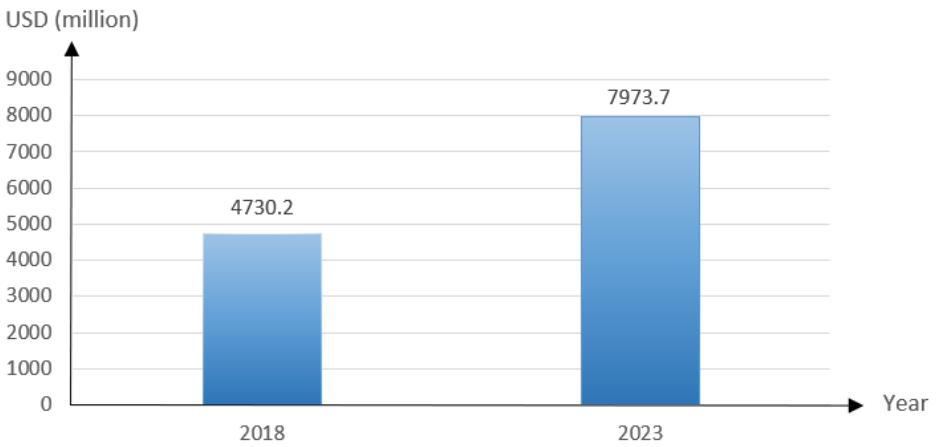

Figure 1.2: The Market of Water and Wastewater Management in the Mining Sector (Research and Markets, 2019).

Since sludge is a by-product of wastewater treatment, the statistic indirectly proves the amount of sludge generated in the mining sector.

In order to ensure the safety and health of living things and the environment, all of the coal mining sludge needs to be well-handled and treated before being disposed of in the environment. In this instance, the procedure is known as sludge management. Typically, the sludge must first undergo a thickening process before being transported to a biological digestion process for stabilisation purposes followed by a dewatering stage. Then, it can be reused for agriculture as fertiliser depending on the chemicals in it. If the sludge still contains some hazardous chemicals, it can also simply be incinerated until it is reduced to ash, and then it can be buried in a sanitary landfill.

1.2 Problem Statement

The current sludge management plan might seem trouble-free for the coal mining industry, but a more thorough study and research would reveal the problems in question.

The major components of coal mining sludge typically include chemically treated water and solid particles of rock, soil, coal, and clay (Herter, 2012). These solid particles are usually found in sludge in fine particle form, thus resulting in a greater surface area per mass and improving the sludge's ability to retain water. Additionally, residual coal itself naturally possesses a porous structure, which further adds to the high-water retention capacity of coal mining sludge. As a result, even after the thickening process, the sludge will still have a high moisture content, which is not ideal.

On top of that, according to Herter (2012), a wide variety of water-soluble heavy metals, including lead, iron, and cadmium, as well as organic compounds like polycyclic aromatic hydrocarbons (PAHs), are commonly encountered in rock, coal, and clay. Except for those toxic heavy metals, anaerobic digestion will also not be able to decompose PAHs due to their stable aromatic ring structures. Thus, instead of being dumped in landfills, the hazardous compounds will first go through the incineration process. However, when the sludge is burned in furnaces, it is likely to "transfer" rather than "eliminate" the chemical's toxic effects. As the heavy metals and PAHs

undergo combustion, they are released into the air in gas form, contributing to air pollution and threatening life on Earth. It can also be seen that, by incineration, most of the valuable heavy metal will be wasted.

For all of these reasons, the study is taking place to determine the characteristics of coal mining sludge in-depth and discover more sustainable alternatives for its treatment and purification.

1.3 Importance of the Study

Due to the concerns discussed in Section 1.2, the study is essential because it might help resolve the crisis in coal mining sludge management along with achieving some of the Sustainable Development Goals (SDGs).

First and foremost, the result of this study can act as a reference for other researchers, enabling them to precisely identify the composition and properties of coal mining sludge through various characterisation methods. Once they have those details, they may use them to come up with more effective purification techniques. They can also evaluate the technique against the current sludge treatment process and decide which is more sustainable. If it is feasible, they may even be able to integrate and modify the process. Therefore, it can be drawn that the study is in line with SDG 9 (Industry, Innovation and Infrastructure) as it promotes sustainable industrial practices and fosters innovation in the coal mining sludge management field. In particular, the incineration might be replaced by another better technology that can help remove unwanted compounds instead of burning them in the air. By doing so, the sludge management is upgraded, ensuring human health and safety with SDG 3 (Good Health and Well Being) and preventing the emission of pollutants to the atmosphere, contributing to SDG 13 (Climate Action) as well.

Meanwhile, the study of purification techniques can help to recover certain valuable substances, including heavy metals, minerals, lipids, and coal particles from sludge and reuse them again. This practice, which turns waste into a resource, not only supports the circular economy concept but also benefits the coal mining industry with SDG 12 (Responsible Consumption and Production).

Globally speaking, the study can even help with SDG 17 (Partnerships for the Goals). It is because the data from the study enables researchers, scholars, and developers to engage in a mutual exchange of ideas and opinions with foreign elites to establish effective treatment solutions and address the limitations of current sludge management.

1.4 Aim and Objectives

This project aims to investigate the characteristics of sludge from the coal mining industry and propose appropriate purification techniques that can be employed to treat the sludge. Thus, more specific objectives are listed below:

- To characterise the physical and chemical properties of sludge from the coal mining industry.
- To investigate the effect of sulfation roasting temperature, mass ratio of sludge to ammonium sulphate, sulfation roasting time, water leaching temperature, solid-liquid ratio and water leaching time on the aluminium extraction.
- To determine the percentage of silica recovery in sludge after the treatment process.

1.5 Scope and Limitation of the Study

The sludge sample in this study will be collected from the coal mining industry. Besides, the sludge sample is categorised as primary sludge as it is formed by the sedimentation process after adding alum for coagulation and flocculation purposes.

After reading the relevant journal papers, a variety of characterisation techniques, namely Scanning Electron Microscopy with Energy Dispersive X-ray spectroscopy (SEM-EDX), Thermogravimetric Analysis (TGA), Brunauer-Emmett-Teller (BET), Fourier Transform Infrared (FTIR) and X-ray Diffraction (XRD) will be used to analyse the physical and chemical properties of coal mining sludge. The project will also focus on identifying the elements present in the sludge, such as organic compounds, minerals, and heavy metals.

Then, the purification method will be studied based on the sludge's characteristics to remove or recover certain substances from it. At this moment,

an experiment is conducted to demonstrate the validity of the selected techniques. Finally, the purified sludge is recharacterised again to assess the efficiency of that method.

However, this study does have certain limitations. Since the sample for this study is coal mining sludge, there are not many journal publications available for the literature review, making it difficult to do a comprehensive review and comparative analysis. Thus, it is necessary to find similar topics in different industries for a deeper understanding, but doing so could lead to inaccurate results. On top of that, the findings and conclusions derived from this project might only apply to the coal mining sector but are not transferable to other industries due to the variations in sludge composition across industries.

CHAPTER 2

LITERATURE REVIEW

2.1 Type of Coal Mining Sludge

In the wastewater treatment plant of coal mining industry, the sludge can generally be divided into three principal categories: primary, secondary (waste-activated), and tertiary (chemical). In terms of sources, three of them can be obtained during the wastewater treatment with different types of treatment principles. The primary coal mining sludge is produced in the primary clarifier through a sedimentation process after the wastewater has gone through a series of mechanical pre-treatments. Most of the time, it will contain a mixture of biodegradable organic materials, settable solids, and some human pathogens. The secondary coal mining sludge, however, is thought to be the product of biological reactions carried out by microorganisms. Along with the microbes and biodegradable organic matter essential to the reaction, the sludge likewise includes some organic compounds that cannot be broken down, such as proteins and carbohydrates, as well as trace amounts of inorganic materials and heavy metals. On the other hand, when tertiary advanced treatment is necessary, the treated wastewater will be chemically injected for flocculation and coagulation, generating the tertiary coal mining sludge following the filtration process. Normally, this kind of sludge will only consist of fine suspended solids and nutrients (Canziani & Spinosa, 2019). The general process flow of the wastewater treatment plant, including the origin of sludge, is depicted in Figure 2.1 for better understanding.

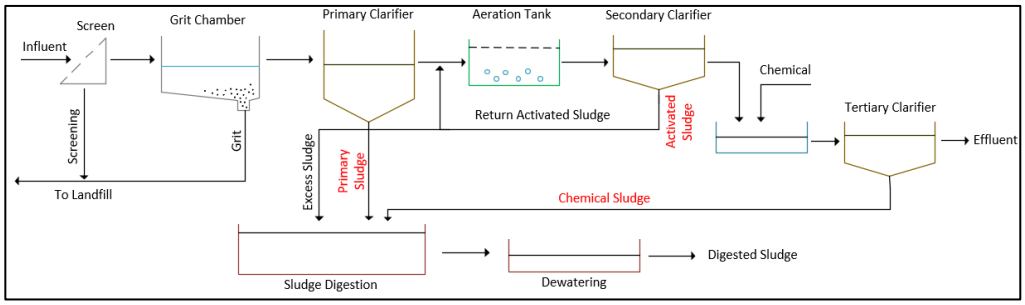

Figure 2.1: Generation of Different Types of Coal Mining Sludge in Wastewater Treatment Plant (Guangyin & Youcai, 2017).

2.2 Sludge Management

To have a deeper understanding of the current sludge management, this subsection would describe how the sludge is being processed in detail with the aid of Figure 2.2.

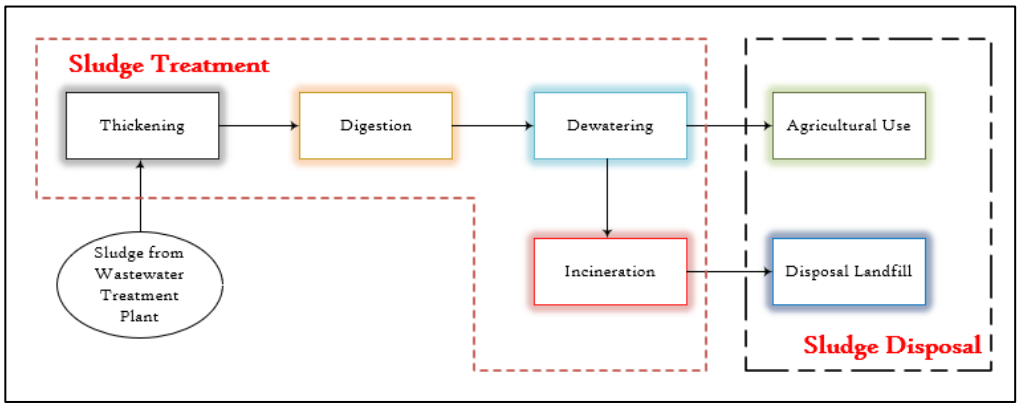

Figure 2.2: Sludge Management Plan (Kroiss, et al., 2011).

After being removed from the wastewater treatment plant, the sludge is treated using some techniques before it is disposed of in the environment. To reduce the overall volume of sludge, it must first undergo a thickening process in a specialised tank known as a gravity thickener. This procedure is required since thicker sludge will be more manageable throughout the following stages of treatment. Additionally, thick sludge enables improved mixing and encourages high rates of reaction, which leads to high treatment efficiency. The thick sludge will then be transported to a biological digestion process for stabilisation purposes. The digestion of sludge usually takes place in two stages. The sludge will first be heated and mixed with acid-forming bacteria in a sealed tank for anaerobic digestion. As shown in Figure 2.3, these bacteria can help to break down the large and complex molecules in sludge into smaller water-soluble substances by hydrolysis. The partially digested sludge is transferred into the second tank, where it is further broken down by other bacteria, producing carbon dioxide and methane that can be used again to produce electricity.

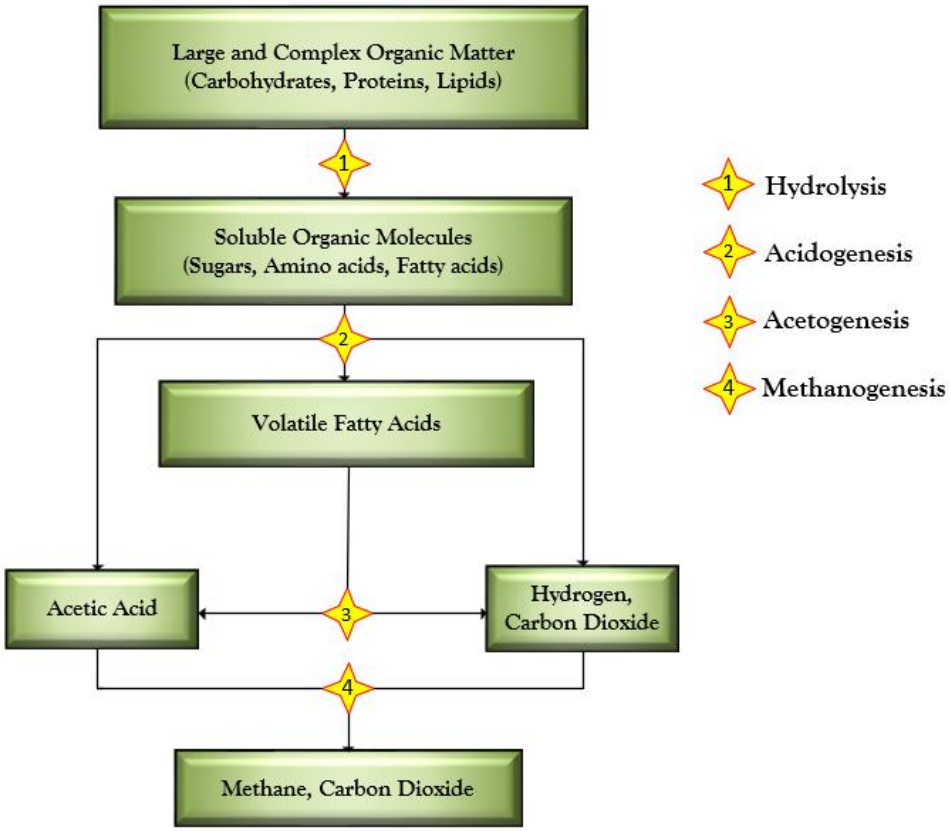

Figure 2.3: Two-phase Anaerobic Digestion Process (Mothe & Polisetty, 2020).

As such, this stage is viewed as crucial in the treatment process because the majority of organic compounds have broken down into substances that are safe to release into the environment and able to regenerate other energy sources, paving the way for a high level of energy efficiency. Before final disposal, the digested sludge needs to be dewatered. It is suggested to use a centrifuge since it helps recover all the water and makes handling solid waste easier, taking less time and costing less money. After the sludge has been successfully dewatered, it can be reused for agriculture as fertiliser depending on the chemicals in it. If the sludge still contains some hazardous chemicals, it can also simply be incinerated until it is reduced to ash, and then it can be buried in a sanitary landfill (Patel, 2018).

2.3 Sludge Characterisation Techniques

This section will explore various analytical techniques to reveal the chemical and physical properties of coal mining sludge. Each subsection will also include the relevant sample preparation method, instrument setup, and result interpretation that can help determine the properties of the sludge.

2.3.1 Thermogravimetric Analysis (TGA)

According to Silva, et al. (2012), TGA is a very powerful analytical method to study the thermal stability and decomposition behaviour of sludge. It provides insight into the temperature range at which various components of the coal mining sludge decompose or transform. Also, TGA demonstrates how the weight of material changes over time as heat is supplied (George, et al., 2023). By observing the weight loss patterns during the thermal decomposition, it is possible to study the moisture content and chemical composition of coal mining sludge.

2.3.1.1 Sample Preparation & Instrument Setup

A general sample preparation method for TGA was suggested by several journal papers. Firstly, Silva, et al. (2012) claimed that the collected sludge sample was dewatered in a centrifuge system. However, S.P. & Swaminathan (2022) proposed another drying method, which was to expose the sludge to the sun. Both were acceptable since they could remove the moisture content. Following this, the dried or dewatered sludge should be ground in a cutting mill for homogenisation purposes to improve the precision of the result (S.P. & Swaminathan, 2022). Then, the powered sludge was weighed and put into crucibles for thermal analysis later (Francioso, et al., 2010; Silva, et al., 2012).

Before operating the TGA machine, some instrument setups need to be determined including the temperature range, heating rate, surrounding atmosphere, and atmospheric flow rate. However, the setting largely depends on the instrument specifications, sample sensitivity, and composition. After completing the tare weight of crucible in the machine, the prepared sample was filled in and the program could be run with a predetermined setup.

2.3.1.2 Results & Analysis

Initially, the weight loss of the sludge is usually caused by the evaporation of water molecules due to their weak hydrogen bond. In a study conducted by Rodrigues, et al. (2023) as illustrated in Figure 2.4, it was observed that the initial weight loss of sludge was associated with the loss of water molecules which took place between 30 ℃ and 150 ℃. A report done by Silva, et al. (2012) also found similar findings with water weight loss at 70 ℃. Besides water weight loss, there was also some weight loss of light or easily volatile substances due to their low boiling point at this temperature range (S.P. & Swaminathan, 2022; Jerez, et al., 2021).

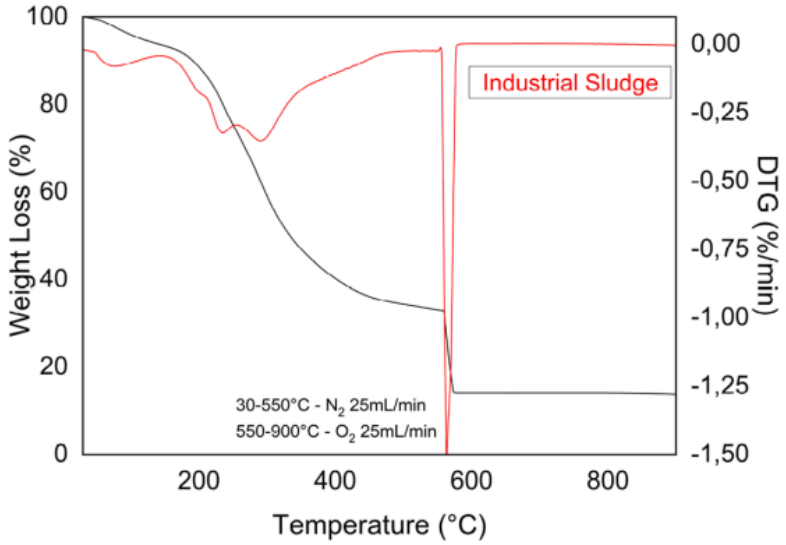

Figure 2.4: TGA Results (Rodrigues, et al., 2023).

The weight loss that followed was caused by the breakdown of thermally labile components including protein and carboxylic acid groups at temperatures between 150 ℃ and 350 ℃. To be more precise, these thermally labile components were normally decomposed at 300 ℃ due to their simpler structure and bonding (Francioso, et al., 2010; Silva, et al., 2012).

At 350 ℃ to 550 ℃, weight loss due to the breakdown of complex hydrocarbons such as long-chain n-alkyls, saturated aliphatic chains, and aromatic rings was then discovered. Specifically, the decomposition of the aforementioned substances was around 450 ℃ (Francioso, et al., 2010; Silva, et al., 2012). Not only complex hydrocarbons, but the majority of the volatile organic substances and macromolecular organic compounds also had a weight

loss between 200 ℃ and 550 ℃ (S.P. & Swaminathan, 2022; Jerez, et al., 2021). Thus, it could be deduced that all the complex and large organic molecules decomposed at around 200 ℃ to 550 ℃.

As the temperature rose, the inorganic compounds which had stronger chemical bonds would begin to decompose. Based on the findings from Rodrigues, et al. (2023), the weight loss attributed to the volatilisation of amorphous carbonaceous residues and the breakdown of inorganic compounds such as calcium carbonate was between 550 ℃ and 600 ℃. S.P. & Swaminathan (2022) and Jerez, et al. (2021) also agreed with this result. However, by observing the black line in the figure, it was also noticeable that the trend had become constant from 580 ℃ onwards, proving the slow decomposition rate of inorganic compounds. So, when the temperature reached higher than 900 ℃, the decomposition of inorganic compounds was solely accountable for the weight loss. As stated in S.P. & Swaminathan (2022), once the temperature exceeded 860 ℃, the weight loss was attributed to the inorganic materials including kaolin and calcium carbonate, which indirectly supported the previous argument.

In short, the results from different journal papers with different instrument setups displayed a similar trend in the thermal degradation behavior of sludge. There was only a slight difference in terms of sludge content due to their respective origins, as shown in Table 2.1.

Table 2.1: Results Comparison for the TGA Analysis.

Sources	Instrument Setups	Results		References
Industrial Sludge	Temperature range: 30 ℃ - 950 ℃ Heating rate: 10 ℃/ min Surrounding atmosphere: Nitrogen and oxygen Atmospheric flow rate: 25 ml/min & 25 ml/min	30 ℃ - 150 ℃ 150 ℃ - 350 ℃ 350 ℃ - 550 ℃ 550 ℃ - 600 ℃ > 900 ℃	Loss of water molecules Decomposition of thermally labile components Decomposition of complex hydrocarbons Volatilisation of amorphous carbonaceous residues & decomposition of inorganic materials Decomposition of inorganic materials	(Rodrigues, et al., 2023)
Sewage Sludge	Temperature range: 25 ℃ - 600 ℃ Heating rate: 10 ℃/ min Surrounding atmosphere: Nitrogen Atmospheric flow rate: 50 ml/min	70 ℃ 300 ℃ 450 ℃	Loss of water molecules Decomposition of thermally labile components Decomposition of complex hydrocarbons	(Silva, et al., 2012)

Table 2.1 (Continued)

Sources	Instrument Setups	Results		References
Municipal Sludge	Temperature range: 30 ℃ - 700 ℃ Heating rate: 10 ℃/ min Surrounding atmosphere: Oxygen Atmospheric flow rate: 50 L/h	300 ℃ 450 ℃	Decomposition of thermally labile components Decomposition of complex hydrocarbons	(Francioso, et al., 2010)
Textile Lime Sludge	Temperature range: 35 ℃ - 950 ℃ Heating rate: 10, 15, 20 ℃/ min Surrounding atmosphere: Oxygen Atmospheric flow rate: -	50 ℃ - 200 ℃ 200 ℃ - 550 ℃ 550 ℃ - 860 ℃ > 860 ℃	Loss of water molecules, small portion of volatile matter Decomposition of macromolecular organic compound, volatile matter Decomposition of lime Degradation of fixed carbon and inorganic materials	(S.P. & Swaminathan, 2022)

Table 2.1 (Continued)

Sources	Instrument Setups	Results		References
Oily Sludge	Temperature range: 30 ℃ - 1000 ℃ Heating rate: 10 ℃/ min Surrounding atmosphere: Nitrogen Atmospheric flow rate: 100 ml/min	< 260 ℃	Removal of light components of the mixture	(Jerez, et al., 2021)
		280 ℃ - 460 ℃	Decomposition of organic compounds of oily fraction	
		460 ℃ - 620 ℃	Decomposition of heavy components, reduction of metals	

2.3.2 Brunauer-Emmett-Teller (BET)

BET can be employed to estimate the sludge surface area. A higher surface area always indicates more active sites, which can infer coal mining sludge adsorption capacity and surface reactivity. Furthermore, BET can also be applied to measure the pore volume and pore size, which are related to the sludge's permeability (Amanda & Moersidik, 2019; Munyengabe, et al., 2020).

2.3.2.1 Sample Preparation & Instrument Setup

Several preparation steps were required to be carried out before placing the sludge sample into the analysis chamber of BET machine. As proposed by Munyengabe, et al. (2020), the collected sludge sample was dried at 105 ℃ in an oven for 24 hours. Then, the dried sample was pulverised and sieved with 100 mesh to get a uniform size (Amanda & Moersidik, 2019). Next, Munyengabe, et al. (2020) also stated that the sample was degassed with nitrogen at 120 ℃ to remove the moisture content. Finally, the sample was ready for the BET analysis.

BET analysis is initiated by setting the adsorption pressure range and equilibration time in the machine program. By doing so, the nitrogen gas will be introduced into the chamber at low pressure, then step by step, gradually raising the pressure while giving the sample enough time to reach the adsorption equilibrium for each pressure increment (Connelly, 2017). During this period, the BET machine will automatically record the data and show the result afterward.

2.3.2.2 Results & Analysis

Based on Table 2.2, synthetic acid mine drainage (AMD) sludge had the greatest specific surface area (31.50 ± 0.03 m^2/g) whereas waste activated sludge (WAS) had the lowest (0.97 m^2/g). The difference in surface area is usually affected by a lot of factors, while particle size has the largest influence among them (Wołowiec, et al., 2019). The WAS sample for BET analysis was prepared with a particle size of around 300 µm which was larger than both AMD sludges that use 149 µm (100 mesh). So, when the particle size of sludge increases, it will decrease the sludge specific surface area for adsorption, resulting in a lower value after the BET analysis.

On top of that, synthetic AMD sludge which was chemically treated with liquid sodium ferrate (VI) would have a greater pore size and volume than AMD sludge. According to Munyengabe, et al. (2020), liquid sodium ferrate (VI) was known as a coagulant and could therefore help to remove the impurities from the sludge, leaving a larger pore size and volume and eventually enhancing the specific surface area.

Table 2.2: Results Comparison for the BET Analysis.

Sources	Results	References
AMD Sludge	Surface Area: 22.60 ± 0.20 m^2/g Pore Volume: 0.06 cm^3/g Pore Size: 10.71 nm	(Amanda & Moersidik, 2019)
Synthetic AMD Sludge	Surface Area: 31.50 ± 0.03 m^2/g Pore Volume: 0.41 cm^3/g Pore Size: 37.50 nm	(Munyengabe, et al., 2020)
WAS	Surface Area: 0.97 m^2/g Pore Volume: - Pore Size: -	(Veenhuyzen, et al., 2021)

2.3.3 Scanning Electron Microscopy with Energy Dispersive X-ray spectroscopy (SEM-EDX)

Veenhuyzen, et al. (2021) described that the sludge's morphology could be studied using SEM. In this instance, SEM can generate high-resolution images of the coal mining sludge's surface, revealing its overall structure as well as its size and shape. Additionally, the elements present in the coal mining sludge can be identified through EDX, an integrated approach with SEM. Such technology is crucial for determining the types and concentrations of different elements that may be present in the sludge.

2.3.3.1 Sample Preparation & Instrument Setup

Before performing SEM-EDX analysis, the collected sludge sample was dried in an oven with 105 ℃ for 24 hours to remove moisture content. The dried sample was then ground, mounted with double-sided carbon tape on a metal stub, and coated with gold (Veenhuyzen, et al., 2021).

In order to carry out SEM-EDX analysis, a vacuum condition is created in the machine chamber to avoid any gas particles that may interfere with the result. Next, some of the settings including the acceleration voltage and beam current are determined in the program. Following this, the sample is aligned with the electron beam for analysis using the control system.

2.3.3.2 Results & Analysis

In Figure 2.5 depicted by Munyengabe, et al. (2020), the synthetic AMD sludge had an irregularly shaped mesh-like structure with an inner surface that appeared spongy and very porous, but the outer edges had a rough surface with a mainly flake-like appearance.

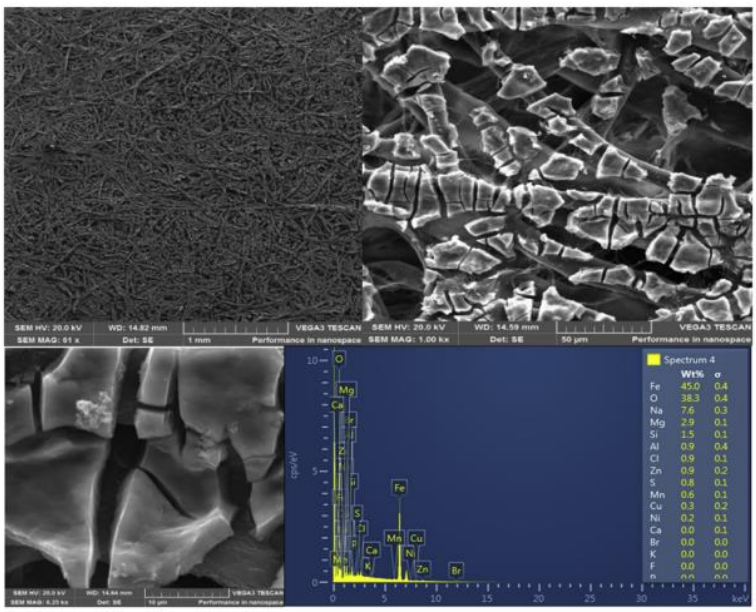

Figure 2.5: SEM Result of Synthetic AMD Sludge (Munyengabe, et al., 2020).

The result was supported by Amanda & Moersidik (2019) who stated that the AMD sludge would normally appear in a mesh-like structure with a certain level of porosity and had outer edges with a flake-like appearance. Both

articles agreed that those flaky structures were due to the presence of silica dioxide, while the spongy side was composed of iron oxide. However, in terms of water treatment sludge, the surface was smooth due to the film created by the organic compounds. After the thermal treatment, the surface would change to become rougher and more porous due to the decomposition of organic substances, leaving behind the flake-like appearance of crystalline materials (Nguyen, et al., 2023). Hence, it can be concluded that sludge with a flake-like appearance usually contains low organic content, while a smooth surface always implies a high content of organic matter.

From the perspective of EDX data tabulated in Table 2.3, the oxygen concentration in AMD sludge and water treatment sludge was the highest which was 38.33 wt% and 44.16 wt% respectively. As claimed by Nguyen, et al. (2023), this might indicate the sludge contained elements in an oxidised form including silica dioxide and iron oxide. Apart from that, the aluminium content was high in water treatment sludge whereas the silica content was high in AMD sludge. The former might be attributed to the sludge's origin as alum sludge while the latter was due to the soil and sediment at the mining site. On the other hand, the synthetic AMD sludge had a high concentration of iron, oxygen, and sodium which was caused by the liquid sodium ferrate (VI) used in the sludge treatment (Munyengabe, et al., 2020).

Table 2.3: Results Comparison for the EDX Analysis.

Sources	**Results**		**References**
AMD Sludge	O	38.33 wt%	(Amanda & Moersidik, 2019)
	Si	28.34 wt%	
	Al	17.16 wt%	
Synthetic AMD Sludge	Fe	45.0 wt%	(Munyengabe, et al., 2020)
	O	38.3 wt%	
	Na	7.6 wt%	
Water Treatment Sludge	O	44.16 wt%	(Nguyen, et al., 2023)
	Al	30.26 wt%	
	Si	16.82 wt%	

2.3.4 X-ray Diffraction (XRD)

Amanda & Moersidik (2019) stated that XRD could detect the minerals presented in coal mining sludge. The mineral phase in the sludge can even be identified by matching the diffraction pattern of sludge with the known patterns of various minerals. Moreover, XRD provides insight into the crystal structure of minerals in the sludge. For instance, the crystallographic orientation and crystal symmetry of the minerals can be defined, providing valuable information for the mineralogical properties of sludge (Bakar, et al., 2022).

2.3.4.1 Sample Preparation & Instrument Setup

Several studies recommended that the sludge sample be dried first in an oven at 105 ℃ overnight, followed by a crushing step, and sieved through a 100-mesh fine screen for homogenisation purposes. Subsequently, the powdered sample was mounted onto a sample holder for XRD analysis later (Amanda & Moersidik, 2019; Munyengabe, et al., 2020).

After placing the sample holder into the XRD machine, some instrument setup is required. For example, an appropriate X-ray source proposed by Amanda & Moersidik (2019) with Cu K(α) radiation at 1.54 A wavelength is decided. Then, the sample is positioned in the instrument's goniometer and ready for analysis. The resulting diffraction patterns will be interpreted by the available software.

2.3.4.2 Results & Analysis

Research conducted by Amanda & Moersidik (2019) found that the AMD sludge contained significant amounts of quartz and kaolinite. As shown in Table 2.4, the quartz had a diffraction peak at 20.9°, 26.7°, 36.5°, 50.1° and 60.0°. This was consistent with the findings from Jerez, et al. (2021) and Wang, et al. (2022). Although the sludge source was different from AMD sludge, they reported similar diffraction peaks for quartz which were 21.0°, 26.9°, 36.8°, 50.1° and 60.0° for oily sludge, and 20.859°, 26.639° and 36.546° for coal gangue. However minor differences occurred as the quartz diffraction peaks at 50.1° and 60.0° were absent from coal gangue. This was possible seeing as the crystal structure of quartz varied in coal gangue. The presence of

quartz could be attributed to the contamination of sediments or soil during the drilling and extraction processes.

Besides, the coal mining process will disturb the natural geological layers, weathering the clays and releasing kaolinite particles onto the site. Thus, the diffraction peaks at 12.4°, 20.9°, 25.0°, 26.8°, 36.7°, 39.5°, 46.0°, 55.0° and 62.2° proved the presence of kaolinite in the AMD sludge. In support of this, Yang, et al. (2016) also revealed a similar diffraction pattern at 12.9°, 20.9°, 25.0°, 27.0°, 36.8°, 39.4°, 46.0°, 55.7° and 63.0° for coal gangue 2.

Table 2.4: Results Comparison for the XRD Analysis.

Sources	Results		References
AMD Sludge	Quartz (SiO_2)	20.9°, 26.7°, 36.5°, 50.1°, 60.0°	(Amanda & Moersidik, 2019)
	Kaolinite ($Al_2Si_2O_5(OH)_4$)	12.4°, 20.9°, 25.0°, 26.8°, 36.7°, 39.5°, 46.0°, 55.0°, 62.2°	
Oily Sludge	Quartz (SiO_2)	21.0°, 26.9°, 36.8°, 50.1°, 60.0°	(Jerez, et al., 2021)
Coal Gangue	Quartz (SiO_2)	20.859°, 26.639°, 36.546°	(Wang, et al., 2022)
Coal Gangue 2	Kaolinite ($Al_2Si_2O_5(OH)_4$)	12.9°, 20.9°, 25.0°, 27.0°, 36.8°, 39.4°, 46.0°, 55.7°, 63.0°	(Yang, et al., 2016)

2.3.5 Fourier Transform Infrared (FTIR)

The main function of FTIR is to allow for the identification of functional groups present in coal mining sludge (Munyengabe, et al., 2020; Veenhuyzen, et al., 2021). The functional groups always correspond to the specific chemical bond and molecular structure of organic or inorganic substances. When the infrared light passes through the sludge sample, the molecules will absorb the specific wavelength that matches the vibrational modes of the chemical bonds

within the molecule. To put it another way, FTIR can also disclose the molecular structure of a compound. As a result, it is possible to predict the sludge's chemical composition and reactivity.

2.3.5.1 Sample Preparation & Instrument Setup

To remove the moisture, the sludge sample was initially dried at 105 ℃ using an oven for 24 hours. Next, the dried sample was ground into a fine powder using mortar grinder (Nguyen, et al., 2023). Rodrigues, et al. (2023) mentioned that the powdered sample was then prepared with potassium bromide (KBr) in the form of pellets for FTIR analysis.

In order to have an accurate result, the sample chamber of FTIR machine is purged by nitrogen gas to remove carbon dioxide and water. Then, a plain KBr pellet is put into the sample holder to have a background spectrum to remove any interference. After that, the prepared pellet is inserted into the machine to replace the plain KBr pellet (Washington. Edu, n.d.). The measurement parameters including the wavenumber range (400 cm^{-1} – 4000 cm^{-1}), resolution (4 cm^{-1}), and acquisition time (64 scans) are set in the machine program and ready for analysis (Rodrigues, et al., 2023).

2.3.5.2 Results & Analysis

In a recent paper published by Ren, et al. (2020), it claimed that the absorption peaks at 3695 cm^{-1} and 3620 cm^{-1} represented the bond stretching of free – OH while the peak appearing near 3407 cm^{-1} represented the stretching of O – H in the intermolecular hydrogen bonding. The results were compatible with the findings of Veenhuyzen, et al. (2021) and Rodrigues, et al. (2023). The former mentioned that the O-H stretching in variegated hydrogen bonding would have a broad band at 3600 cm^{-1} – 3000 cm^{-1} whereas the latter further argued that the peak near 3397 cm^{-1} could be related to the O – H stretching of acids and alcohols.

From Figure 2.6, it could be observed that there was a band between 3000 cm^{-1} and 2800 cm^{-1}, implying the presence of C – H stretching. Veenhuyzen, et al. (2021) believed that the C – H stretching asymmetrically and symmetrically in the hydrocarbon chain could be observed by the peaks near 2924 cm^{-1} and 2854 cm^{-1}.

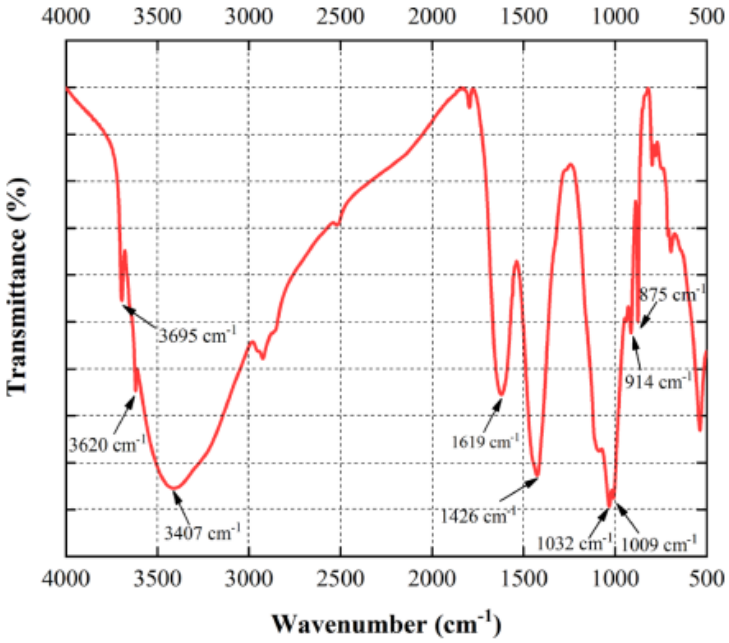

Figure 2.6: FTIR spectrum of Coal Mine Sludge (CMS) (Ren, et al., 2020).

Moreover, peaks at 1619 cm^{-1} and 1426 cm^{-1} represented the antisymmetric and symmetric stretching of – COO^- respectively. Compared to the results obtained by other authors, it was confirmed that carboxylate groups were stretching symmetrically near 1407 cm^{-1} but bands with 1630 cm^{-1} were ascribed to C = O stretching from primary amide (Veenhuyzen, et al., 2021). Even so, the CMS was treated with partially hydrolysed polyacrylamide (HPAM). Thus, it could be considered that the antisymmetric stretching of – COO^- was from the amide group in HPAM.

Ren, et al. (2020) also asserted that there was C – O stretching vibration in alcohol at absorption peaks 1032 cm^{-1} and 1009 cm^{-1}. But Rodrigues, et al. (2023) offered an alternative perspective to the absorption band at 1045 cm^{-1} for the C – O stretching vibration in polysaccharides. Both refer to the C – O stretching but correspond to different molecules. Yet, the authors also emphasised that the band near 1045 cm^{-1} might be attributed to the Si – O stretching of silicates due to their similar bond strength and length. The argument aligned with the interpretation of another report, which showed that the Si – O stretch was likely to be presented at the absorption band 1031 cm^{-1} indicating that the aforementioned 1032 cm^{-1} was also possible to represent the Si – O stretching vibration (Nguyen, et al., 2023).

Another similar scenario could be discussed by using – NH vibration and Al – O stretching. Ren, et al. (2020) had proven that the – NH vibration in HPAM could be detected at peak 875 cm^{-1} while Nguyen, et al. (2023) criticised the spectra between 468 cm^{-1} and 912 cm^{-1} was typically attributed to Al – O. Thus, the only reason that can explain this phenomenon will be the chemical bond of NH becomes weaker due to the hydrolysis process that breaks down the amide group of HPAM, alternating its chemical structure (Berdugo-Clavijo, et al., 2019).

In order to have a better view, the aforementioned results are summarised in Table 2.5.

Table 2.5: Results Comparison for the FTIR Analysis.

Sources	**Results**		**References**
CMS	O – H	3695, 3620, 3407	(Ren, et al., 2020)
	C – H	3000 – 2800	
	$-COO^-$	1619, 1426	
	C – O	1032, 1009	
	– NH	875	
WAS	O – H	3600 – 3000	(Veenhuyzen, et al., 2021)
	C – H	2924, 2854	
	$-COO^-$	1407	
	C = O	1630	
Industrial Sludge	O – H	3397	(Rodrigues, et al., 2023)
	C – O	1045	
	Si – O	1045	
Water Treatment Sludge	Si – O	1031	(Nguyen, et al., 2023)
	Al – O	468 – 912	

2.4 Sludge Purification Techniques

After characterising the coal mining sludge, certain separation processes can be used to extract valuable substances including zinc, cadmium, aluminium, and silica from the sludge. Through a variety of methods, it is even possible to retrieve small quantities of organic compounds that were created during the processing of coal. In order to have more in-depth knowledge regarding the appropriate treatment approach, the following subsections will describe and discuss their experiment setup, the effect of parameters, and the possible outcomes.

2.4.1 Acid Leaching

Acid leaching extracts the heavy metal from the coal mining sludge by chelation. Ethylenediamine tetraacetic acid (EDTA) is well-known as an effective chelating agent involved in the extraction process due to its stable metal complexes and excellent solubility. However, it has been said to have poor biodegradability, which means it could cause secondary pollution to the environment. Thus, it is gradually replaced by other eco-friendlier chelators such as glutamic acid (GLDA) and citric acid (CA) (Guo, et al., 2020; Wu, et al., 2015). Both of them were successful in achieving high removal efficiency for some heavy metals, which will be explained in more detail in the following part.

2.4.1.1 Pre-treatment & Experiment Setup

According to Wu, et al. (2015), the collected sludge was first dried with air at room temperature. It was then crushed and sieved to a size of 150 µm. In order to perform the acid leaching process, 0.5 g of sludge sample and 25 ml of chelator were put into a conical flask. The flask was shaken at 200 rpm at room temperature for some reaction time. After that, the tube was centrifuged at 3500 rpm for 20 minutes and the supernatant was collected using a 0.45 µm filter membrane. Before analysis, the solution was stored at 4 ℃. The general step of the procedure was consistent with another researcher Guo, et al. (2020). The experiment was repeated with different reaction times (2 – 72 h), molar ratio of GLDA: M(II) (1:1 – 10:1), and pH (1 – 12) to determine the optimum condition for heavy metal removal.

2.4.1.2 Effect of Parameter Studies

i. Reaction Time

Several studies have pointed out that the removal efficiency of heavy metals grew rapidly with the reaction time until a certain level, at which point the leaching performance would become lower (Hu, et al., 2022; Guo, et al., 2020; Wu, et al., 2015). In the study of Wu, et al. (2015) as shown in Figure 2.7, the removal efficiency of cadmium (Cd) and copper (Cu) with GLDA demonstrated a relatively fast increase within 24 h. After 24 h, the efficiency exhibited only a slight increase.

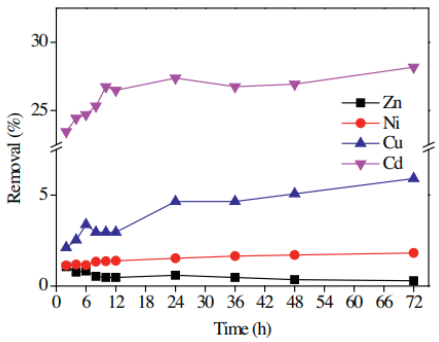

Figure 2.7: Effect of Reaction Time on The Extraction of Heavy Metals at GLDA: M(II) = 1:1, pH 12 (Wu, et al., 2015).

The trend was likely aligned with the study done by Guo, et al. (2020) which mentioned that the removal efficiency of Cd and Cu with GLDA+CA spiked up within 8 h and then continued to increase with time until 24 h, followed by a slight increase afterward.

ii. pH

Prior research had shown heavy metals would have high removal efficiency at low pH. In the words of Wu, et al. (2015), it could be seen from Figure 2.8, the removal efficiency of heavy metals was decreasing with the rise of pH.

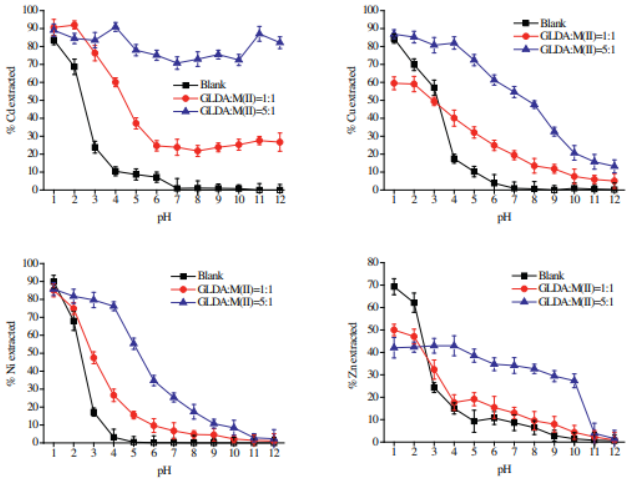

Figure 2.8: Effect of pH on The Extraction of Heavy Metals within 24 h (Wu, et al., 2015).

Guo, et al. (2020) validated the trend and explained the concept behind it was that when the pH is low, the proton movement in the solution will intensify, facilitating the removal of heavy metals. Contrary to this, when the pH value is higher, the alkaline environment will promote the heavy metal ions to precipitate, hindering the leaching process.

iii. Chelator Concentration

Generally, the removal efficiency of heavy metals will increase with the concentration of the chelator. High concentration implied that more ligand was present to interact with metal ions, promoting the complexing reaction and forming more chelate, which was good for the leaching process (Wu, et al., 2015). From Figure 2.9 presented by Wu, et al. (2015), the removal efficiency of heavy metals only climbed until a certain level of GLDA concentration, then showed a decline in leaching performance afterward.

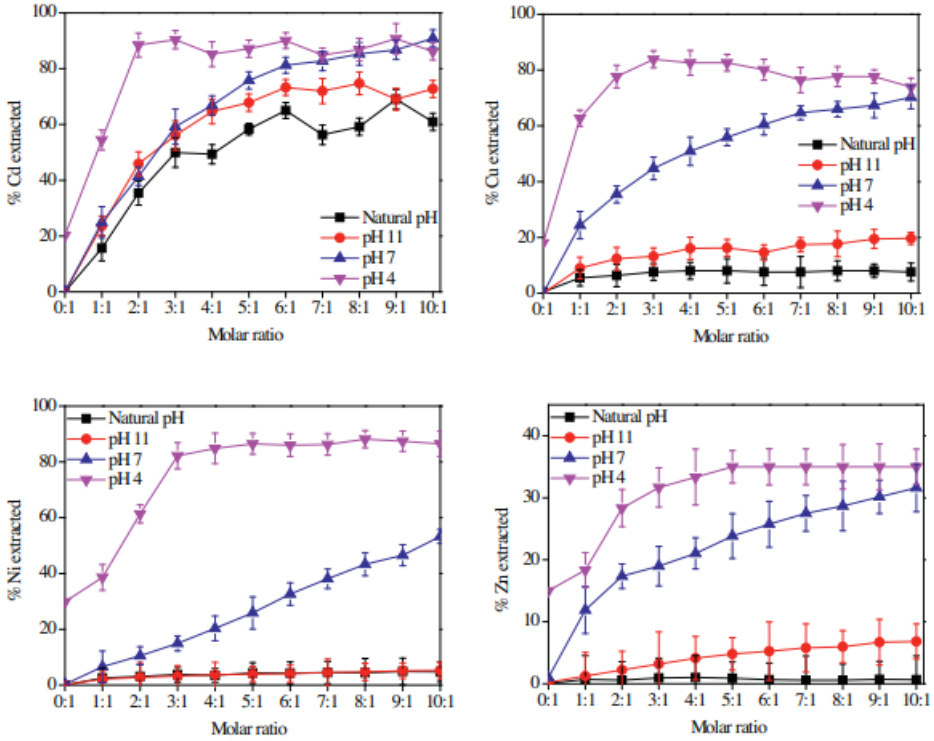

Figure 2.9: Effect of GLDA concentration on The Extraction of Heavy Metals with 24 h at different pH (Wu, et al., 2015).

The result was further supported by Guo, et al. (2020) which stated that the effect of chelator concentration was similar to the effect of reaction time, where the trend only climbed until a certain level. As mentioned by the researchers, this was most likely due to the fact that most of the exchangeable and reducible heavy metal fractions in the sludge were removed, and the remaining fractions were not accessible by excess chelators.

2.4.1.3 Optimum Condition

In short, the Cd, Ni, and Cu removal efficiency might be attained at 89 %, 82 %, and 84 % respectively, at the optimum condition of a 24 h reaction time with a 3:1 GLDA: M(II) molar ratio at pH 4 (Wu, et al., 2015).

2.4.2 Sulfation Roasting & Water Leaching

A novel and less harsh technique that combines roasting and leaching to separate the heavy metal from the coal mining sludge has been devised. Compared with conventional acid leaching, which has the potential to harm

the environment and corrode equipment, it is more effective and sophisticated. In a recent paper published by Ballou, et al. (2022), the sulfation roasting phase enabled the conversion of major mineral substances into soluble metal sulphates which facilitated the leaching stage afterward. It has been found that a few heavy metals, particularly aluminium (Al) and silicon (Si), might be recovered using this method. The details of the experiment will be reviewed in the following subsection.

2.4.2.1 Pre-treatment & Experiment Setup

Initially, the collected sludge was dried in the air for four nights. Then, the sludge sample was steamed at 105 ℃ for 24 h to eliminate the moisture content, followed by grinding and finally sieving through a 63 μm mesh, ready for the experiment (Ballou, et al., 2022).

Besides the sludge sample, ammonium sulphate, $(NH_4)_2SO_4$ was also ground with a mortar grinder. Next, $(NH_4)_2SO_4$ powder would be mixed with powdered sludge to a desired ratio and ground again to enhance the solid-solid interaction and the specific surface area. The mixture was then transferred into a quartz-made crucible and placed inside the furnace that operated under an air atmosphere with a 5 ℃/min heating rate. Three parameters namely roasting temperature (200 ℃ - 700 ℃), mass ratio of sludge to ammonium sulphate (1:1 – 1:4), and roasting time (20 min – 140 min) were systematically varied in the roasting experiment to determine the optimum conditions for heavy metal extraction. Later, the roasted sludge was cooled to 25 ℃ and ground again to get rid of the agglomerates that formed during the roasting process.

Subsequently, the processed sludge was leached with hot distilled water (80 ℃) at a solid-liquid ratio of 1:100 for 1 hour. The leaching stage was performed with 500 rpm magnetic stirring while being refluxed in a double-walled glass beaker attached to a thermostatic bath. The solution was filtered using 0.45 μm filter paper and the residues were rinsed with hot water before being put into the oven for drying purposes. Eventually, both filtrates and residues were required for analysis to examine the extraction efficiency of the experiment (Ballou, et al., 2022). The overall procedure described above for the roasting and leaching experiment was in line with the study of Zhang, et al. (2021), establishing that this is the proper method for experimenting.

2.4.2.2 Effect of Parameter Studies

i. Roasting Temperature

As illustrated by Figure 2.10, the Al extraction efficiency grew with the roasting temperature. The result agreed with the finding of Shekhar, et al. (2021) which also presented an increasing trend for the effect of roasting temperature on heavy metal leaching performance.

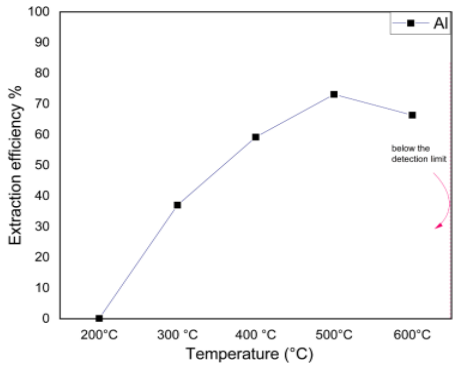

Figure 2.10: Effect of Roasting Temperature on The Al Extraction (Ballou, et al., 2022).

It was because when the roasting temperature increased, it would break the mineral structure inside the sludge, creating a larger surface area for the leaching process and enhancing the heavy metal extraction efficiency. Besides, as mentioned by Ballou, et al. (2022), the $(NH_4)_2SO_4$ and raw sludge would decompose and begin to react with each other, producing various products as the temperature increased. Eventually, generating the soluble metal sulfate ($Al_2(SO_4)_3$) at 500 ℃. Therefore, the highest Al extraction efficiency was shown during the leaching process. The extraction efficiency was then reduced with temperature due to the decomposition of $Al_2(SO_4)_3$ into insoluble Al_2O_3 which hindered the leaching process afterward (Ballou, et al., 2022; Shekhar, et al., 2021). Hence, it can be concluded that the roasting temperature helps to increase the extraction efficiency until a certain level, where the soluble metal sulfate begins to decompose into an insoluble substance.

ii. Mass Ratio

Based on Figure 2.11, Al extraction efficiency rose with the mass ratio and exhibited little effect from mass ratio 1:3 onward. The same result was also found in the case of Shekhar, et al. (2021) with the manganese (Mn) extraction efficiency increasing along the sawdust dosage until a certain point when the effect of dosage became negligible. So, it is undeniable that when more reacting agents are mixed with the sludge, more interaction can occur to produce the desired product which benefits the leaching process, and leads to higher extraction efficiency.

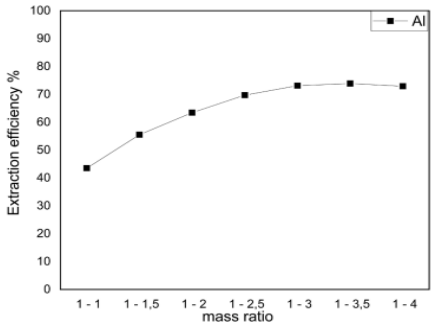

Figure 2.11: Effect of Mass Ratio on The Al Extraction (Ballou, et al., 2022).

iii. Roasting Time

By referring to Figure 2.12, the graph implied that the Al extraction efficiency increased with time. In other words, the interaction between the sludge and $(NH4)_2SO_4$ requires more time to produce the desired product such as soluble metal sulfate which can boost the performance of the leaching process for high extraction efficiency.

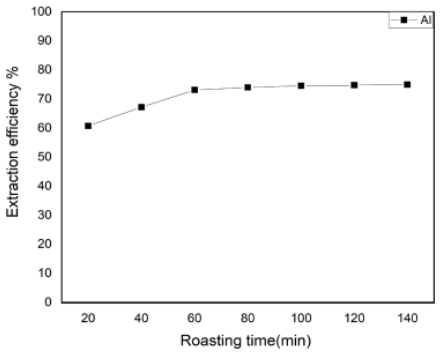

Figure 2.12: Effect of Roasting Time on The Al Extraction (Ballou, et al., 2022).

The argument was further endorsed by Zhang, et al. (2021) who had similar results on the trend. Also, as stated by Ballou, et al. (2022), rapid volatilisation would happen after 60 min, leading to a loss of SO_x that eventually accumulated on the sludge surface, resulting in a small increment in extraction efficiency. Thus, it was evident that the extraction efficiency would reach an optimum point over time, and after that, the performance of the leaching process would not be significant due to the formation of unwanted products.

2.4.2.3 Optimum Condition

To summarise, 74 % of Al could be successfully recovered at the optimum conditions of 500 ℃ roasting temperature, 100 min roasting time, and 1:3 mass ratio. As well, it was found that there was a high percentage (35.8 %) of silicon present in the leaching residue. Thus, it could be deduced that both Al and Si could be recovered as valuable products through the combination of roasting and leaching processes.

2.4.3 Solvent Extraction & Freeze-Thaw

Except for heavy metals, some organic compounds (oil) may also be recovered from coal mining sludge through solvent extraction. It is a straightforward technique that involves combining the sludge with a solvent in the proper quantities to ensure optimal oil miscibility while removing water and particles as unwanted contaminants by centrifugation or gravity. However, if the sludge contains a high moisture content, it can lead to the formation of emulsified water during the extraction process. As a result, the water cannot be effectively separated by gravity, contaminating the extractant and degrading the oil recovery rate. Thus, it is encouraged to integrate the extraction process with freeze-thaw treatment, which aids in extractant dewatering and optimises the quality of recovered oil (Abdulqawi, et al., 2023; Hua, et al., 2015). Cyclohexane (CHX) is known as one of the typical solvent types used during the process and its performance will be evaluated in the following part.

2.4.3.1 Pre-treatment & Experiment Setup

First and foremost, the collected sludge should be stirred manually to ensure a well-mixed condition before being applied to the experiment. It was highlighted that the solvent extraction experiment would be repeated a few times by using different ratios of solvent to sludge (1:1 – 8:1) and durations of extraction (5 min – 90 min) to determine the optimum conditions for oil recovery (Hua, et al., 2015).

Hua, et al. (2015) and Abdulqawi, et al. (2023) agreed that each experiment began by putting 5 g of sludge sample and an appropriate volume of solvent into a 50 ml centrifugation tube. Then, the tube was sealed and placed into a shaker for processing at 150 rpm. After shaking for a certain time, the mixture was settled for 24 h at 25 ℃. Later, it was observed that three layers were formed, as illustrated in Figure 2.13. The extractant layer (oil, solvent, and emulsified water) was transferred into a 100 ml round-bottom flask that was placed in a vacuum rotary evaporator operating at 40 ℃ for distillation. The distillate (solvent) was condensed for recovery while the bottom was placed in the fume hood to eliminate any residual solvent using air drying, and the product left in the flask was referred to as the recovered oil. The water layer was removed using a Pasteur pipette, whereas the solids layer, was air-dried in the fume hood for 48 h and weighed for analysis purposes.

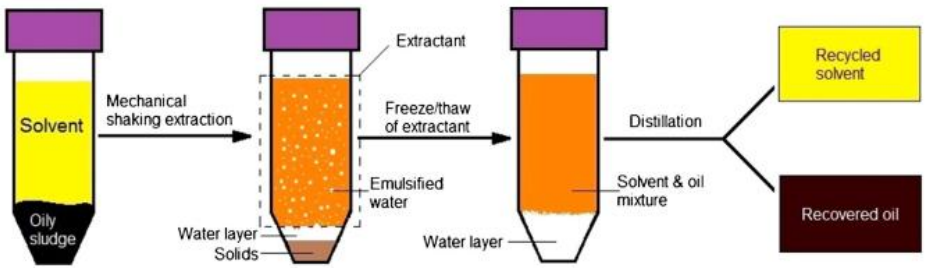

Figure 2.13: Schematic Diagram of the Integration of Solvent Extraction and Freeze-Thaw Treatment (Hua, et al., 2015).

In order to study the effectiveness of freeze-thaw treatment, another three groups of experiments with the identified optimal conditions were carried out, namely solvent extraction alone, freeze-thaw alone, and the integration of both techniques. In terms of solvent extraction alone, the

experiment was performed the same as the procedure described above. For freeze-thaw, it was started by mixing the pure water and sludge sample, followed by a shaking process and finally transferred to a freezer at -20 ℃ for 12 h then thawed at 25 ℃. For the last group experiment, it was just a combination of steps from both groups mentioned before and using solvent instead of water (Abdulqawi, et al., 2023; Hua, et al., 2015).

2.4.3.2 Effect of Parameter Studies

i. Solvent to Sludge Ratio

From Figure 2.14 reported by Hua, et al. (2015), the oil recovery rate was increasing with the solvent-to-sludge ratio until reaching equilibrium. It was due to the fact that when the ratio climbed, the oil solubility in solvent was boosted as well, thus improving the oil recovery rate. A similar finding was also obtained from Abdulqawi, et al. (2023).

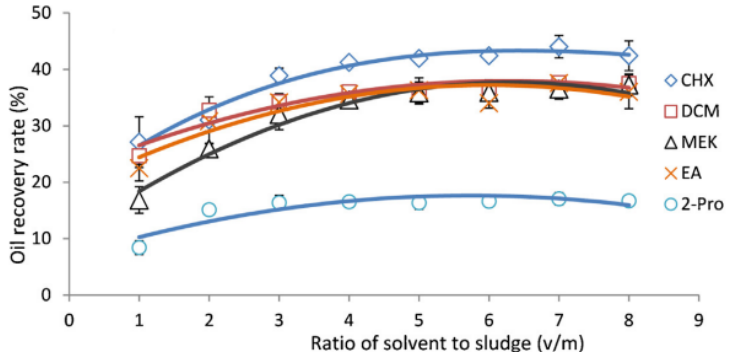

Figure 2.14: Effect of Solvent to Sludge Ratio on Oil Recovery Rate (Hua, et al., 2015).

On top of that, Hua, et al. (2015) pointed out that the waste reduction rate in terms of sludge mass was increasing with the ratio of solvent to sludge until a certain point which is 4:1. Therefore, 4:1 might be the suitable solvent-to-sludge ratio which was further confirmed by Abdulqawi, et al. (2023).

ii. Extraction Duration

From the viewpoint of extraction duration, Hua, et al. (2015) discussed that if the time duration was long enough, the oil could be dissolved by the solvent and the impurities could assemble into bigger particles to be settled out of the

liquid phase. The statement aligned with the trend in Figure 2.15 which showed that the oil recovery rate rose with the extraction time until a certain level where equilibrium was achieved, indicating the complete extraction of oil.

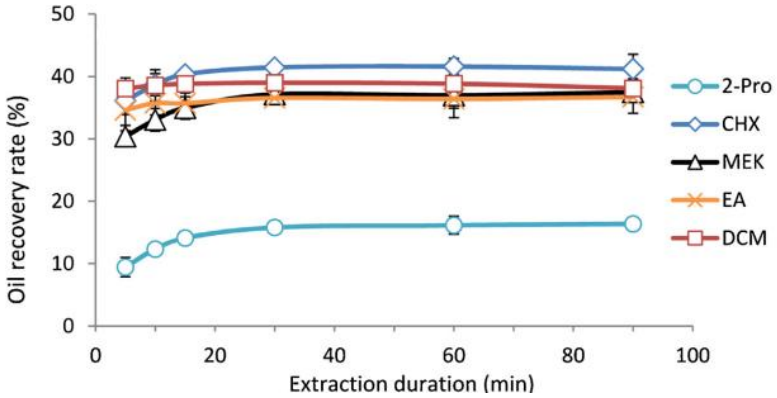

Figure 2.15: Effect of Extraction Duration on Oil Recovery Rate (Hua, et al., 2015).

In this case, Hua, et al. (2015) and Abdulqawi, et al. (2023) concluded that the optimum duration for extraction was 30 min which could accomplish a high oil recovery rate and waste reduction rate.

iii. Effectiveness of Freeze-Thaw Treatment

As studied by Hua, et al. (2015) and Abdulqawi, et al. (2023), both reports validated that freeze-thaw alone was unable to recover any oil from sludge. Abdulqawi, et al. (2023) explained that it was because the water was incapable of dissolving any complex organic compound present in sludge. In addition, it was true that for the solvent extraction alone, large amounts of emulsified water were detected in the extractant, which made it impossible to separate them using gravitational settling. However, if the freezing process was employed, the emulsified water droplets were transformed into an ice lattice, while the solvent and oil remained in their original forms. Subsequently, the water droplets would coalesce during the thawing process, forming a larger water droplet that was readily separated by gravity. Thus, it was noted that the freeze-thaw treated sample had a higher separated water layer than that without treatment, proving the effectiveness of freeze-thaw treatment

dewatering ability and ensuring the quality of recovered oil (Hua, et al., 2015; Abdulqawi, et al., 2023).

2.4.3.3 Optimum Condition

In a word, a solvent (CHX) extraction with freeze-thaw treatment experiment could be conducted under a 4:1 solvent-to-sludge ratio and 30 min duration to obtain around 40 % oil recovery.

CHAPTER 3

METHODOLOGY AND WORK PLAN

3.1 List of Material and Equipment

The material and equipment used for the characterisation and purification experiments are outlined and discussed in Sections 3.1.1 and 3.1.2.

3.1.1 Materials

The coal mining sludge used in this study was collected from a foreign company in Indonesia. Besides, all the chemicals involved in the experiment are tabulated in Table 3.1 with their respective brand, purity, and purpose.

Table 3.1: Materials Required in the Experiment.

Chemicals	Brand	Purity	Purpose
Ammonium Sulphate	Merck	≥ 99.5%	Reacting agent for sulfation roasting

3.1.2 Equipment / Apparatus

All the equipment or apparatus involved in the experiment are summarised in Table 3.2 with their respective specification and purpose.

Table 3.2: Equipment/Apparatus Required in the Experiment.

Equipment/Apparatus	Specification	Purpose
Oven	Memmert	Drying of sludge
Mortar Grinder	GM-800S1	Grinding of sludge
Sieve	300 µm mesh size	Sieving of sludge
Electronic Balance	AND FX-300i	Weighing of sludge powder and ammonium sulphate
Vacuum Pump	Rocker 300	Filter the leachate

Table 3.2 (Continued)

Equipment/Apparatus	Specification	Purpose
Crucible	Alumina	Load the mixture (sludge and ammonium sulphate)
Muffle Furnace	LT Furnace	Roasting of sludge and ammonium sulphate
Heating Mantle	Mtops	Maintain the desired temperature during leaching process
Thermogravimetric Analyser (TGA)	Perkin Elmer STA8000	Analysis of thermal decomposition behaviour of sludge
Brunauer-Emmett-Teller (BET)	Micromeritics 3Flex	Determination of specific surface area, pore size, and pore volume of sludge
Scanning Electron Microscope Equipped with Energy Dispersive X-ray spectroscopy (SEM-EDX)	Hitachi S3400N	Identification of surface morphology and chemical elements in the sludge
X-ray Diffractometer (XRD)	Shidmazu XRD-6000	Analysis of crystalline phase and mineralogical properties of sludge
Fourier Transform Infrared Spectrometer (FTIR)	Nicolet IS10	Identification of functional group present in the sludge

3.2 Overall Experiment Methodology and Flowchart

The overview of the experiment methodology is illustrated in Figure 3.1.

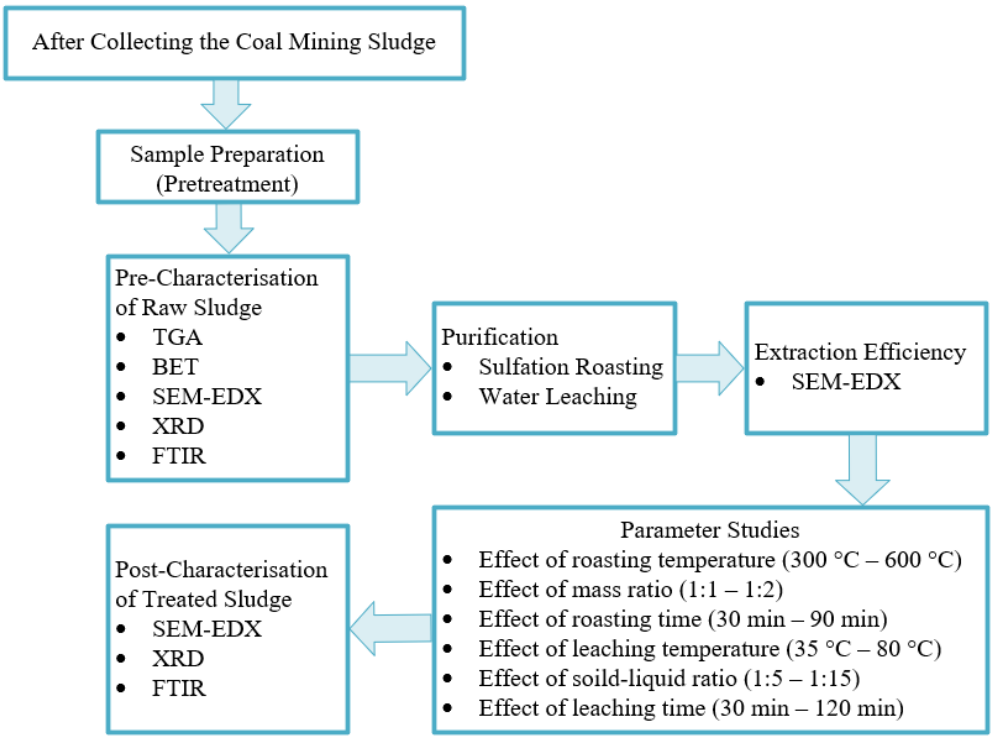

Figure 3.1: Overview of the Experiment Methodology.

3.3 Experimental Procedures

3.3.1 Sample Preparation

The collected coal mining sludge will have to go through several preparation steps before carrying out the characterisation experiment. TGA, BET, SEM-EDX, XRD and FTIR all require the sample to be prepared in solid form.

Initially, the sludge sample was dried in an oven at 105 ℃ for 24 hours to remove the moisture content. The dried sample was then crushed using a mortar grinder before being sieved with 60 mesh (300 µm) for homogenisation purposes to improve the precision of the result (Amanda & Moersidik, 2019).

3.3.2 Pre or Post Characterisation

3.3.2.1 TGA

The TGA machine was programmed with a temperature range of 30 ℃ to 1000 ℃ and a heating rate of 10 ℃/ min. In addition, the analysis was conducted under 20 ml/min of nitrogen atmosphere. 40 mg of powdered coal mining sludge sample was weighted on an electronic balance and loaded into a crucible for thermal analysis. Upon program completion, a TGA curve was obtained.

3.3.2.2 BET

The degassing chamber was initially loaded with 1.2 g of powdered coal mining sludge sample. Then, it was degassed at 90 °C by nitrogen for 60 min with a heating rate of 10 ℃/min to eliminate impurities and moisture. Following this, the temperature was increased to 100 ℃ with a heating rate of 10 ℃/min and held for 8 hours After that, the sample was moved to the analysis chamber where it would be subjected to a nitrogen analysis at 77 K (Munyengabe, et al., 2020; Veenhuyzen, et al., 2021). Eventually, the BET software would calculate the specific surface area, pore size, and pore volume based on the adsorption isotherm.

3.3.2.3 SEM-EDX

To initiate the SEM-EDX experiment, the powdered coal mining sludge sample was mounted with double-sided carbon tape on an SEM stub and coated with gold (Munyengabe, et al., 2020). The SEM machine was then set at 15 kV for accelerating voltage and 3000X, 4000X, and 5500X for image magnification. Also, the elemental composition of sludge was determined through EDX spectra by choosing a specific point on the sample.

3.3.2.4 XRD

Firstly, the powdered coal mining sludge sample was mounted onto a sample holder and placed into the XRD machine. An X-ray source with Cu K(α) radiation at 1.54 A wavelength in 40 kV and 30 mA was selected (Amanda & Moersidik, 2019). As well, the machine was configured to perform continuous

step scans with a 0.02° stepping size over a range of 5° to 85°, 2θ. After finishing, diffraction patterns of the sample were produced.

3.3.2.5 FTIR

Before beginning the FTIR analysis, 5 mg of the powdered coal mining sludge sample was put into the sample holder and held at the fixed position using the pressure tower and compression tip. At a resolution of 4 cm^{-1} across 64 scans, the FTIR machine was operated in the 400 cm^{-1} to 4000 cm^{-1} wavenumber range (Rodrigues, et al., 2023). The process was completed with the generation of a sample's FTIR spectrum.

3.3.3 Purification

Considering the collected sample was an alum sludge originating from the coal mining wastewater treatment plant and the contribution of natural geology, it was reasonable to presume that there would be the presence of aluminium (Al) and silicon (Si) as major elements in the sludge. Thus, a sophisticated treatment method was proposed as follows to extract the aluminium and recover the silica content in the sludge.

3.3.3.1 Sulfation Roasting

First and foremost, the coal mining sludge sample was prepared and pre-treated as described in Section 3.3.1. Then, a reacting agent, ammonium sulphate, $(NH_4)_2SO_4$ was ground with a mortar and pestle. After that, it was mixed with 8 g of powdered coal mining sludge with a 1:1.5 mass ratio and ground again to enhance the solid-solid interaction and the specific surface area. The mixture was then loaded into an alumina-made crucible and put inside the muffle furnace which combusts at 300 °C at a rate of 5 °C/min for 90 min, as shown in Figure 3.2. Later, the roasted sludge was cooled to 25 °C and processed once more to remove the agglomerates that developed during the roasting process. The process was repeated by systematically altering three parameters: roasting temperature (300 °C - 600 °C), mass ratio of sludge to ammonium sulphate (1:1 - 1:2), and roasting time (30 min - 90 min) to

determine the ideal conditions for aluminium extraction (Ballou, et al., 2022). The details of the condition for each parameter are listed in Table 3.3.

Table 3.3: The Condition of Each Parameter for the Roasting Process.

Groups	Parameter Studies	Conditions
1	Roasting temperature	300 °C - 600 °C 1:1.5 ratio 90 min
2	Mass ratio	1:1 - 1:2 Optimum roasting temperature 90 min
3	Roasting time	30 min – 90 min Optimum roasting temperature Optimum mass ratio

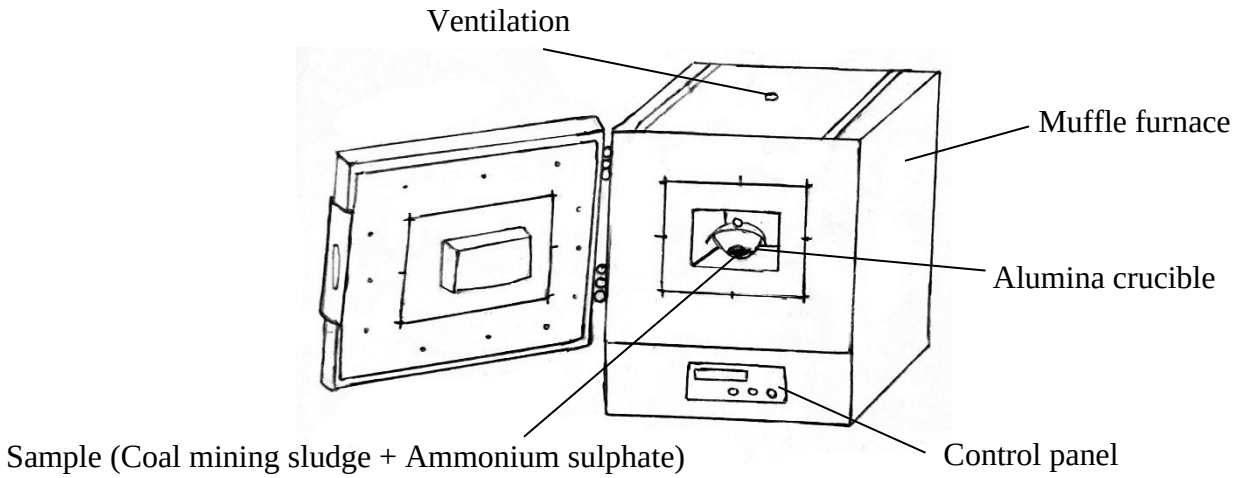

Figure 3.2: The Experiment Setup of the Roasting Process.

3.3.3.2 Water Leaching

As stated by Ballou, et al. (2022), the processed sludge was next leached for 60 min with hot distilled water (80 °C) at a solid-liquid ratio of 1:10. This process was conducted under reflux in a round bottom flask with a heating mantle and being stirred at 500 rpm as illustrated in Figure 3.3. The mixture was filtered using filter paper before being dried in an oven at 80 ℃ for 2 hours. Eventually, the residues were required for SEM-EDX analysis to

examine the extraction efficiency of the experiment. The analysis would be collected for three different locations of a sample to obtain an average result. It was highlighted that after determining the optimum roasting condition for aluminium extraction, the leaching process would be also varied with three different parameters as presented in Table 3.4 to further improve the aluminium extraction performance.

Table 3.4: The Condition of Each Parameter for the Leaching Process.

Groups	Parameter Studies	Conditions
1	Leaching temperature	35 °C - 80 °C 1:10 ratio 60 min
2	Solid-liquid ratio	1:5 - 1:15 Optimum leaching temperature 60 min
3	Leaching time	30 min – 120 min Optimum leaching temperature Optimum solid-liquid ratio

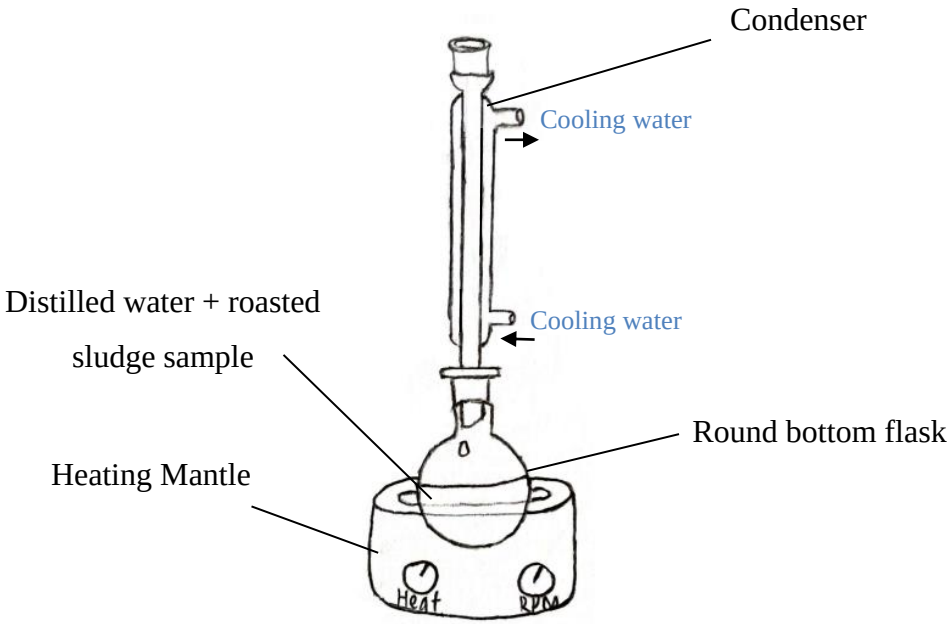

Figure 3.3: The Experiment Setup of the Leaching Process.

3.3.3.3 Extraction Efficiency

The Al extraction efficiency was calculated using equation 3.1.

$$\eta_{Al} = \frac{w_B - w_A}{w_B} \times 100\ \% \tag{3.1}$$

Where:

$\eta = Al\ extraction\ efficiency\ (\%)$

$w_B = Weightage\ of\ Al\ in\ the\ sludge\ before\ experiment\ (wt.\%)$

$w_A = Weightage\ of\ Al\ in\ the\ sludge\ after\ experiment\ (wt.\%)$

CHAPTER 4

RESULTS AND DISCUSSION

4.1 Raw Sludge Characteristics

The coal mining sludge was characterised through various analytical methods including Thermogravimetric Analysis (TGA), Brunauer-Emmett-Teller (BET), Scanning Electron Microscopy with Energy Dispersive X-ray spectroscopy (SEM-EDX), X-ray Diffraction (XRD) and Fourier Transform Infrared (FTIR) to determine the physical and chemical properties of sludge before the subsequent treatment stage.

4.1.1 TGA

The thermal stability and decomposition behaviour of coal mining sludge are illustrated in Figure 4.1. It was observed that the weight loss at the temperature range of 30 ℃ to 130 ℃ was contributed by the evaporation of water molecules and the loss of light or easily volatile components. The former was due to the breakage of weak hydrogen bonds while the latter was attributed to their low boiling point (Rodrigues, et al., 2023; S.P. & Swaminathan, 2022; Jerez, et al., 2021).

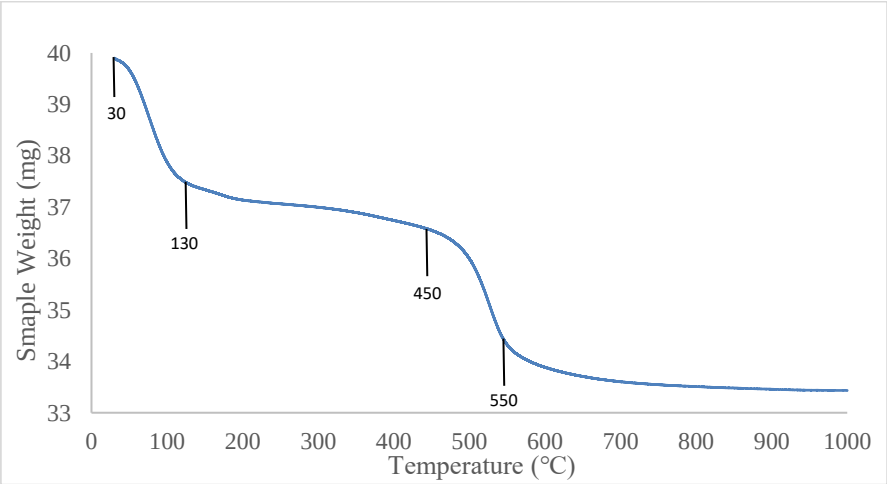

Figure 4.1: TGA Curve of Raw Coal Mining Sludge.

Following this, the sample experienced weight loss due to the decomposition of thermally labile components and complex hydrocarbon at the temperature

range of 130 ℃ to 450 ℃ (Rodrigues, et al., 2023; Silva, et al., 2012). Also, it was remarkable that there was a rapid decreasing trend between 450 ℃ to 550 ℃ due to the volatilisation of amorphous carbonaceous residues. At the same time, it was noted that the breakdown event of inorganic materials such as kaolin and heavy metals would begin. By observing the trend from 550 ℃ onward, it was relatively becoming constant, showing the slow decomposition rate of inorganic compounds due to their strong chemical bonds (Rodrigues, et al., 2023). To mention, it could be said that the thermal stability of coal mining sludge only achieved after 700 ℃. In general, the TGA curve of coal mining sludge displayed a similar pattern with the previous studies as demonstrated in Table 4.1.

Table 4.1: Thermal and Decomposition Behaviour of Raw Coal Mining Sludge.

Behaviour	**Temperature Range (℃)**	**References**
Evaporation of water molecules The loss of light or easily volatile components	30 ℃ - 130 ℃	(Rodrigues, et al., 2023; S.P. & Swaminathan, 2022; Jerez, et al., 2021).
Decomposition of thermally labile components and complex hydrocarbon	130 ℃ - 450 ℃	(Rodrigues, et al., 2023; Silva, et al., 2012)
Volatilisation of amorphous carbonaceous residues Decomposition of inorganic compounds	450 ℃ - 550 ℃	(Rodrigues, et al., 2023)
Decomposition of inorganic compounds	> 550 ℃	

4.1.2 Surface Analysis

The surface area, pore size, and pore volume of coal mining sludge could be known with the aid of adsorption-desorption isotherm as illustrated in Figure 4.2.

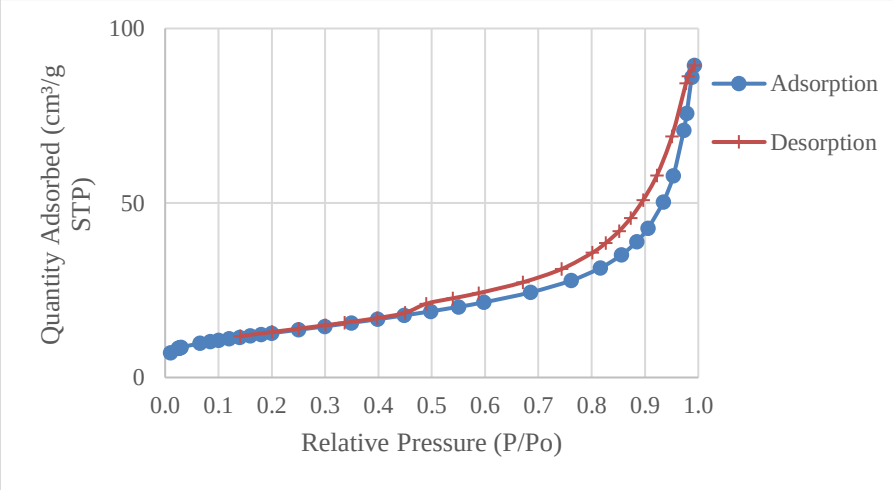

Figure 4.2: BET Isotherm Linear Plot.

According to the International Union of Pure and Applied Chemistry (IUPAC), the plot is represented as a Type II isotherm which is similar to the findings from Munyengabe, et al. (2020). Nevertheless, the results also displayed with hysteresis loop that was different from the researchers. To further elaborate, it was a Type II isotherm with the H3 Hysteresis model. In this instance, the hysteresis hinted at the presence of porosity in terms of mesopores and macropores. As well, such loops are possible when the pore network is composed of macropores that are not filled with pore condensate, or in the case of non-rigid aggregates of plate-like particles (such as certain clays). Moreover, it was evident that there was an abrupt closure of the desorption isotherm to the adsorption due to the cavitation or bubble formation phenomena during the desorption phase, leading to the insignificant desorption isotherm for describing the porous characteristics. The statement was also supported by the BJH (Barrett-Joyner-Halenda) pore size distribution where the plot was dominated by the sharp peak centered at around 3.8 nm that was caused by the loop closure rather than the real porosity within the sample (Thommes, et al., 2015; MCA Services, 2022). In short, it was determined that

the BET surface area of coal mining sludge was 44.97 m^2/g and its pore volume and pore size were 0.09 cm^3/g and 12.42 nm respectively. The findings of the study, presented in Table 4.2, might be considered to be fairly comparable.

Table 4.2: Comparison of BET Results.

Material	Surface Area (m^2/g)	Pore Volume (cm^3/g)	Pore Size (nm)	References
Acid Mine Drainage Sludge	22.60 ± 0.20	0.06	10.71	(Amanda & Moersidik, 2019)
Coal Mining Sludge	44.97	0.09	12.42	This study

4.1.3 SEM-EDX

The surface morphology of coal mining sludge was depicted in Figure 4.3 at three different resolutions. Overall, the images showed that the samples had a slightly porous irregular structure, with an uneven flake-like appearance at the outside borders, which is consistent with the pattern reported in the literature review (Amanda & Moersidik, 2019).

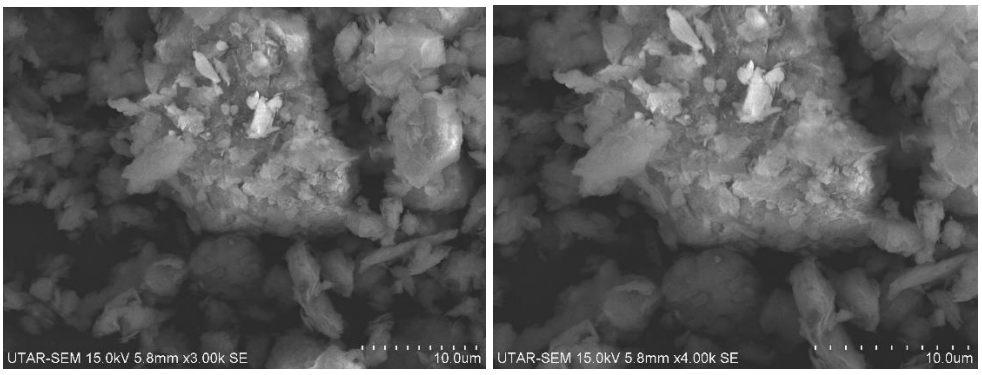

(a) (b)

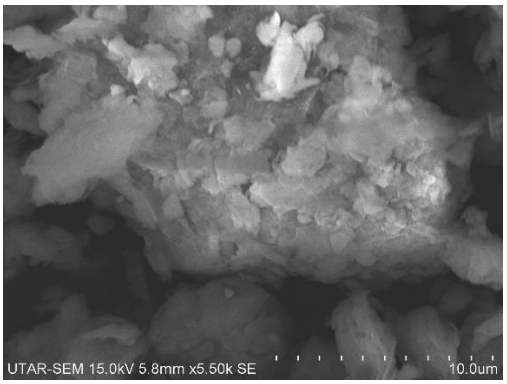

(c)

Figure 4.3: SEM images of Raw Coal Mining Sludge at (a) 3000 x resolution, (b) 4000 x resolution and (c) 5500 x resolution.

As studied by Amanda & Moersidik (2019), while the flaky structure was attributed to silica oxide, it had been speculated that the porous part was made up of iron oxide particles. Also, it could be observed that the surface of coal mining sludge was rougher, indicating low organic content.

According to Table 4.3, the chemical composition of coal mining sludge was analysed by EDX. In line with the outcomes of the literature review, the primary elements of the coal mining sludge were oxygen, silicon, and aluminium. Given the presence of oxygen, the sludge was likely composed of oxidised components notably silica dioxide and iron oxide. Regarding silicon and aluminium, the former was related to the mining site's soil and sediment, while the latter was brought on by the usage of aluminium sulphate during the coagulation treatment phase or just occurred in nature. Minor elements such as magnesium, lead, tin, iron, and cesium were thought to have started as naturally occurring substances found in coal seams and certain geographical areas (Zhao, et al., 2017; Amanda & Moersidik, 2019).

Table 4.3: Chemical Composition of Raw Coal Mining Sludge.

Element	**Wt.%**
O	32.27
Mg	1.28
Al	21.90
Si	34.80

Table 4.3 (Continued)

Element	Wt.%
Pb	1.76
Sn	2.10
Cs	1.42
Fe	4.45

4.1.4 XRD

Figure 4.4 revealed the major minerals and their respective crystallographic orientation and crystal symmetry present in the coal mining sludge.

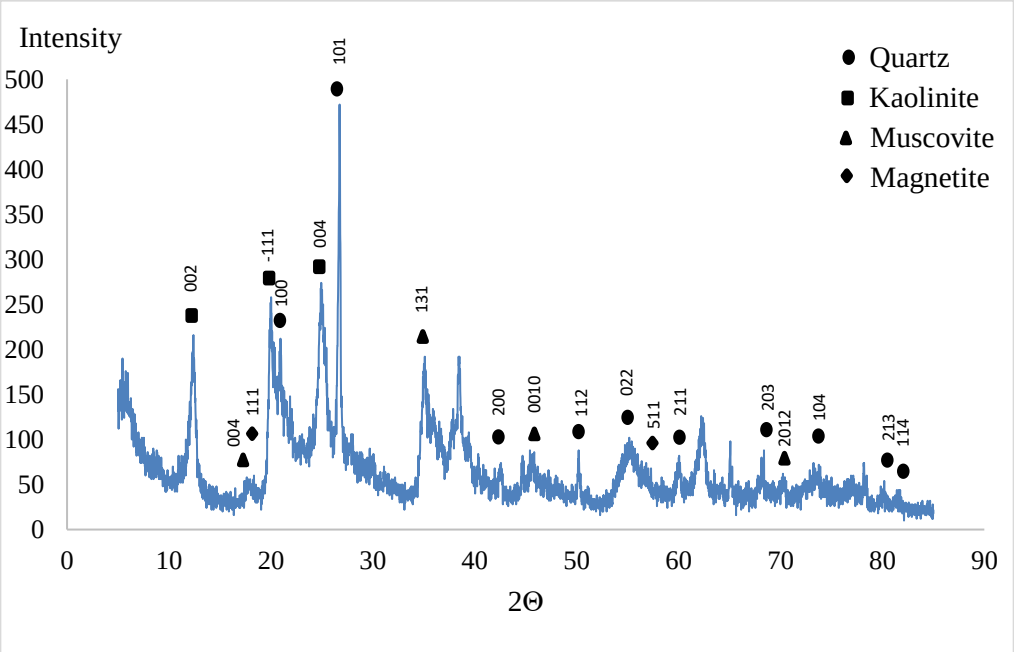

Figure 4.4: XRD Pattern of Raw Coal Mining Sludge.

The findings were compatible with the studies done by Amanda & Moersidik (2019) as they also managed to analyse similar results in AMD sludge. As well, the results further prove the validity of the existence of those major heavy metals (Si, Al, and Fe). The diffraction pattern was compared with the database named American Mineralogist Crystal Structure Database (AMCSD) based on the respective minerals' code listed in Table 4.4 and the summary of their characteristic peaks at 2Θ would be presented in Table 4.5.

Table 4.4: Mineral Identified in The Raw Coal Mining Sludge by AMCSD Code.

Minerals	AMCSD Code
Quartz	0006212
Kaolinite	0017947
Muscovite	0000854
Magnetite	0000945

Since the coal mining process would disturb the natural geological layers, weathering the rocks, clay and sand, it contributed to the existence of quartz, kaolinite, muscovite, and magnetite in the coal mining sludge.

Table 4.5: Characteristic Peaks of Each Mineral in Raw Coal Mining Sludge.

Minerals	Peak Value
Quartz (SiO_2)	20.84º (100), 26.63º (101), 42.41º (200), 50.12º (112), 59.91º (211), 54.85º (022), 68.14º (203), 73.50º (104), 79.85º (213), 81.19º (114)
Kaolinite ($Al_2Si_2O_5(OH)_4$)	12.37º (002), 20.16º (-111), 24.90º (004)
Muscovite ($KAl_2(Si_3Al)O_{10}(OH)_2$)	17.74º (004), 35.02º (131), 45.34º (0010), 70.19º (2012)
Magnetite (Fe_3O_4)	18.30º (111), 57.00º (511)

4.1.5 FTIR

To further confirm the chemical composition of coal mining sludge, a spectrum generated by FTIR analysis was shown in Figure 4.5. Initially, Ballou, et al. (2022) stated that the absorption peaks at 3692 cm^{-1} and 3620 cm^{-1} indicated the vibrational stretching mode of O-H bond of the surface and internal hydroxyl cluster in silicates respectively, which also agreed by Ren, et al. (2020). Following this, Ballou, et al. (2022) described the angular deformation of H-O-H group of water molecules at wavelength 1636 cm^{-1}.

Also, the researchers mentioned another O-H deformation of internal hydroxyls associated with Al was justified at 908 cm^{-1}. The absorption bands at 992 cm^{-1} and 796 cm^{-1} referred to the stretching vibration of Si-O in kaolinite and quartz respectively which is different from the previous studies that have different sludge compositions (Ballou, et al., 2022).

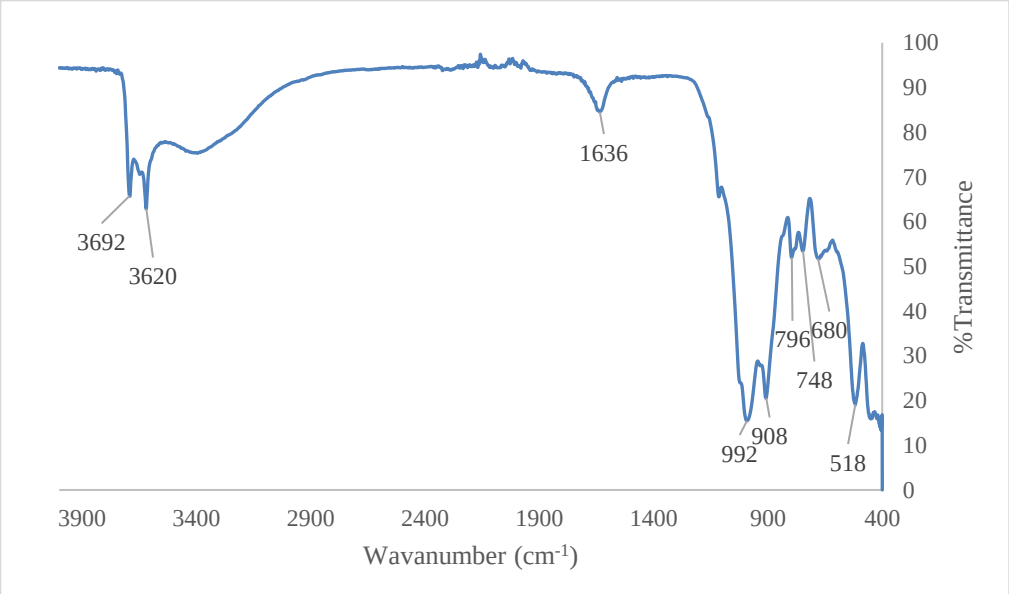

Figure 4.5: FTIR Spectra of Raw Coal Mining Sludge.

In terms of Si-O-Al bending vibration mode in kaolinite and muscovite, it was represented by the absorption band at 518 cm^{-1}. Apart from that, the absorption bands at 748 cm^{-1} and 680 cm^{-1} revealed two possible results each. As claimed by Ballou, et al. (2022), the former interfered with the existence of Al-OH stretching vibration in kaolinite and Al-O-Al stretching, Si-O-Al vibration in muscovite. The latter interpreted the bending vibration of Si-O in quartz and the stretching vibration of Si-O-Al in kaolinite. A summary of the aforementioned analysis was tabulated in Table 4.6 for a better view.

Table 4.6: Functional Groups Present in the Raw Coal Mining Sludge.

Bonds	**Wavelength (cm^{-1})**	**References**
O-H in silicates	3692 3620	(Ballou, et al., 2022; Ren, et al., 2020)
O-H in water	1636	(Ballou, et al., 2022)
Al-O-H	908	
Si-O in kaolinite	992	
Si-O in quartz	796	
Si-O-Al in kaolinite	518	
Si-O-Al in muscovite		
Al-O-Al and Si-O-Al in muscovite	748	
Al-OH in kaolinite		
Si-O in quartz	680	
Si-O-Al in kaolinite		

4.2 Sludge Treatment

As revealed through the characterisation phase, the coal mining sludge featured a high aluminium level, and the mineral composition rendered it more appropriate for the suggested treatment methodology. In theory, the sulfation roasting (Stage 1) would aid in the conversion of the major minerals into metal sulphate, which would subsequently dissolve in the water during the leaching process (Stage 2). Thus, the technique's effectiveness will be explored in the following section, which also goes into great depth on the effects of various parameters during the experiment.

4.2.1 Sulfation Roasting Parameter Study

4.2.1.1 Effect of Roasting Temperature

As seen in Figure 4.6, the roasting temperature enhanced the extraction efficiency of aluminium to a certain extent, which was consistent with research conducted by Ballou, et al. (2022) and Shekhar, et al. (2021) who studied the extraction of heavy metals from sludge.

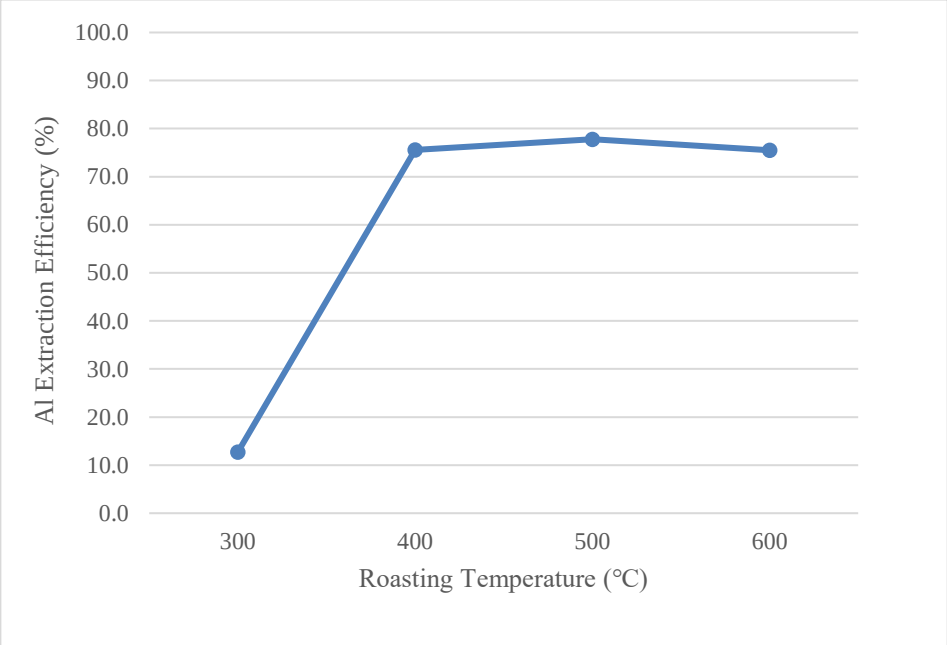

Figure 4.6: Effect of Roasting Temperature on Aluminium Extraction Efficiency at 1:1.5 Sludge to Ammonium Sulphate Mass Ratio, 90 minutes Roasting Time, 80 °C Leaching Temperature, 1:10 Solid-Liquid Ratio, 60 minutes Leaching Time.

As claimed by Ballou, et al. (2022), the ammonium sulphate (reacting agent) was decomposed at 300 °C, forming the ammonium bisulfate, NH_4HSO_4. At the same time, the ammonium bisulfate would react with the kaolinite to produce water-soluble ammonium metal sulfates including ammonium aluminium sulfate, $(NH_4)_3Al(SO_4)_3$. Following this, the ammonium aluminium sulfate would react again with the unreacted kaolinite and muscovite, generating ammonium alum, $NH_4Al(SO_4)_2$, and potassium alum, $KAl(SO_4)_2$ simultaneously. Then, the reaction continued to occur when the temperature rose to 400 °C, indicating more ammonium alum and potassium alum formed. It was worth noting that at 500 °C, the ammonium alum started to decompose

into the target compound namely, aluminium sulphate, $Al_2(SO_4)_3$. In contrast, the ammonium alum tends to decompose into aluminium oxide, Al_2O_3 which was insoluble in water at 600 ℃. For a better view, the aforementioned reaction mechanism was presented as follows:

300 ℃	→	$(NH_4)_2SO_4 \rightarrow NH_4HSO_4$
-		$NH_4HSO_4 + \text{Kaolinite} \rightarrow (NH_4)_3Al(SO_4)_3$
500 ℃		$(NH_4)_3Al(SO_4)_3 + \text{Kaolinite} \rightarrow NH_4Al(SO_4)_2$
		$(NH_4)_3Al(SO_4)_3 + \text{Muscovite} \rightarrow KAl(SO_4)_2$
500 ℃	→	$NH_4Al(SO_4)_2 \rightarrow Al_2(SO_4)_3$
600 ℃	→	$NH_4Al(SO_4)_2 \rightarrow Al_2O_3$

Given the previously described reaction mechanism, 300 ℃, which had an aluminium extraction efficiency of 12.7 %, could be interpreted as having low performance because it was merely the reaction's initiation temperature and produced just a little water-soluble product. As the temperature grew, it was evident that more desired products were formed, achieving 75.6 % efficiency at 400 ℃ and continuing to rise to 77.8 % at 500 ℃ due to the formation of the target product. Eventually, the efficiency declined to 75.5 % when the temperature climbed to 600 ℃, which promoted the decomposition of ammonium alum to insoluble product. Thus, it was concluded that 500 ℃ was selected as the optimum roasting temperature for the subsequent parameter studies.

4.2.1.2 Effect of Mass Ratio of Sludge to Ammonium Sulphate

Corresponding to the outcomes obtained by the researchers, Figure 4.7 demonstrates that the mass ratio of sludge to ammonium sulphate had a major impact on the extraction efficiency of aluminium (Ballou, et al., 2022). When the mass ratio increased from 1:1 to 1:1.5, the statistic surged substantially from 51.9 % to 77.8 %, and at 1:2, it reached 91.6 %. Clearly, adding more ammonium sulphate to the coal mining sludge would increase the area covered for the reaction to trigger more interaction to form more aluminium sulphate that is soluble in water and thus attains high extraction efficiency of aluminium. To note, a ratio of more than 1:2 would tend to cause unfavourable

events during the roasting process as more ammonium sulphate could enhance the formation of lead sulphate. However, the lead sulphate was known as insoluble salt and could coat or encapsulate the water-soluble substances, impeding their dissolution in the leaching process afterward. The findings obtained by Chen, et al., (2021) proved that a high amount of reagent would bring undesired reaction, affirming the aforementioned statement. As such, a 1:2 mass ratio would be ideal for succeeding parameter studies.

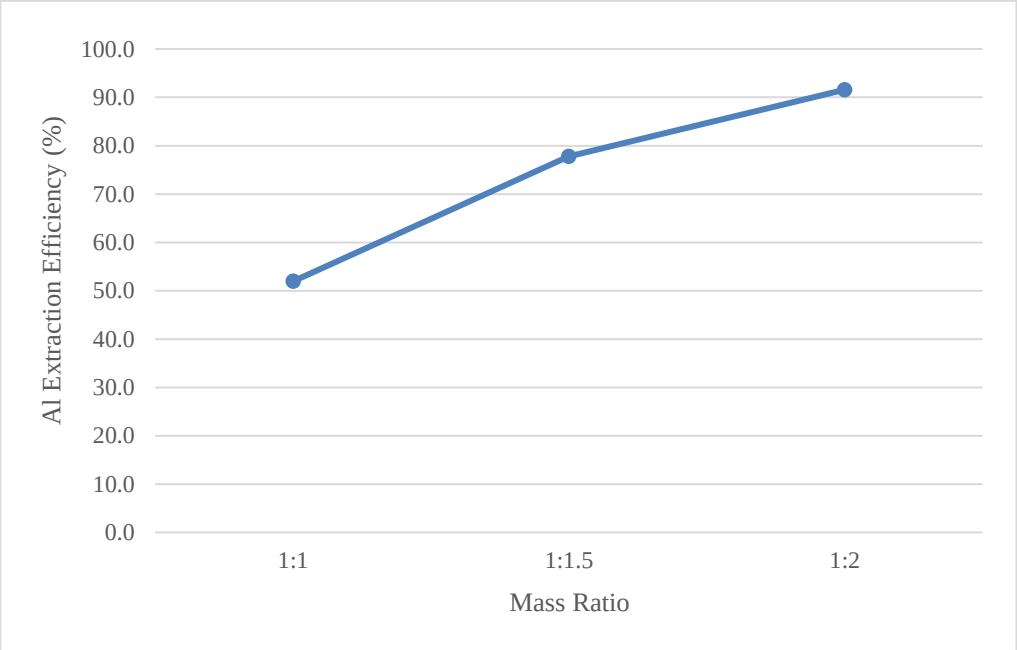

Figure 4.7: Effect of Mass Ratio of Sludge to Ammonium Sulphate on Aluminium Extraction Efficiency at 500 ℃ Roasting Temperature, 90 minutes Roasting Time, 80 ℃ Leaching Temperature, 1:10 Solid-Liquid Ratio, 60 minutes Leaching Time.

4.2.1.3 Effect of Roasting Time

Figure 4.8's trend of extraction efficiency suggested that an increase in roasting time would increase aluminium extraction efficiency since it would create more contact time for reaction. Yet, the effect of roasting time was small. Ballou, et al. (2022) who did similar study provide more explanation for this behaviour, stating that while kaolinite and muscovite might convert into ammonium alum and potassium alum in 30 and 60 minutes, respectively, it took 90 minutes for the compound to fully transform into aluminium sulphate.

As a result, the efficiency grew from 87.8 % at 30 minutes to 88.5 % for 60 minutes and finally achieved 91.6 % at 90 minutes. Such small changes were contributed by the reaction products generated and coated on the surface of minerals, hindering the gas diffusion like ammonia and water during the leaching phase (Li, et al., 2017). Nonetheless, in the consequent experiment, the roasting time was kept constant at 90 minutes.

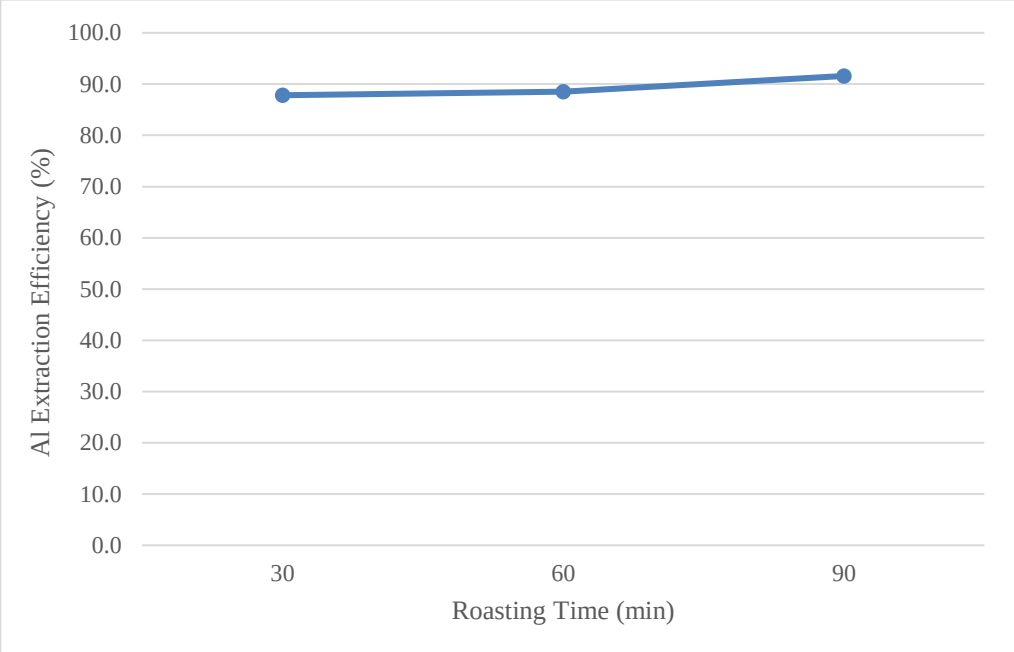

Figure 4.8: Effect of Roasting Time on Aluminium Extraction Efficiency at 500 ℃ Roasting Temperature, 1:2 Sludge to Ammonium Sulphate Mass Ratio, 80 ℃ Leaching Temperature, 1:10 Solid-Liquid Ratio, 60 minutes Leaching Time.

4.2.2 Water Leaching Parameter Study

4.2.2.1 Effect of Leaching Temperature

The solute's solubility in a solvent and its diffusion from the material to the surface and thereafter to the bulk of the solution have a major impact on the leaching process' effectiveness. In this case, the operating temperature can easily have an impact on both of them (Anantharaman & Begum, 2011). The solubility of ionic solids, notably aluminium sulphate, should theoretically increase with temperature as the particles gain more kinetic energy to move

faster and vibrate. This breaks the intermolecular forces between the molecules in the sludge and allows for more interaction with the solvent molecules, thereby resulting in more dissolving in the water (Fu, et al., 2023). The results by Lv et al. (2022) also showed that the temperature had a direct correlation with the diffusion rate, whereby a higher temperature could cause the target solute to transfer into the solvent more quickly, extracting more solute than at a lower temperature during the same duration of time.

As the leaching temperature went up, Figure 4.9 plainly shows that the efficiency of extracting aluminium increased. Additionally, the statistics highlighted that the efficiency only reached 76.7 % and 77.4 % at 35 °C and 50 °C, respectively, signaling a relatively low value in comparison to 65 °C (89.8 %) and 80 °C (91.6 %). Stated differently, it was possible to further improve the solubility and diffusion rate of ionic solids at higher temperatures, particularly at 80 °C, which has an efficiency of 91.6 % and would be useful for forthcoming parameter studies.

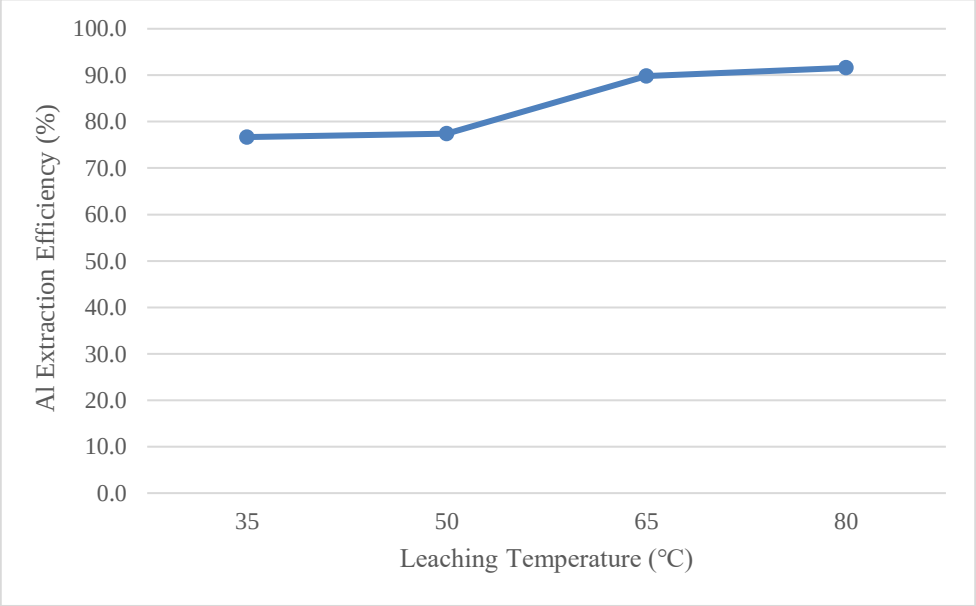

Figure 4.9: Effect of Leaching Temperature on Aluminium Extraction Efficiency at 500 °C Roasting Temperature, 1:2 Sludge to Ammonium Sulphate Mass Ratio, 90 minutes Roasting Time, 1:10 Solid-Liquid Ratio, 60 minutes Leaching Time.

4.2.2.2 Effect of Solid-Liquid Ratio

The effect of solid-liquid ratio on the extraction efficiency of aluminium is displayed in Figure 4.10.

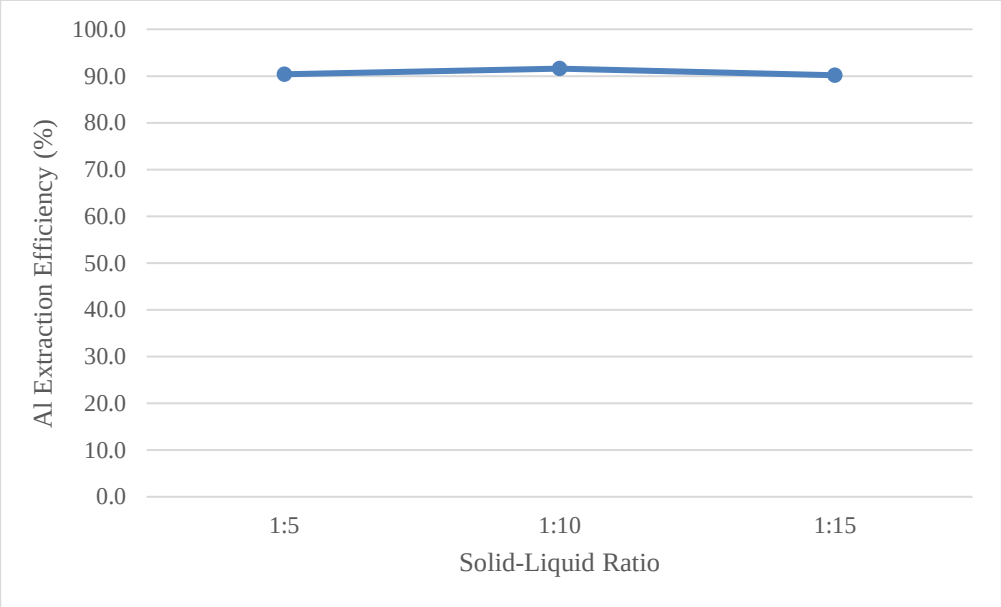

Figure 4.10: Effect of Solid-Liquid Ratio on Aluminium Extraction Efficiency at 500 ℃ Roasting Temperature, 1:2 Sludge to Ammonium Sulphate Mass Ratio, 90 minutes Roasting Time, 80 ℃ Leaching Temperature, 60 minutes Leaching Time.

The pattern and effect of the trend were found to be comparable to that of the research done by Thamilselvi & Balamurugan (2018) on the extraction of alumina from coal fly ash which was nearly constant. Increasing the liquid ratio could decrease the viscosity of the slurry, which is a mixture of sludge and water, as well as improve the concentration difference of aluminium ions on the solid-liquid interface, promoting the mass transfer phenomena during the leaching process (Lv, et al., 2022). Overall, the solid-liquid ratios of 1:15 (90.2 %) and 1:5 (90.4 %) were found to work similarly; hence, the optimum solid-liquid ratio for more experimentation would be 1:10 with a 91.6 % efficiency.

4.2.2.3 Effect of Leaching Time

Figure 4.11 pointed out that leaching time had a positive effect on the extraction efficiency of aluminium. In the period between 30 and 90 minutes, the efficiency grew steadily from 88.9% to 91.6% and, ultimately, to 93.2% because there was sufficient contact time for the mass transfer process. However, at 120 minutes, the extraction efficiency had slightly dropped to 92%. This could be considering the system was already approaching the equilibrium state for the dissolution of aluminium sulphate, and even more time would not improve it—rather, the extraction of other metals would result in a diminishing return (Thamilselvi & Balamurugan, 2018). As agreed by Ahmed, et al., (2016), such decreasing behavior might be attributed to the competition between the aluminium with other elements such as iron, tin, and magnesium. Accordingly, 90 minutes would be a suitable leaching time in this scenario.

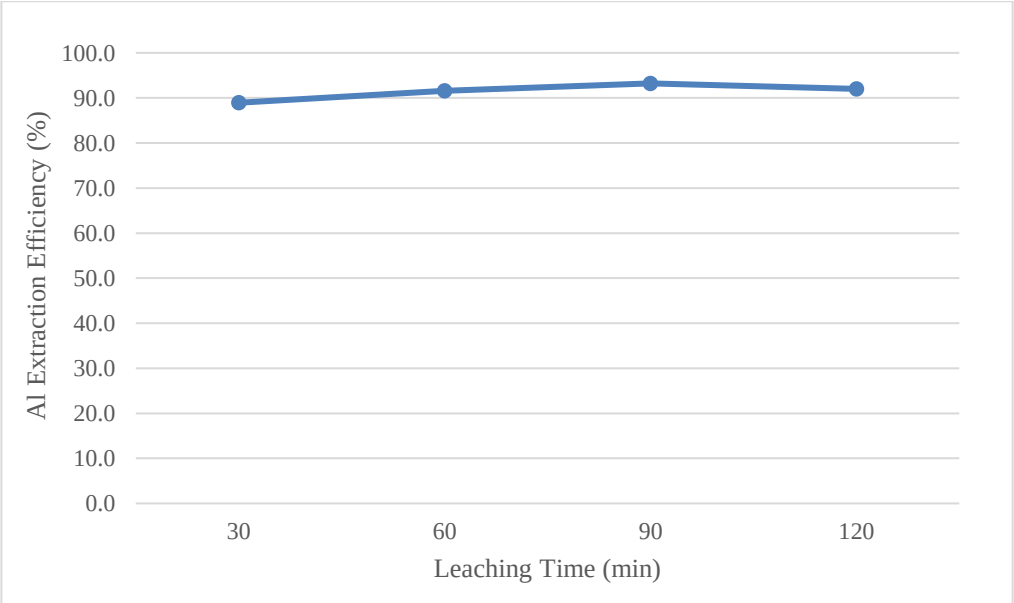

Figure 4.11: Effect of Leaching Time on Aluminium Extraction Efficiency at 500 ℃ Roasting Temperature, 1:2 Sludge to Ammonium Sulphate Mass Ratio, 90 minutes Roasting Time, 80 ℃ Leaching Temperature, 1:10 Solid-Liquid Ratio.

4.2.3 Optimum Condition

Following a series of experiments, it was discovered that the best conditions for extracting aluminium were 500 °C for roasting at a mass ratio of 1:2 sludge to ammonium sulphate for 90 minutes, and 80 °C for hot water leaching at a 1:10 solid-liquid ratio for 90 minutes, yielding a 93.2% efficiency.

Moreover, the extraction efficiency of various elements under the effect of different factors was displayed in Figures 4.12 and 4.13. Six graphs demonstrated how various elements behave differently depending on the situation. In the optimum conditions, the best extraction efficiencies for Mg, Sn, Cs, and Fe were discovered to be 64.0 %, 65.1 %, 16.9 %, and 69.2 %, in that order. As well, no extraction efficiency was observed for Pb and Si because lead sulphate is insoluble in water and silicon was less likely to react during the roasting condition. More specifically, the results of the studies conducted by Ballou et al. (2022) and Meng et al. (2020) supported the removal of Al from the experiment rather than Si. To elucidate, the recovery of Si in this study was approximately 44 %, which raised the possibility that silica content is accessible.

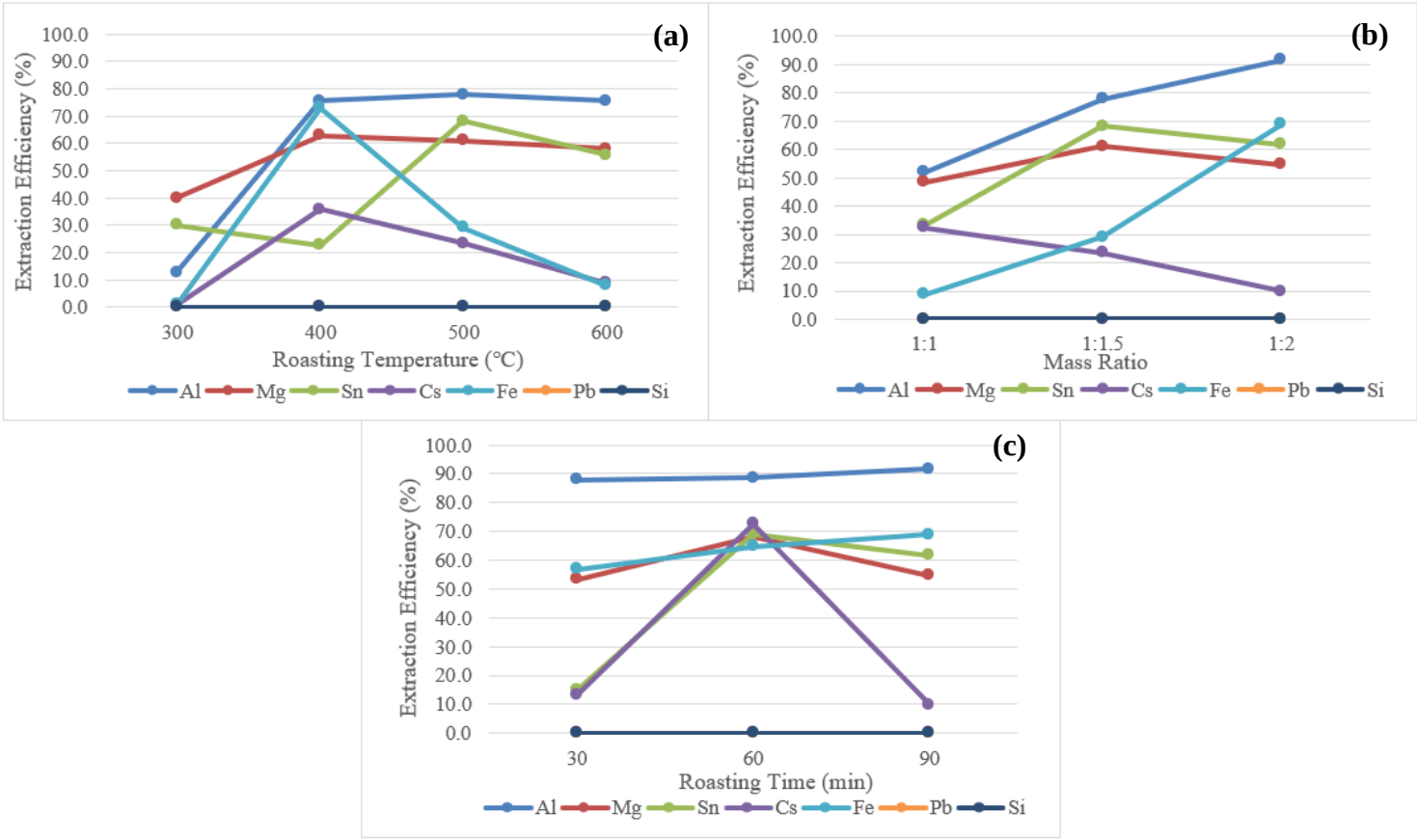

Figure 4.12: Extraction Efficiency of Different Elements in Coal Mining Sludge as a Function of (a) Roasting Temperature, (b) Mass Ratio and (c) Roasting Time.

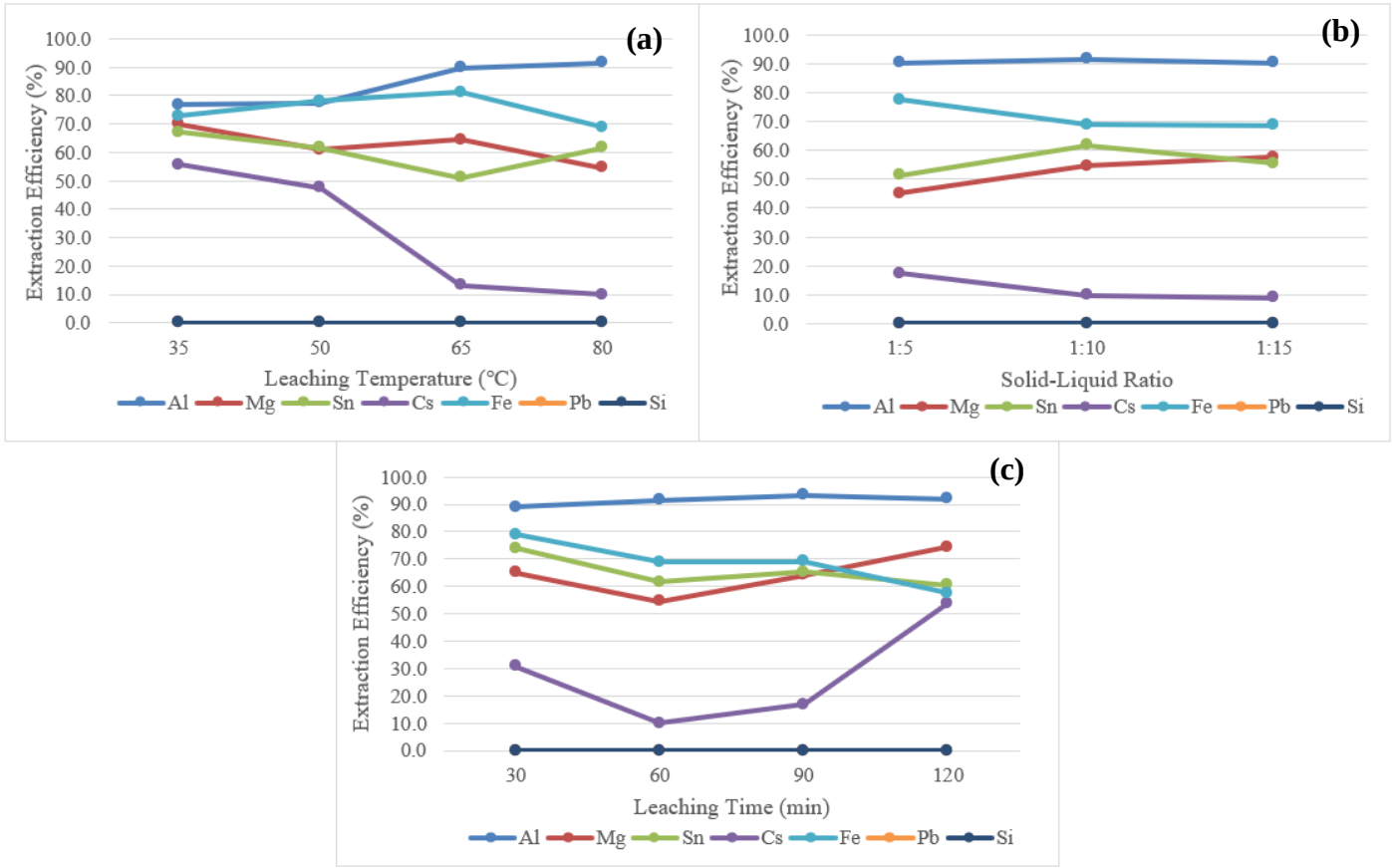

Figure 4.13: Extraction Efficiency of Different Elements in Coal Mining Sludge as a Function of (a) Leaching Temperature, (b) Solid-Liquid Ratio and (c) Leaching Time.

4.3 Treated Sludge Characteristics

After the purification stage, it was anticipated that there would be certain differences in the physical and chemical characteristics of coal mining sludge, which would be covered in the succeeding subsections.

4.3.1 SEM-EDX

The surface morphology of treated coal mining sludge is illustrated in Figure 4.14. Compared to the images captured during pre-characterisation, it was observed that the surface of the sludge became smoother as most of the spiky structures were decomposed into water-soluble products and dissolved in the leaching process. Also, the treated sludge was mainly composed of a flaky structure, implying the presence of silica oxide as discussed in Section 4.2.3 since it could not be removed throughout the treatment process (Amanda & Moersidik, 2019; Ballou, et al., 2022).

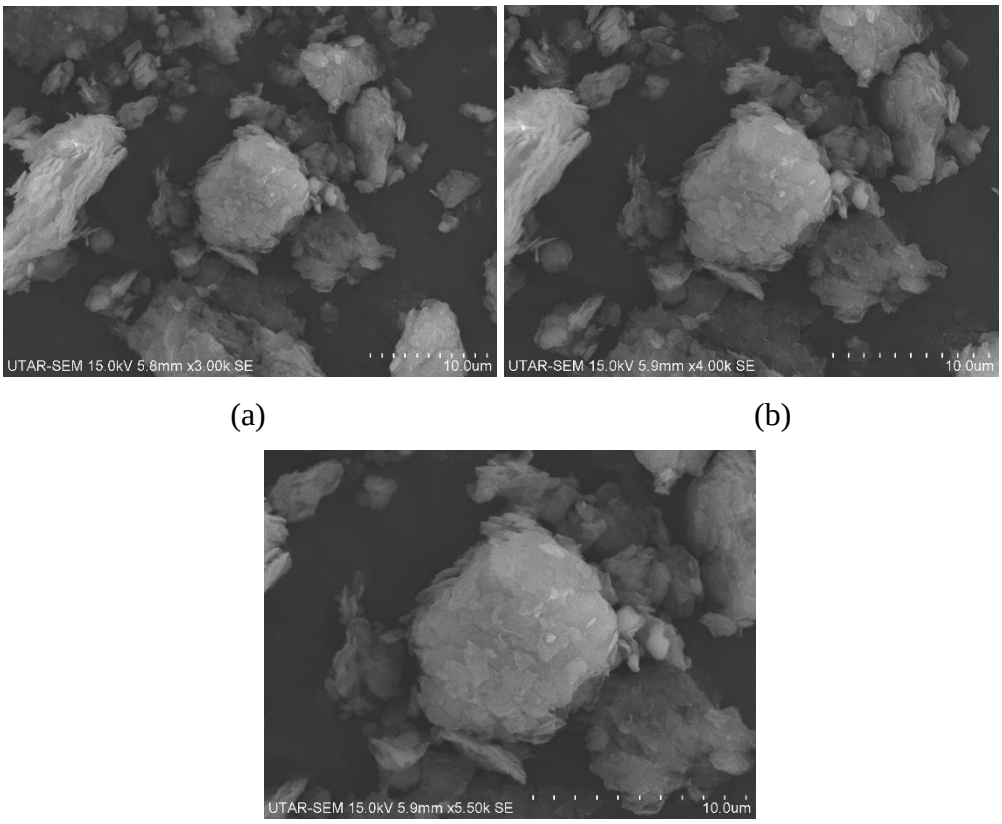

(a) (b)

(c)

Figure 4.14: SEM images of Treated Coal Mining Sludge at (a) 3000 x resolution, (b) 4000 x resolution, and (c) 5500 x resolution.

From the perspective of EDX as tabulated in Table 4.7, it was given that most of the elements left in the coal mining sludge were silicon and oxygen, further verifying the existence of silica dioxide instead of other compounds, especially after the treatment process. In this instance, the weightage of aluminium reduced significantly from 21.90 wt.% to 1.48 wt.%, along with some decreasing trend for minor elements such as iron, magnesium and, tin with the removal percentage of 69 %, 64 % and, 65 % respectively, proving the effectiveness of the treatment method.

Table 4.7: Chemical Composition of Treated Coal Mining Sludge.

Element	**Wt%**
O	42.19
Mg	0.46
Al	1.48
Si	50.23
Pb	2.34
Cs	0.73
Sn	1.18
Fe	1.37

4.3.2 XRD

Compared to the XRD pattern analysed during pre-characterisation, except for quartz and muscovite, it was evident from Figure 4.15 that the other pre-analysed minerals like kaolinite and magnetite had vanished and had been replaced by a new one: steklite. Indeed, the absence of kaolinite and magnetite was attributed to the roasting process performed in the treatment stage where the minerals have decomposed into a water-soluble product such as aluminium sulphate and iron sulphate, thus be removed during the water leaching stage (Ballou, et al., 2022).

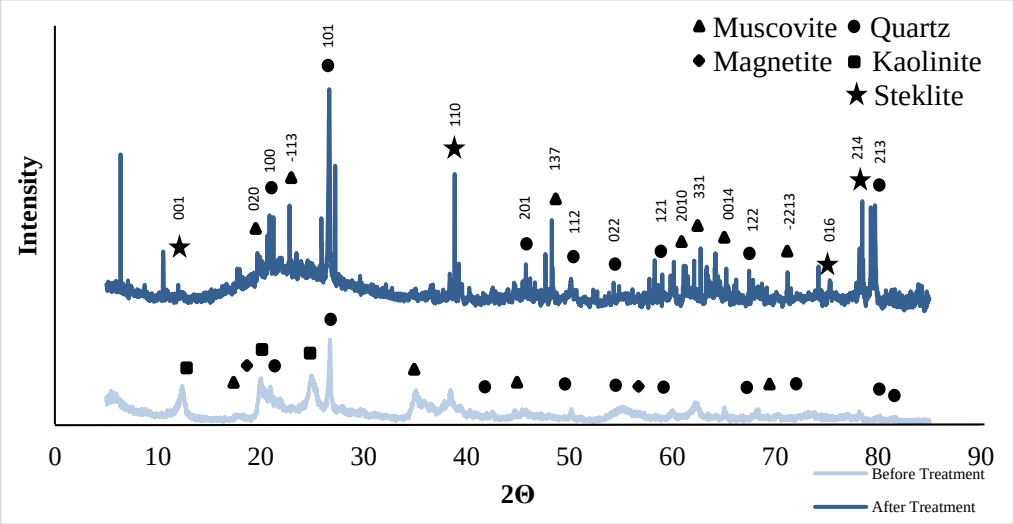

Figure 4.15: Comparison of XRD Pattern of Coal Mining Sludge.

Moreover, as stated in Section 4.2.1.1, where steklite was represented as potassium alum, the formation of the new mineral was induced by sulfation during the roasting phase. Furthermore, since only 93.2% extraction efficiency was attained, it may also be inferred that some of them were not completely dissolved during the water-leaching process and were left in the sludge. Moreover, the 93.2 % value could be attributed to the existence of muscovite due to the incomplete transformation during the roasting phase and thus insoluble in water. On the other hand, since quartz did not react, it remained natural in the sludge, which was in agreement with the experiment's outcomes as reported by Ballou et al. (2022). It was also noted that each mineral's crystal structure was further explored through a database that was summarised in Table 4.8.

Table 4.8: Minerals Identified in The Treated Coal Mining Sludge.

AMCSD	
Minerals	**Code**
Quartz	0006212
Steklite	0018101
Muscovite	0000854
Characteristic Peaks of Each Mineral	

Table 4.8 (Continued)

Minerals	Peak Value
Quartz (SiO_2)	20.84º (100), 26.63º (101), 45.76º (201), 50.12º (112), 54.85º (022), 59.91º (121), 67.70º (122), 79.85º (213)
Steklite ($KAl(SO_4)_2$)	11.12º (001), 38.25º (110), 75.34º (016), 78.53º (214)
Muscovite ($KAl_2(Si_3Al)O_{10}(OH)_2$)	19.67º (020), 22.90º (-113), 48.51º (137), 61.38º (2010), 62.68º (331), 65.31º (0014), 71.21º (-2213)

4.3.3 FTIR

As in the pre-characterisation phase, FTIR analysis was used to confirm the treated coal mining sludge's chemical composition, as can be seen in Figure 4.16.

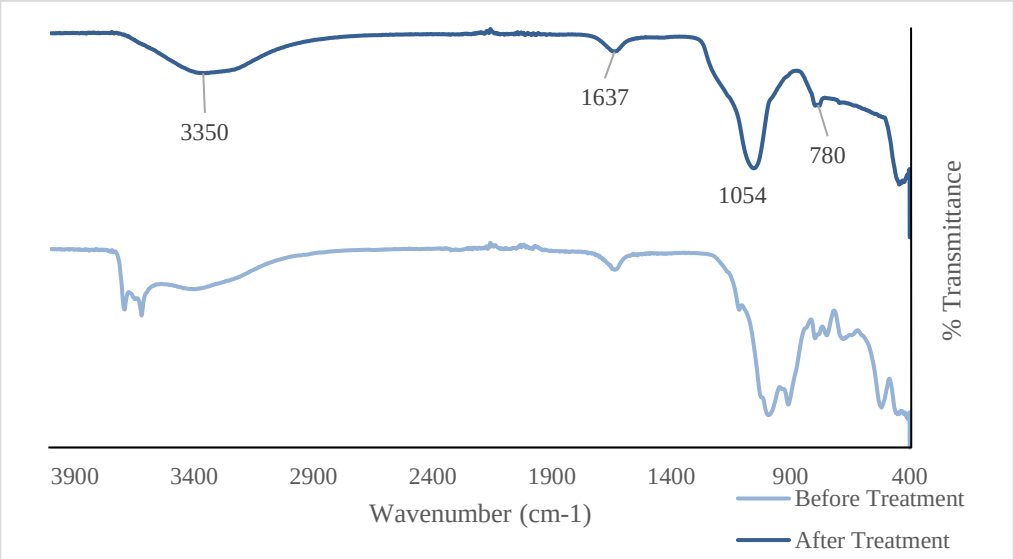

Figure 4.16: Comparison of FTIR Spectrum of Coal Mining Sludge.

Figure 4.16 signified that there was a considerable alternation in the pattern after the purification process as compared to the pre-charaterisation phase, particularly in the 500–1000 cm^{-1} spectrum range. This was again caused by the event that took place during sulfation roasting, which broke the bond between the kaolinite and muscovite molecules and led them to disappear from

the FTIR spectrum. The present functional group in the treated coal mining sludge is thus shown in Table 4.9. The O-H bond in water creates vibrations and angular deformation, which were symbolised by the broad band at 3350 cm^{-1} and the peak at 1637 cm^{-1}, respectively, as indicated by the researchers. As well, the absorption peaks at 1054 cm^{-1} and 780 cm^{-1}, both indicated the Si-O stretching vibration in quartz or muscovite.

Table 4.9: Functional Groups Remaining in the Treated Coal Mining Sludge.

Bonds	**Wavelength (cm^{-1})**	**References**
O-H in water	3350	(Ballou, et al., 2022)
	1637	
Si-O in quartz or muscovite	1054	
	780	

4.4 Comparison of The Aluminium Extraction Efficiency with Other Studies

The experiment demonstrated the effective removal of aluminium from coal mining sludge using sulfation roasting and water leaching. As Table 4.10 summarises, the outcomes of this study highlighted fairly high performance when compared to previous works that utilise similar separation techniques with a different matrix.

Table 4.10: Comparison of Aluminium Extraction Efficiency with Other Works.

Type of Matrices	**Extraction Efficiency (%)**	**References**
Coal Fly Ash	95.0 %	(Doucet, et al., 2016)
	46.6 %	(Merwe, et al., 2017)
Platinum Group Metals Tailings	60.0 %	(Mohamed, et al., 2016)
Coal Gangue	24.2 %	(Qin, et al., 2022)

Table 4.10 (Continued)

Type of Matrices	Extraction Efficiency (%)	References
Drinking Water Treatment Sludge	74.0 %	(Ballou, et al., 2022)
Coal Mining Sludge	93.2 %	This Study

Aside from that, the high aluminium content found in raw coal mining sludge was comparable with that in the bauxite. In this instance, the extraction of aluminium from the bauxite was vastly different from the method employed in this study. To briefly describe, the techniques could be divided into two stages: the Bayer process and the Hall-Héroult process. The former involved crushing, washing and drying phases of bauxite before mixing with sodium hydroxide to produce an alumina-precipitated solution under high temperature and pressure. Following this, the latter would mainly utilise the principle of electrolysis with molten cryolite under huge currents to dissolve and convert the alumina into pure aluminium metal. Thus, in terms of cost-effectiveness, sulfation roasting with water leaching would be preferred due to its less energy consumption and more economical acquisition of materials (Clark, 2015).

CHAPTER 5

CONCLUSIONS AND RECOMMENDATIONS

5.1 Conclusions

In a nutshell, the physical and chemical properties of coal mining sludge were investigated through various analytical methods including Scanning Electron Microscopy with Energy Dispersive X-ray spectroscopy (SEM-EDX), Thermogravimetric Analysis (TGA), Brunauer-Emmett-Teller (BET), Fourier Transform Infrared (FTIR) and X-ray Diffraction (XRD). To note, the coal mining sludge was dried, ground, and sieved before continuing to the characterisation and purification phase. The TGA curve proved the coal mining sludge only achieved thermal stability after 700 ℃. Additionally, BET discovered that the coal mining sludge was classified as a Type II isotherm with the H3 Hysteresis model. It had a surface area of 44.97 m^2/g and was made up of mesopores, which have pore volumes and sizes of 0.09 cm^3/g and 12.42 nm, respectively. From the perspective of sludge's morphology, SEM determined a slightly porous irregular structure, with an uneven flake-like appearance at the outside borders which should be attributed to silica. In terms of chemical composition, EDX, FTIR, and XRD further verified the presence of silicon, oxygen, and aluminium as major elements in the coal mining sludge.

Following this, sulfation roasting with water leaching was suggested as a separation method to extract the aluminium from coal mining sludge while retaining the silica content. Various parameters including roasting temperature, mass ratio of sludge to ammonium sulphate, roasting time, leaching temperature, solid-liquid ratio, and leaching time were studied to identify the best condition of extraction. In this context, it was found that under the optimum condition of 500 ℃ roasting temperature, 1:2 sludge to ammonium sulphate mass ratio, 90-minute roasting period, 80 ℃ leaching temperature, 1:10 solid-liquid ratio, and 90-minute leaching time, the process was able to yield 93.2 % of aluminium extraction efficiency. Concurrently, it came to light that the suggested approach disclosed efficacy in eliminating other metals, including magnesium, tin, and iron, with removal percentages of

64.0 %, 65.1 %, and 69.2 %, respectively. Put differently, it had the potential to recover 44 % of silica content in coal mining sludge, but this has to be further confirmed through characterisation.

In the post-characterisation stage, the treated coal mining sludge was analysed using SEM-EDX, XRD, and FTIR to mainly examine the effectiveness of the proposed method. SEM analysis displayed that the sludge's surface morphology was smoother and its flaky structure was notably more apparent signifying the presence of silica oxide. The EDX results, which demonstrated that silicon and oxygen became the main elements in the sludge, supported the statement. Furthermore, the presence of quartz and its functional groups affirmed that the coal mining sludge's current composition was primarily silica-based. Thus, the coal mining sludge was now likely an active product that may be utilised again for other purposes.

In short, all the objectives in this project were achieved with success. The coal mining sludge from Indonesia was treated effectively and turned into a more valuable product that could be applied for other applications such as glass and ceramic ingredients in the future. As well, the Sustainable Development Goals 9 (Industry, Innovation and Infrastructure), 12 (Responsible Consumption and Production), and 17 (Partnership for the Goals) can be attained through this project.

5.2 Recommendations for future work

Following the project’s objectives and scopes, the experiment was completed with success. Still, few recommendations are made to enhance the pertinent studies in the future for a more thorough result.

a) More data points must be included for each parameter study to improve the extraction efficiency of aluminium extraction.
b) The leachate from the water leaching process must be analysed using an appropriate instrument such as Inductively Coupled Plasma Optical Emission Spectroscopy (ICP-OES) to further confirm the aluminium extraction efficiency.
c) The experiment for each parameter study is suggested to be conducted repetitively to improve the accuracy and reliability of results.

REFERENCES

Ahmed, I., Nayl, A. & Daoud, J., 2016. Leaching and recovery of zinc and copper frombrass slag by sulfuric acid. *Journal of Saudi Chemical Society,* Volume 20, pp. 280-285.

Amanda, N. & Moersidik, S. S., 2019. Characterization of Sludge Generated from Acid Mine Drainage Treatment Plants. *Journal of Physics: Conference Series,* Volume 1351, pp. 1-6.

Anantharaman, N. & Begum, K. M. M. S., 2011. Leaching. In: *Mass Transfer - Theory and Practice.* New Delhi: PHI Learning Private Limited, pp. 355-385.

Bakar, N. F. A., Sidek, M. N. M., Suharman, S. M. & Rahman, N. A., 2022. Characterization and evaluation of dried automotive paint sludge as cement-based composite. *Materials Today: Proceedings*, Volume 63, pp. 301-305.

Ballou, I. et al., 2022. A new approach of aluminum extraction from drinking water treatment A new approach of aluminum extraction from drinking water treatment. *Minerals Engineering* , Volume 189, pp. 1-12.

Berdugo-Clavijo, C. et al., 2019. High temperature utilization of PAM and HPAM by microbial communities enriched from oilfield produced water and activated sludge. *AMB Express,* 9(46), pp. 1-10.

Canziani, R. & Spinosa, L., 2019. Sludge from wastewater treatment plants. In: M. N. Vara, P. J. d. C. Favas, M. Vithanage & S. V. Mohan, eds. *Industrial and Municipal Sludge: Emerging Concerns and Scope for Resource Recovery.* s.l.:Elsevier Science, pp. 3-30.

Chen, G. et al., 2021. Leaching kinetics of manganese from pyrolusite using pyrite as a reductant under microwave heating. *Separation and Purification Technology,* Volume 277, pp. 1-10.

Clark, J., 2015. *ALUMINIUM.* [Online] Available at: https://www.chemguide.co.uk/inorganic/extraction/aluminium.html [Accessed 13 May 2024].

Connelly, A., 2017. *BET surface area.* [Online] Available at: https://andyjconnelly.wordpress.com/2017/03/13/bet-surface-area/ [Accessed 12 July 2023].

Doucet, F. J. et al., 2016. Thermochemical processing of a South African ultrafine coal fly ash using ammonium sulphate as extracting agent for aluminium extraction. *Hydrometallurgy,* Volume 166, pp. 174-184.

Francioso, O. et al., 2010. Chemical characterization of municipal wastewater sludges produced by two-phase anaerobic digestion for biogas production. *Journal of Hazardous Materials,* Volume 175, pp. 740-746.

Fu, S., Lu, J., Walder, I. & Wu, D., 2023. Effect of temperature on the leaching of heavy metals from nickel mine tailings in the arctic area, Norway. *International Journal of Agricultural and Biological Engineering,* 16(2), pp. 152-158.

George, O. S., Dennison, M. S. & Yusuf, A. A., 2023. Characterization and energy recovery from biomass wastes. *Sustainable Energy Technologies and Assessments,* Volume 58, pp. 1-8.

Government of Canada, 2023. *Coal Facts.* [Online] Available at: https://natural-resources.canada.ca/our-natural-resources/minerals-mining/mining-data-statistics-and-analysis/minerals-metals-facts/coal-facts/20071
[Accessed 7 July 2023].

Guangyin, Z. & Youcai, Z., 2017. *Pollution Control and Resource Recovery for Sewage Sludge.* s.l.:Elsevier Science.

Herter, K., 2012. *Chemicals Found in Coal Sludge and Slurry.* [Online] Available at: https://www.sludgesafety.org/chemicals-found-in-coal-sludge-and-slurry/
[Accessed 7 July 2023].

Hua, G., Li, J. & Hou, H., 2015. A combination of solvent extraction and freeze thaw for oil recovery from petroleum refinery wastewater treatment pond sludge. *Journal of Hazardous Materials,* Volume 283, pp. 832-840.

Jerez, S. et al., 2021. Comprehensive characterization of an oily sludge from a petrol refinery: A step forward for its valorization within the circular economy strategy. *Journal of Environmental Management,* Volume 285, pp. 112-124.

Kroiss, H., Rechberger, H. & Egle, L., 2011. Phosphorus in Water Quality and Waste Management. In: S. Kumar, ed. *Integrated Waste Management - Volume II.* s.l.:IntechOpen, p. 484.

Li, J. et al., 2017. The extraction of valuable metals and phase transformation and formation mechanism in roasting-water leaching process of laterite with ammonium sulfate. *Journal of Cleaner Production,* Volume 140, pp. 1148-1155.

Lv, H. et al., 2022. Effective Extraction of the Al Element from Secondary Aluminum Dross Using a Combined Dry Pressing and Alkaline Roasting Process. *Materials (Basel),* 15(16).

MCA Services, 2022. *Gas Adsorption and Desorption Isotherms Explained.* [Online]
Available at: https://www.youtube.com/watch?v=Qc_DYIRrCKY&ab_channel=MCAServices
[Accessed 6 January 2024].

Meng, F. et al., 2020. Selective extraction of scandium from bauxite residue using ammonium sulfate roasting and leaching process. *Minerals Engineering,* Volume 157, pp. 1-9.

Merwe, E. M. v. d. et al., 2017. Ammonium sulphate and/or ammonium bisulphate as extracting agents for the recovery of aluminium from ultrafine coal fly ash. *Hydrometallurgy,* Volume 171, pp. 185-190.

Mohamed, S., Merwe, E. M. v. d., Altermann, W. & Doucet, F. J., 2016. Process development for elemental recovery from PGM tailings by thermochemical treatment: Preliminary major element extraction studies using ammonium sulphate as extracting agent. *Waste Management,* Volume 50, pp. 334-345.

Mothe, S. & Polisetty, V. R., 2020. Review on anaerobic digestion of rice straw for biogas production. *Environmental Science and Pollution Research,* Volume 28, p. 24455–24469.

Munyengabe, A., Zvinowanda, C., Zvimba, J. N. & Ramontja, J., 2020. Characterization and reusability suggestions of the sludge generated from a synthetic acid mine drainage treatment using sodium ferrate (VI). *Heliyon,* Volume 6, pp. 1-6.

Nguyen, M. D. et al., 2023. Phosphorus adsorption and organic release from dried and thermally treated water treatment sludge. *Environmental Research,* Volume 234, pp. 1-8.

Patel, J., 2018. *4-Step Wastewater Sludge Treatment Process.* [Online] Available at: https://www.wateronline.com/doc/step-wastewater-sludge-treatment-process-0001
[Accessed 28 June 2023].

Qin, Q. et al., 2022. An exploratory study on strategic metal recovery of coal gangue and sustainable utilization potential of recovery residue. *Journal of Cleaner Production,* Volume 340, pp. 1-12.

Ren, X. et al., 2020. Study of resource utilization and fire prevention characteristics of a novel gel formulated from coal mine sludge (MS). *Fuel,* Volume 267, pp. 1-10.

Research and Markets, 2019. *Global Mining Water & Wastewater Treatment Market Report 2019-2023: Focus on Growth Opportunities for Sustainable Solutions.* [Online] Available at: https://www.prnewswire.com/news-releases/global-mining-water--wastewater-treatment-market-report-2019-2023-focus-on-growth-opportunities-for-sustainable-solutions-300962194.html
[Accessed 26 June 2023].

Rodrigues, J. L. et al., 2023. Chemical evaluation of pyrolysis oils from domestic and industrial effluent treatment station sludges with perspective to produce value-added products. *Waste Management,* Volume 168, pp. 202-210.

S.P., S. P. & Swaminathan, G., 2022. Thermogravimetric study of textile lime sludge and cement raw meal for co-processing as alternative raw material for cement production using response surface methodology and neural networks. *Environmental Technology & Innovation,* Volume 25, pp. 1-11.

Safeopedia, n.d. *Sludge.* [Online] Available at: https://www.safeopedia.com/definition/2983/sludge
[Accessed 25 June 2023].

Shekhar, S. et al., 2021. Extraction of manganese through baking-leaching technique from high iron containing manganese sludge. *Materials Today: Proceedings,* Volume 46, pp. 1499-1504.

Silva, J. d. O. et al., 2012. Thermal analysis and FTIR studies of sewage sludge produced in treatment plants. The case of sludge in the city of Uberlândia-MG, Brazil. *Thermochimica Acta,* Volume 528, pp. 72-75.

Thamilselvi, J. & Balamurugan, P., 2018. Extraction of Alumina From Coal Fly Ash. *International Research Journal of Engineering and Technology,* 5(4), pp. 2677-2681.

Thommes, M. et al., 2015. Physisorption of gases, with special reference to the evaluation of surface area and pore size distribution (IUPAC Technical Report). *Pure and Applied Chemistry*, 87(9-10), p. 1051–1069.

United States Environmental Protection Agency, 2023. *Coal Mining Effluent Guidelines.* [Online] Available at: https://www.epa.gov/eg/coal-mining-effluent-guidelines [Accessed 7 July 2023].

Veenhuyzen, B. v. et al., 2021. High capacity Pb(II) adsorption characteristics onto raw- and chemically activated waste activated sludge. *Journal of Hazardous Materials,* Volume 416, pp. 1-14.

Wang, B., Liu, X., Zhang, J. & Cheng, F., 2018. Pyrolysis behavior of corncob and coal gangue with modified medical stone and HZSM-5 based additives. *Fuel,* Volume 211, pp. 816-826.

Wang, C.-q.et al., 2022. Lightweight ceramsite made of recycled waste coal gangue & municipal sludge: Particular heavy metals, physical performance and human health. *Journal of Cleaner Production,* Volume 376, pp. 1-16.

Washington. Edu, n.d. *FOURIER TRANSFORM INFRARED SPECTROSCOPY.* [Online] Available at: https://mse.washington.edu/files/research/SOP_FTIR.pdf [Accessed 19 July 2023].

Wołowiec, M. et al., 2019. The properties of sludge formed as a result of coagulation of backwash water from flters removing iron and manganese from groundwater. *SN Applied Sciences ,* 1(639).

Wu, Q., Cui, Y., Li, Q. & Sun, J., 2015. Effective removal of heavy metals from industrial sludge with the aid of a biodegradable chelating ligand GLDA. *Journal of Hazardous Materials,* Volume 283, pp. 748-754.

Yang, Z. et al., 2016. Environmental investigation on co-combustion of sewage sludge and coal gangue: SO2, NOx and trace elements emissions. *Waste Management,* Volume 50, pp. 213-221.

Zhao, C. et al., 2017. Occurrence of rubidium and cesium in Iqe coal, Qinghai-Tibet Plateau: Evidence from sequential chemical extraction experiment. *Energy Exploration & Exploitation*, 35(3), pp. 376-387.

APPENDICES

Appendix A: Raw Coal Mining Sludge Characterisation – BET Analysis

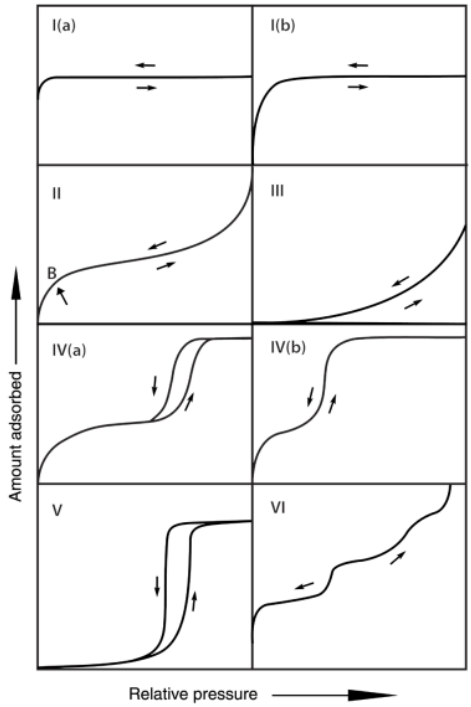

Figure A-1: Classification of Physisorption Isotherms.

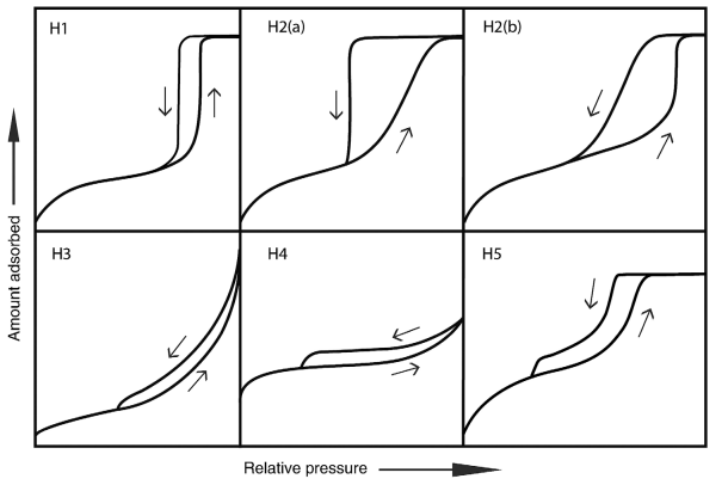

Figure A-2: Classification of Hysteresis Loops.

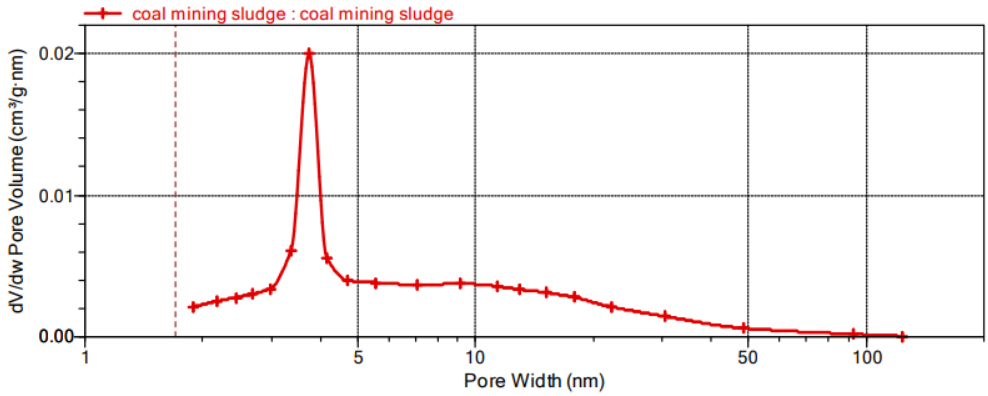

Figure A-3: BJH Desorption dV/dw Pore Volume.

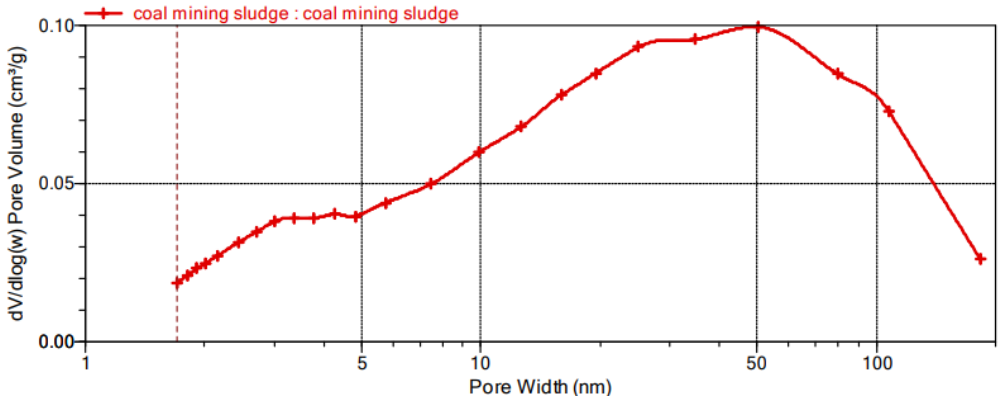

Figure A-4: BJH Adsorption dV/dlog(w) Pore Volume.

BET Surface Area: 44.9686 m²/g

Single point adsorption total pore volume of pores
less than 40.3122 nm width at P/Po = 0.950000000: 0.087283 cm³/g

BJH Adsorption average pore width (4V/A): 12.4219 nm

Figure A-5: BET Report for Surface Area, Pore Volume and Pore Size of Raw Coal Mining Sludge.

Appendix B: Raw Coal Mining Sludge Characterisation – EDX

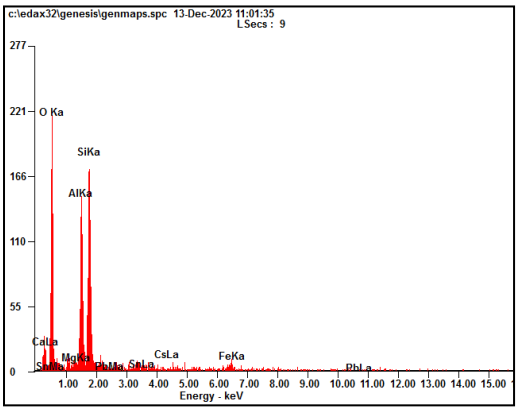

Element	Wt%	At%
OK	34.73	50.93
MgK	01.02	00.99
AlK	20.71	18.01
SiK	32.71	27.32
PbM	03.24	00.37
SnL	01.96	00.39
CsL	01.44	00.25
FeK	04.17	01.75
Matrix	Correction	MThin

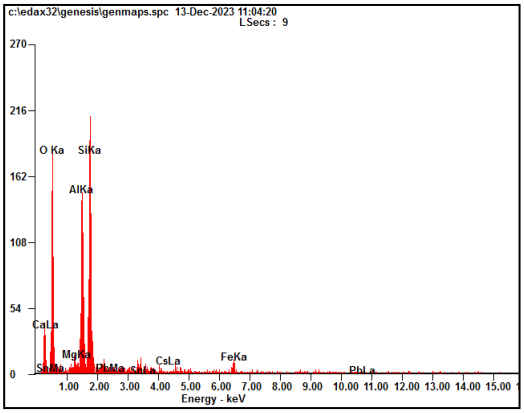

Element	Wt%	At%
OK	30.22	45.23
MgK	01.55	01.52
AlK	22.62	20.08
SiK	35.44	30.21
PbM	02.04	00.24
SnL	02.25	00.45
CsL	01.03	00.19
FeK	04.85	02.08
Matrix	Correction	MThin

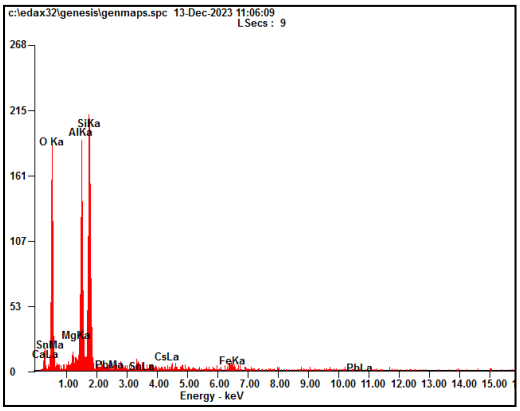

Element	Wt%	At%
OK	31.86	46.61
MgK	01.26	01.21
AlK	22.37	19.41
SiK	36.26	30.22
PbM	00.00	00.00
SnL	02.10	00.42
CsL	01.80	00.32
FeK	04.34	01.82
Matrix	Correction	MThin

Figure B-1: EDX of Raw Coal Mining Sludge from Three Different Locations.

Appendix C: Parameter Studies of Sulfation Roasting Temperature – EDX

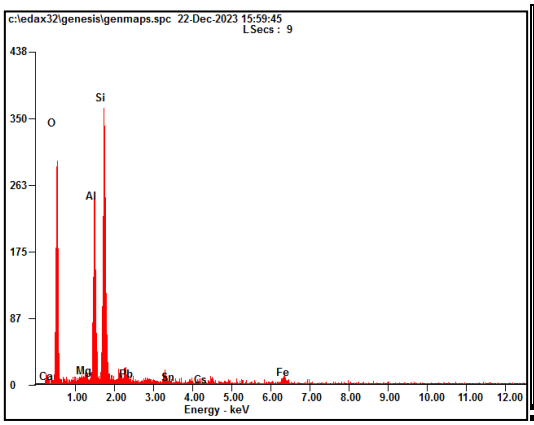

Element	Wt%	At%
OK	31.35	47.10
MgK	00.69	00.69
AlK	19.89	17.72
SiK	37.03	31.69
PbM	06.19	00.72
SnL	00.00	00.00
CsL	00.00	00.00
FeK	04.83	02.08
Matrix	Correction	MThin

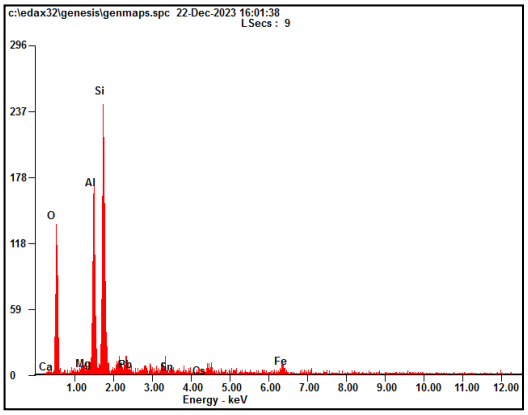

Element	Wt%	At%
OK	18.52	34.62
MgK	00.92	01.13
AlK	19.15	21.23
SiK	34.24	36.47
PbM	15.95	02.30
SnL	03.13	00.79
CsL	02.84	00.64
FeK	05.25	02.81
Matrix	Correction	MThin

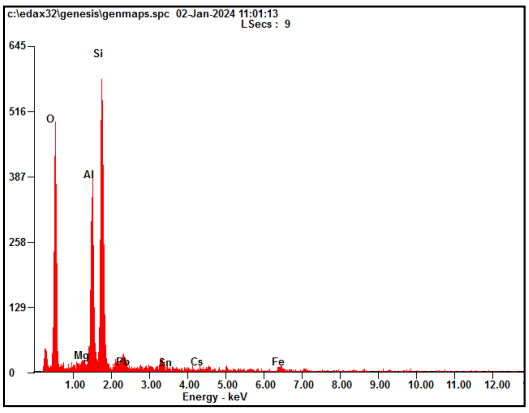

Element	Wt%	At%
OK	28.62	45.72
MgK	00.69	00.73
AlK	18.31	17.35
SiK	36.08	32.84
PbM	10.20	01.26
SnL	01.28	00.28
CsL	01.40	00.27
FeK	03.41	01.56
Matrix	Correction	MThin

Figure C-1: EDX of Water Leaching Residue from Three Different Locations at 300 ℃ Roasting Temperature.

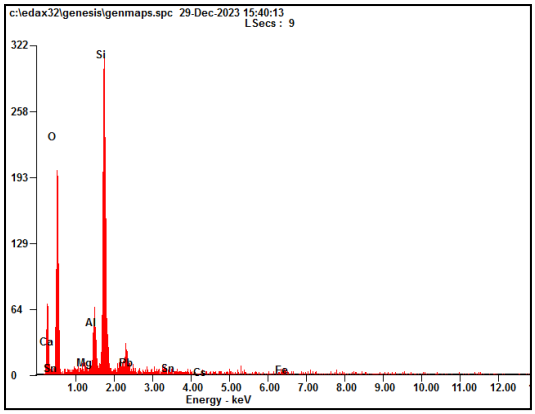

Element	Wt%	At%
OK	26.75	48.04
MgK	00.36	00.42
AlK	05.63	06.00
SiK	40.29	41.21
PbM	23.79	03.30
SnL	01.61	00.39
CsL	00.56	00.12
FeK	01.00	00.52
Matrix	Correction	MThin

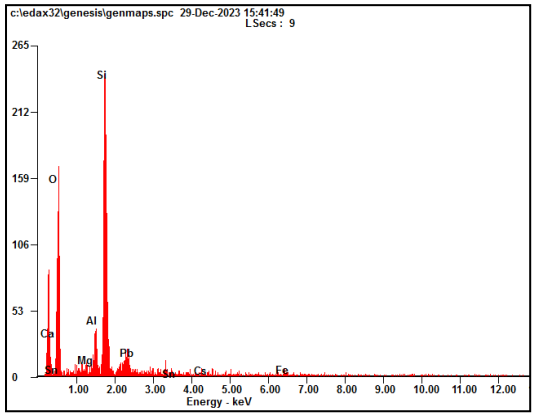

Element	Wt%	At%
OK	25.21	45.50
MgK	00.83	00.99
AlK	04.75	05.08
SiK	42.66	43.86
PbM	21.64	03.01
SnL	02.03	00.49
CsL	01.41	00.31
FeK	01.47	00.76
Matrix	Correction	MThin

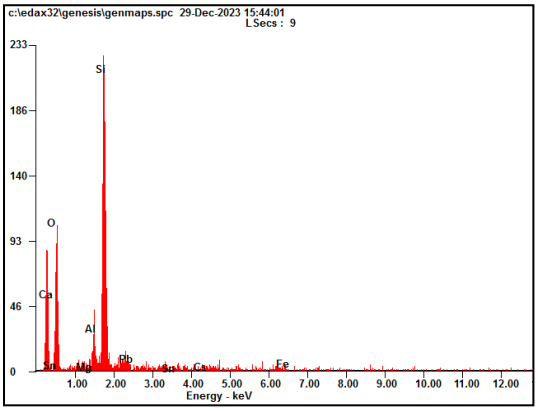

Element	Wt%	At%
OK	23.38	40.25
MgK	00.23	00.26
AlK	05.66	05.78
SiK	51.57	50.57
PbM	16.00	02.13
SnL	01.24	00.29
CsL	00.77	00.16
FeK	01.15	00.57
Matrix	Correction	MThin

Figure C-2: EDX of Water Leaching Residue from Three Different Locations at 400 ℃ Roasting Temperature.

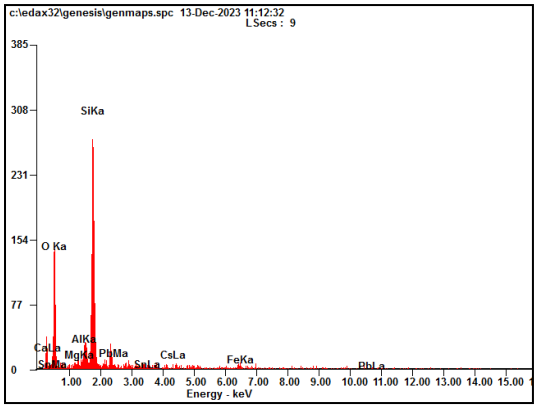

Element	Wt%	At%
OK	23.12	41.58
MgK	01.00	01.18
AlK	04.66	04.97
SiK	46.67	47.83
PbM	20.88	02.90
SnL	00.00	00.00
CsL	01.18	00.26
FeK	02.49	01.28
Matrix	Correction	MThin

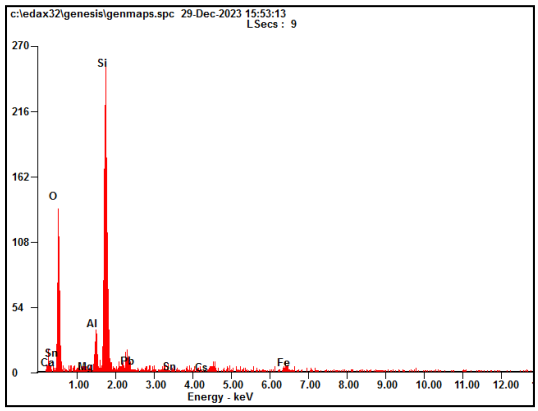

Element	Wt%	At%
OK	24.35	42.41
MgK	00.25	00.28
AlK	05.08	05.25
SiK	47.91	47.54
PbM	17.14	02.31
SnL	00.65	00.15
CsL	00.81	00.17
FeK	03.81	01.90
Matrix	Correction	MThin

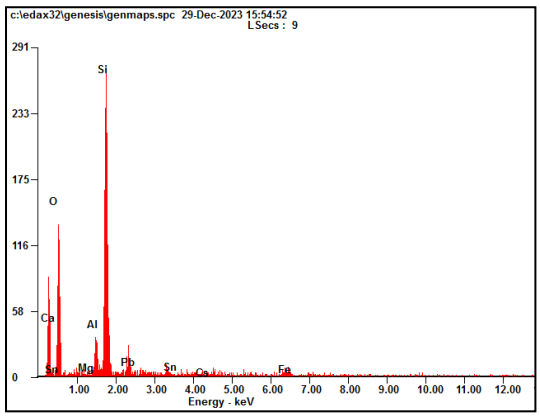

Element	Wt%	At%
OK	22.66	41.65
MgK	00.24	00.29
AlK	04.85	05.29
SiK	45.35	47.49
PbM	21.08	02.99
SnL	01.36	00.34
CsL	01.28	00.28
FeK	03.18	01.67
Matrix	Correction	MThin

Figure C-3: EDX of Water Leaching Residue from Three Different Locations at 500 ℃ Roasting Temperature.

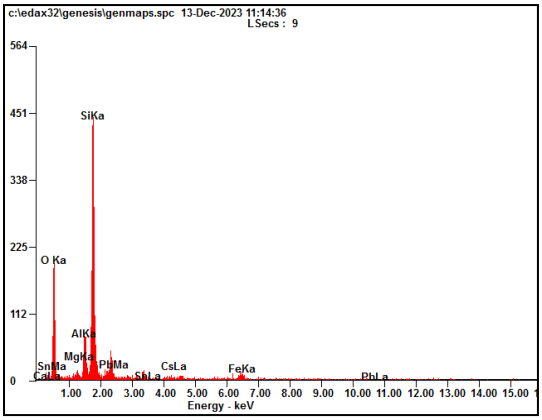

Element	Wt%	At%
OK	20.38	39.65
MgK	00.50	00.64
AlK	05.63	06.49
SiK	41.89	46.42
PbM	26.25	03.94
SnL	00.45	00.12
CsL	00.00	00.00
FeK	04.91	02.74
Matrix	Correction	MThin

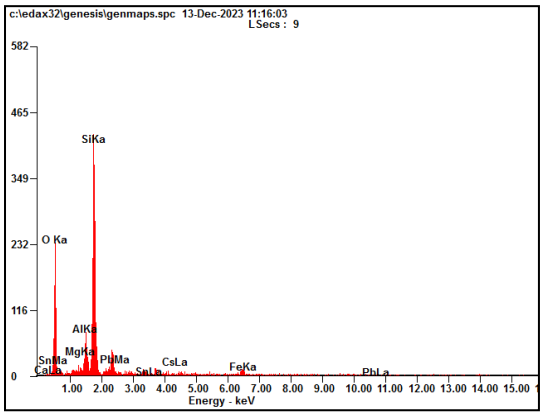

Element	Wt%	At%
OK	20.32	40.21
MgK	00.60	00.78
AlK	05.57	06.54
SiK	40.60	45.77
PbM	26.68	04.08
SnL	01.19	00.32
CsL	01.65	00.39
FeK	03.40	01.93
Matrix	Correction	MThin

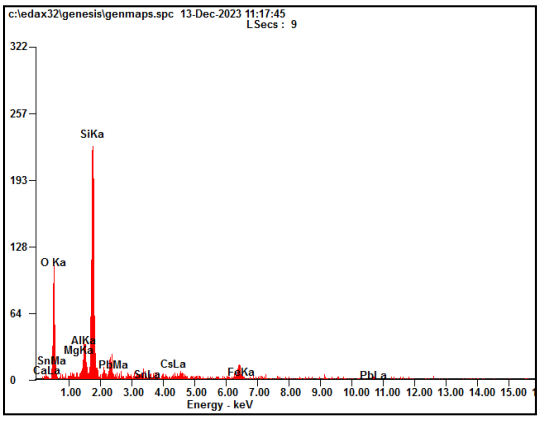

Element	Wt%	At%
OK	16.51	35.13
MgK	00.51	00.72
AlK	04.91	06.20
SiK	40.15	48.66
PbM	28.42	04.67
SnL	01.16	00.33
CsL	02.24	00.57
FeK	06.10	03.72
Matrix	Correction	MThin

Figure C-4: EDX of Water Leaching Residue from Three Different Locations at 600 ℃ Roasting Temperature.

Table C-1: Average EDX Results of Water Leaching Residue at Different Roasting Temperature.

Wt%	Raw	300	400	500	600
OK	32.27	26.16	25.11	23.38	19.07
MgK	1.28	0.77	0.47	0.50	0.54
AlK	21.90	19.12	5.35	4.86	5.37
SiK	34.80	35.78	44.84	46.64	40.88
PbM	1.76	10.78	20.48	19.70	27.12
SnL	2.10	1.47	1.63	0.67	0.93
CsL	1.42	1.41	0.91	1.09	1.30
FeK	4.45	4.50	1.21	3.16	4.80

Table C-2: Extraction Efficiency of Elements at Different Roasting Temperature.

η%	300	400	500	600
O	-	-	-	-
Mg	39.9	62.9	61.1	58.0
Al	12.7	75.6	77.8	75.5
Si	-	-	-	-
Pb	-	-	-	-
Sn	30.1	22.7	68.1	55.6
Cs	0.7	35.8	23.4	8.9
Fe	1.0	72.9	29.0	7.9

SAMPLE CALCULATION

Taking Al wt.% at initial condition (raw) as an example,

$$Average\ Al\ wt.\% = \frac{Location\ 1 + Location\ 2 + Location\ 3}{3}$$

$$Average\ Al\ wt.\% = \frac{20.71 + 22.62 + 22.37}{3}$$

$$Average\ Al\ wt.\% = 21.90$$

Taking Al wt.% at initial condition and 400 ℃ roasting temperature as an example,

$$\eta_{Al} = \frac{w_B - w_A}{w_B} \times 100\ \%$$

$$\eta_{Al} = \frac{w_{raw} - w_{400}}{w_{raw}} \times 100\ \%$$

$$\eta_{Al} = \frac{21.90 - 5.35}{21.90} \times 100\ \%$$

$$\eta_{Al} = 75.6\ \%$$

Appendix D: Parameter Studies of Mass Ratio of Sludge to $(NH_4)_2SO_4$ – EDX

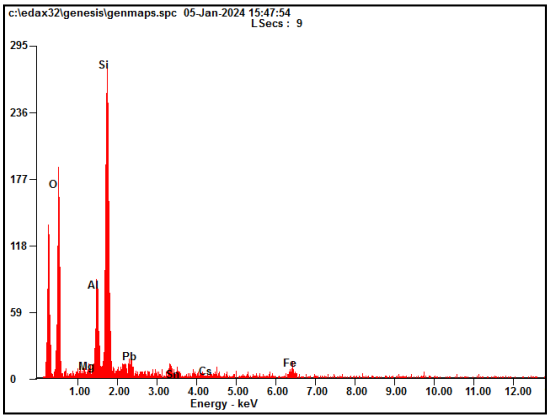

Element	Wt%	At%
OK	26.42	44.34
MgK	00.55	00.61
AlK	10.30	10.25
SiK	42.12	40.26
PbM	13.87	01.80
SnL	01.31	00.30
CsL	00.63	00.13
FeK	04.81	02.31
Matrix	Correction	MThin

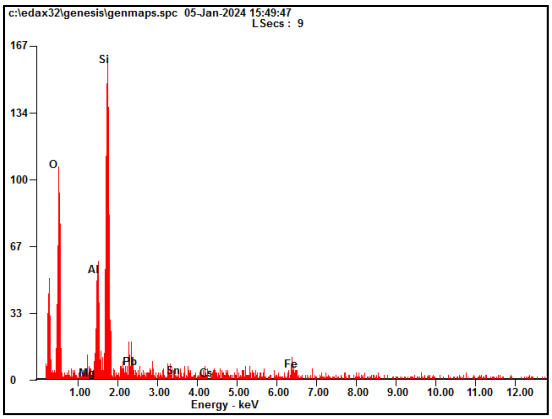

Element	Wt%	At%
OK	23.56	42.81
MgK	01.10	01.32
AlK	10.48	11.30
SiK	37.64	38.96
PbM	20.27	02.84
SnL	01.39	00.34
CsL	01.54	00.34
FeK	04.02	02.09
Matrix	Correction	MThin

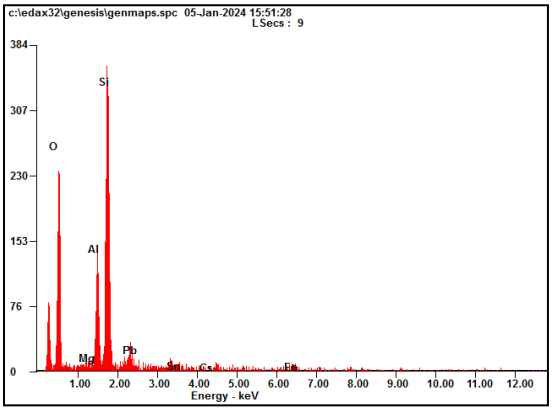

Element	Wt%	At%
OK	26.02	44.51
MgK	00.33	00.38
AlK	10.79	10.94
SiK	40.92	39.87
PbM	16.34	02.16
SnL	01.51	00.35
CsL	00.72	00.15
FeK	03.36	01.65
Matrix	Correction	MThin

Figure D-1: EDX of Water Leaching Residue from Three Different Locations at Mass Ratio of 1:1.

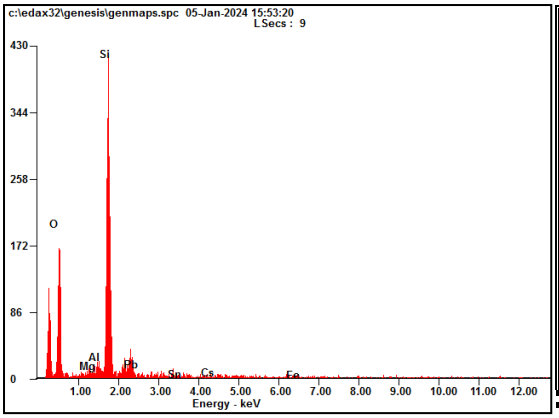

Element	Wt%	At%
OK	22.84	41.42
MgK	00.45	00.54
AlK	01.76	01.90
SiK	50.40	52.06
PbM	21.92	03.07
SnL	00.69	00.17
CsL	00.54	00.12
FeK	01.39	00.72
Matrix	Correction	MThin

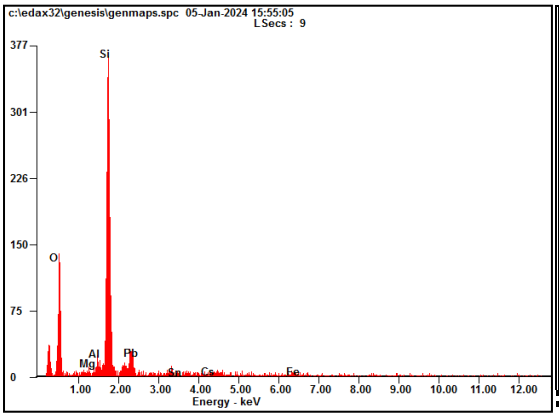

Element	Wt%	At%
OK	17.15	35.09
MgK	00.69	00.93
AlK	02.20	02.67
SiK	47.30	55.12
PbM	27.29	04.31
SnL	01.73	00.48
CsL	02.16	00.53
FeK	01.47	00.86
Matrix	Correction	MThin

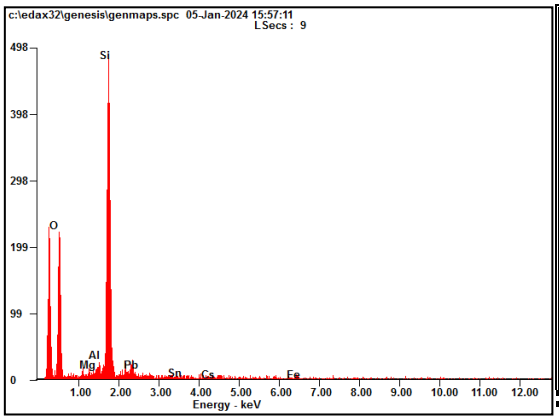

Element	Wt%	At%
OK	25.78	43.42
MgK	00.60	00.66
AlK	01.57	01.57
SiK	53.58	51.41
PbM	16.04	02.09
SnL	00.00	00.00
CsL	01.15	00.23
FeK	01.29	00.62
Matrix	Correction	MThin

Figure D-2: EDX of Water Leaching Residue from Three Different Locations at Mass Ratio of 1:2.

Table D-1: Average EDX Results of Water Leaching Residue at Different Mass Ratio.

Wt%	Raw	1.1	1.1.5	1.2
OK	32.27	25.33	23.38	21.92
MgK	1.28	0.66	0.50	0.58
AlK	21.90	10.52	4.86	1.84
SiK	34.80	40.23	46.64	50.43
PbM	1.76	16.83	19.70	21.75
SnL	2.10	1.40	0.67	0.81
CsL	1.42	0.96	1.09	1.28
FeK	4.45	4.06	3.16	1.38

Table D-2: Extraction Efficiency of Elements at Different Mass Ratio.

η%	1:1	1:1.5	1:2
O	-	-	-
Mg	48.3	61.1	54.6
Al	51.9	77.8	91.6
Si	-	-	-
Pb	-	-	-
Sn	33.3	68.1	61.6
Cs	32.3	23.4	9.8
Fe	8.8	29.0	68.9

Appendix E: Parameter Studies of Sulfation Roasting Time - EDX

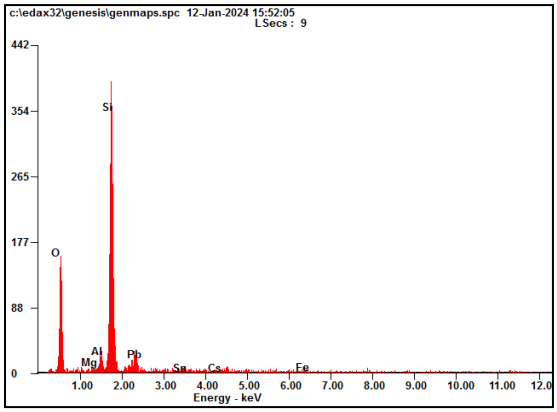

Element	Wt%	At%
OK	19.45	38.43
MgK	00.47	00.61
AlK	02.54	02.97
SiK	46.33	52.13
PbM	25.75	03.93
SnL	02.15	00.57
CsL	01.55	00.37
FeK	01.75	00.99
Matrix	Correction	MThin

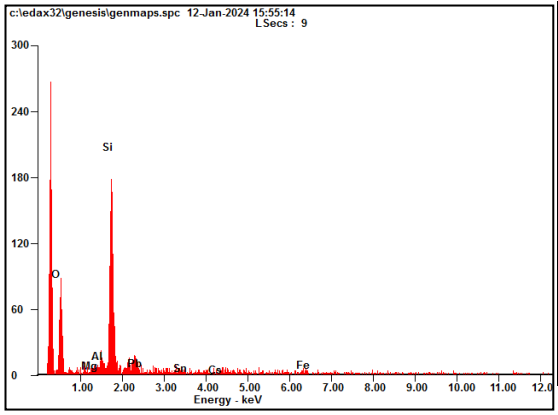

Element	Wt%	At%
OK	20.62	40.62
MgK	00.85	01.10
AlK	02.79	03.26
SiK	43.47	48.77
PbM	26.50	04.03
SnL	02.18	00.58
CsL	01.17	00.28
FeK	02.42	01.36
Matrix	Correction	MThin

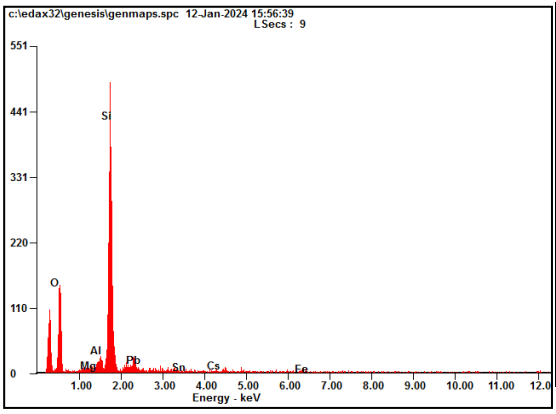

Element	Wt%	At%
OK	20.41	36.35
MgK	00.47	00.55
AlK	02.67	02.82
SiK	55.79	56.59
PbM	15.94	02.19
SnL	01.02	00.24
CsL	02.12	00.45
FeK	01.58	00.81
Matrix	Correction	MThin

Figure E-1: EDX of Water Leaching Residue from Three Different Locations at 30 Minutes Roasting Time.

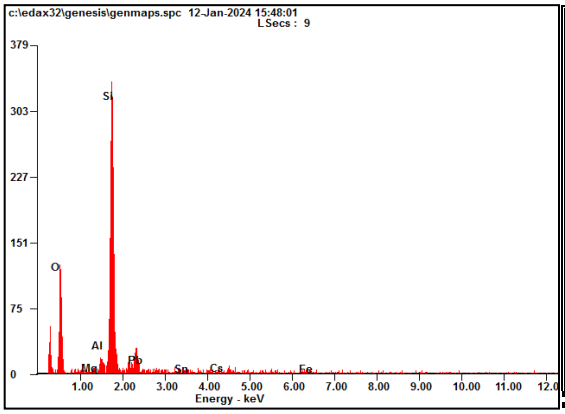

Element	Wt%	At%
OK	19.92	37.68
MgK	00.17	00.21
AlK	01.94	02.17
SiK	51.32	55.30
PbM	23.17	03.38
SnL	00.00	00.00
CsL	02.03	00.46
FeK	01.45	00.79
Matrix	Correction	MThin

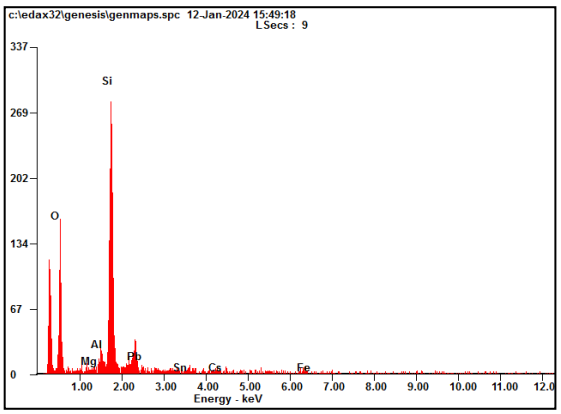

Element	Wt%	At%
OK	22.02	42.18
MgK	00.38	00.48
AlK	02.87	03.26
SiK	44.57	48.63
PbM	24.84	03.67
SnL	00.00	00.00
CsL	03.60	00.83
FeK	01.72	00.95
Matrix	Correction	MThin

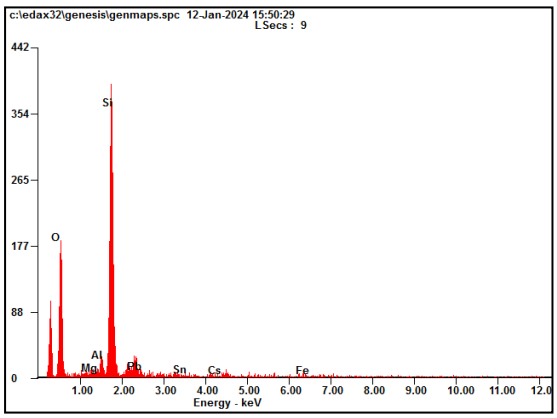

Element	Wt%	At%
OK	23.13	42.09
MgK	00.67	00.81
AlK	02.75	02.97
SiK	47.87	49.62
PbM	20.34	02.86
SnL	01.97	00.48
CsL	01.74	00.38
FeK	01.53	00.80
Matrix	Correction	MThin

Figure E-2: EDX of Water Leaching Residue from Three Different Locations at 60 Minutes Roasting Time.

Table E-1: Average EDX Results of Water Leaching Residue at Different Roasting Time.

Wt%	Raw	30	60	90
OK	32.27	20.16	21.69	21.92
MgK	1.28	0.60	0.41	0.58
AlK	21.90	2.67	2.52	1.84
SiK	34.80	48.53	47.92	50.43
PbM	1.76	22.73	22.78	21.75
SnL	2.10	1.78	0.66	0.81
CsL	1.42	1.61	2.46	1.28
FeK	4.45	1.92	1.57	1.38

Table E-2: Extraction Efficiency of Elements at Different Roasting Time.

η%	30	60	90
O	-	-	-
Mg	53.3	68.1	54.6
Al	87.8	88.5	91.6
Si	-	-	-
Pb	-	-	-
Sn	15.2	68.8	61.6
Cs	13.3	72.6	9.8
Fe	57.0	64.8	68.9

Appendix F: Parameter Studies of Water Leaching Temperature – EDX

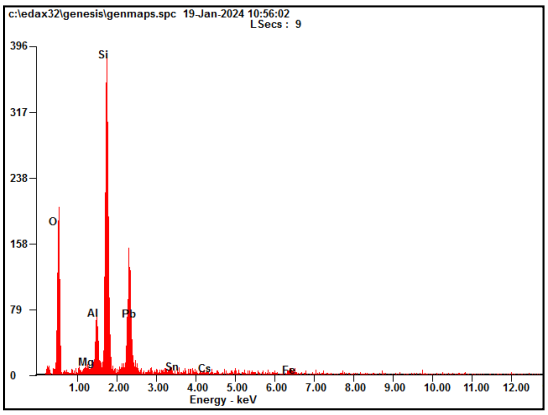

Element	Wt%	At%
OK	32.52	57.92
MgK	00.46	00.54
AlK	05.90	06.23
SiK	30.03	30.47
PbM	29.21	04.02
SnL	00.00	00.00
CsL	00.47	00.10
FeK	01.40	00.72
Matrix	Correction	ZAF

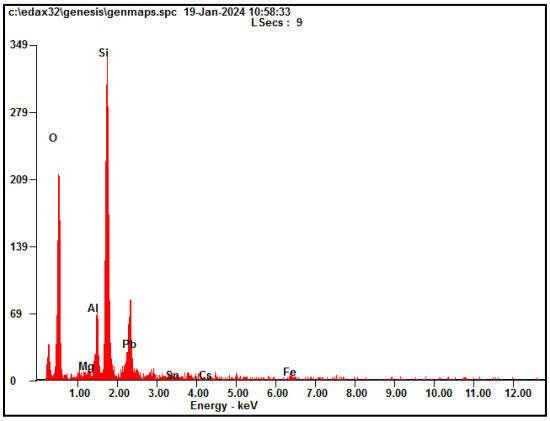

Element	Wt%	At%
OK	41.99	64.27
MgK	00.51	00.51
AlK	05.48	04.97
SiK	31.25	27.24
PbM	17.85	02.11
SnL	01.31	00.27
CsL	00.33	00.06
FeK	01.28	00.56
Matrix	Correction	ZAF

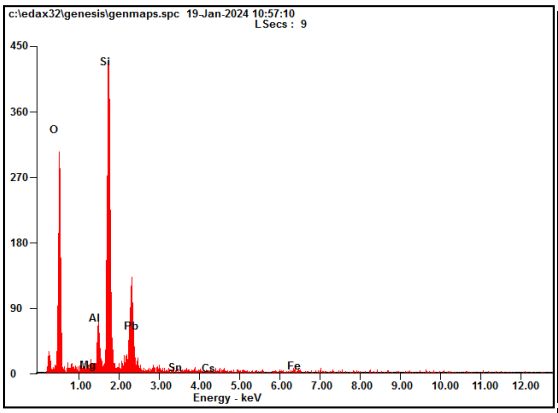

Element	Wt%	At%
OK	41.69	65.80
MgK	00.18	00.19
AlK	03.94	03.69
SiK	29.94	26.92
PbM	21.45	02.61
SnL	00.76	00.16
CsL	01.09	00.21
FeK	00.94	00.42
Matrix	Correction	ZAF

Figure F-1: EDX of Water Leaching Residue from Three Different Locations at 35 ℃ Leaching Temperature.

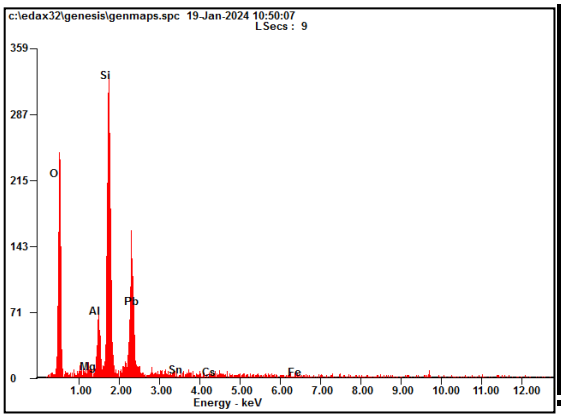

Element	Wt%	At%
OK	38.22	64.52
MgK	00.48	00.54
AlK	05.50	05.51
SiK	26.12	25.12
PbM	26.64	03.47
SnL	00.80	00.18
CsL	01.52	00.31
FeK	00.72	00.35
Matrix	Correction	ZAF

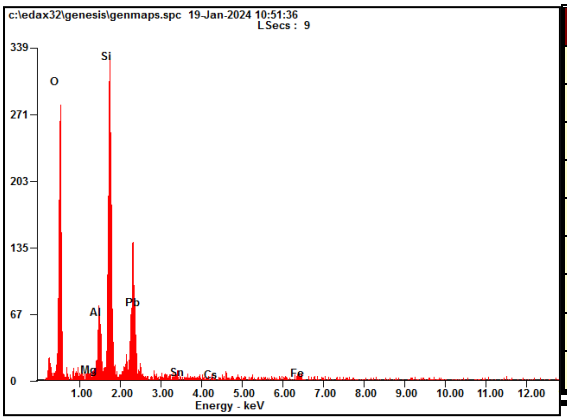

Element	Wt%	At%
OK	43.15	68.89
MgK	00.30	00.32
AlK	05.09	04.82
SiK	24.36	22.16
PbM	25.25	03.11
SnL	00.62	00.13
CsL	00.00	00.00
FeK	01.22	00.56
Matrix	Correction	ZAF

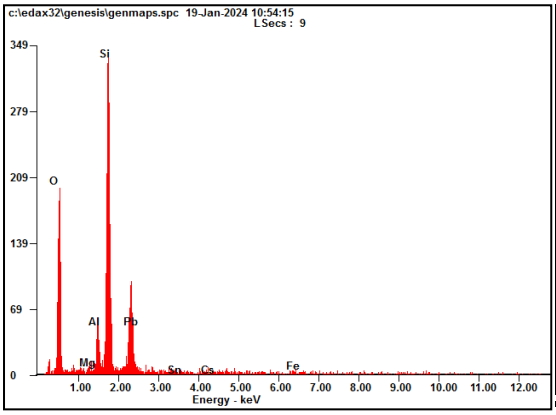

Element	Wt%	At%
OK	38.48	62.34
MgK	00.72	00.77
AlK	04.23	04.06
SiK	31.66	29.22
PbM	22.17	02.77
SnL	01.01	00.22
CsL	00.72	00.14
FeK	01.00	00.46
Matrix	Correction	ZAF

Figure F-2: EDX of Water Leaching Residue from Three Different Locations at 50 ℃ Leaching Temperature.

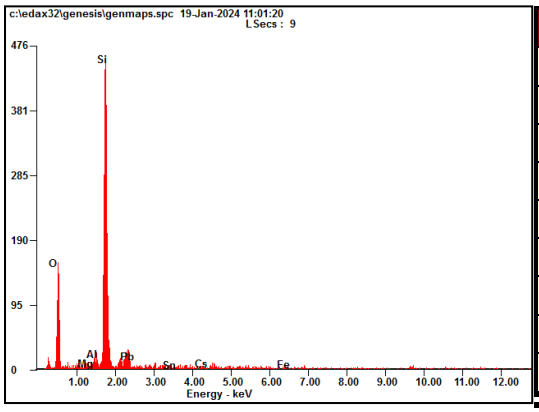

Element	Wt%	At%
OK	36.10	54.11
MgK	00.47	00.46
AlK	01.95	01.73
SiK	48.91	41.76
PbM	09.20	01.06
SnL	01.07	00.22
CsL	01.33	00.24
FeK	00.98	00.42
Matrix	Correction	ZAF

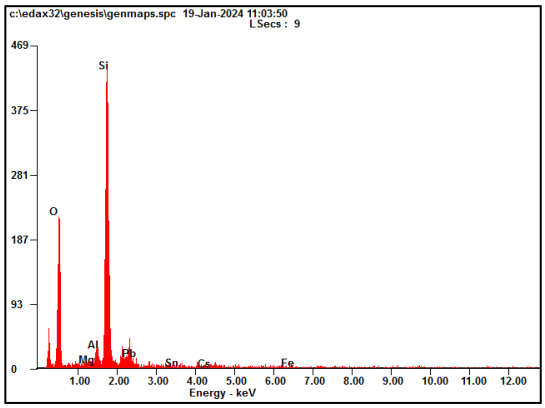

Element	Wt%	At%
OK	42.13	60.98
MgK	00.58	00.55
AlK	02.39	02.05
SiK	41.95	34.59
PbM	09.73	01.09
SnL	01.00	00.20
CsL	01.53	00.27
FeK	00.70	00.29
Matrix	Correction	ZAF

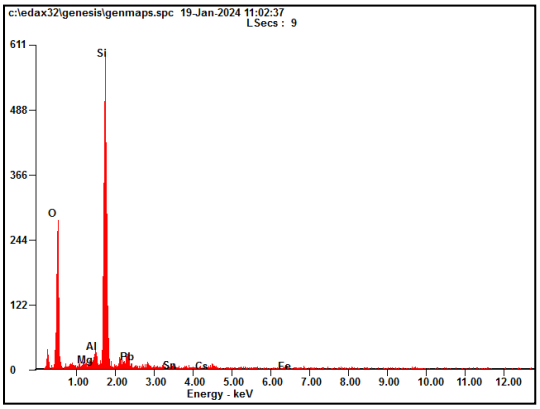

Element	Wt%	At%
OK	43.92	60.95
MgK	00.31	00.28
AlK	02.36	01.94
SiK	44.97	35.54
PbM	05.71	00.61
SnL	01.02	00.19
CsL	00.85	00.14
FeK	00.85	00.34
Matrix	Correction	ZAF

Figure F-3: EDX of Water Leaching Residue from Three Different Locations at 65 ℃ Leaching Temperature.

Table F-1: Average EDX Results of Water Leaching Residue at Different Water Leaching Temperature.

Wt%	Raw	35	50	65	80
OK	32.27	38.73	39.95	40.72	21.92
MgK	1.28	0.38	0.50	0.45	0.58
AlK	21.90	5.11	4.94	2.23	1.84
SiK	34.80	30.41	27.38	45.28	50.43
PbM	1.76	22.84	24.69	8.21	21.75
SnL	2.10	0.69	0.81	1.03	0.81
CsL	1.42	0.63	0.75	1.24	1.28
FeK	4.45	1.21	0.98	0.84	1.38

Table F-2: Extraction Efficiency of Elements at Different Water Leaching Temperature.

η%	35	50	65	80
O	-	-	-	-
Mg	70.0	60.8	64.5	54.6
Al	76.7	77.4	89.8	91.6
Si	-	-	-	-
Pb	-	-	-	-
Sn	67.2	61.5	51.0	61.6
Cs	55.7	47.5	13.1	9.8
Fe	72.9	78.0	81.1	68.9

Appendix G: Parameter Studies of Solid-Liquid Ratio – EDX

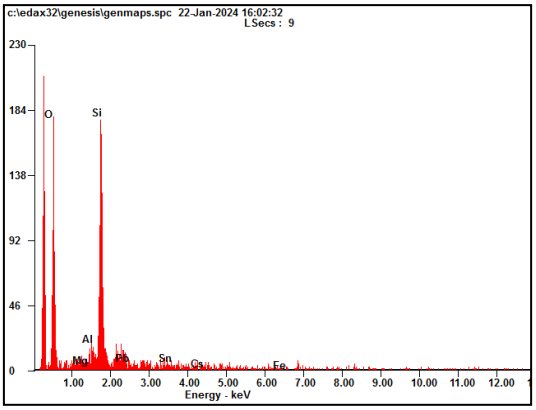

Element	Wt%	At%
OK	49.03	67.10
MgK	01.17	01.05
AlK	02.50	02.03
SiK	36.18	28.21
PbM	06.61	00.70
SnL	02.69	00.50
CsL	01.34	00.22
FeK	00.47	00.19
Matrix	Correction	ZAF

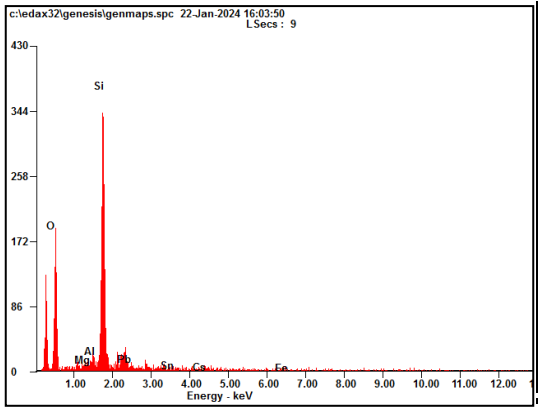

Element	Wt%	At%
OK	41.98	59.42
MgK	00.78	00.73
AlK	02.26	01.90
SiK	45.16	36.42
PbM	07.38	00.81
SnL	00.38	00.07
CsL	00.75	00.13
FeK	01.31	00.53
Matrix	Correction	ZAF

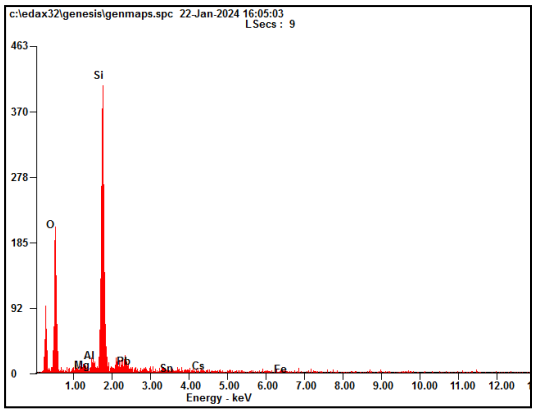

Element	Wt%	At%
OK	44.44	61.62
MgK	00.15	00.14
AlK	01.58	01.30
SiK	45.02	35.56
PbM	06.13	00.66
SnL	00.00	00.00
CsL	01.44	00.24
FeK	01.24	00.49
Matrix	Correction	ZAF

Figure G-1: EDX of Water Leaching Residue from Three Different Locations at Solid-Liquid Ratio of 1:5.

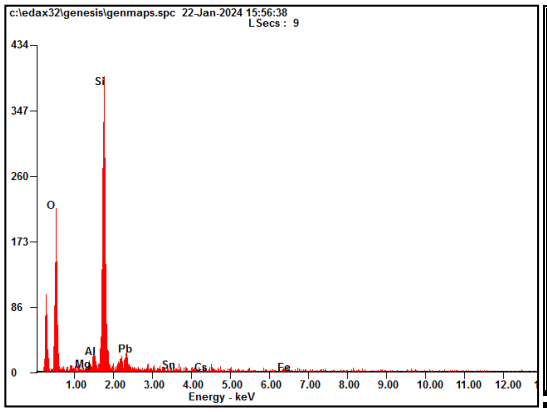

Element	Wt%	At%
OK	42.19	61.00
MgK	00.25	00.24
AlK	02.53	02.17
SiK	41.93	34.53
PbM	09.14	01.02
SnL	00.70	00.14
CsL	01.84	00.32
FeK	01.41	00.58
Matrix	Correction	ZAF

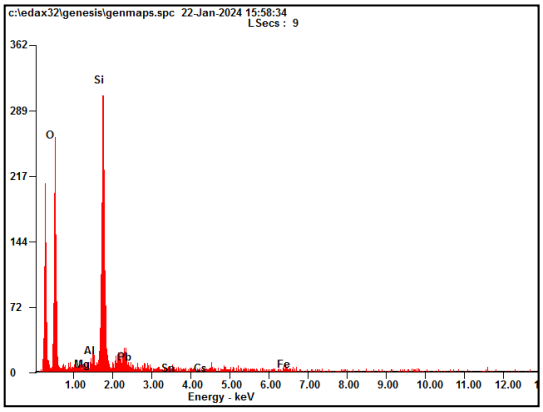

Element	Wt%	At%
OK	50.75	66.62
MgK	00.50	00.43
AlK	02.05	01.60
SiK	40.50	30.29
PbM	04.61	00.47
SnL	00.00	00.00
CsL	00.00	00.00
FeK	01.59	00.60
Matrix	Correction	ZAF

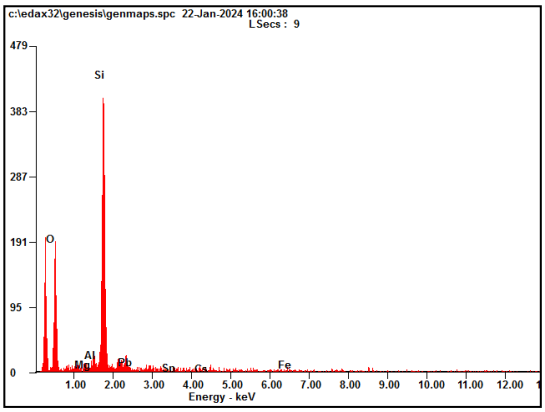

Element	Wt%	At%
OK	39.34	56.98
MgK	00.87	00.83
AlK	01.88	01.61
SiK	46.87	38.68
PbM	05.70	00.64
SnL	02.11	00.41
CsL	02.05	00.36
FeK	01.19	00.49
Matrix	Correction	ZAF

Figure G-2: EDX of Water Leaching Residue from Three Different Locations at Solid-Liquid Ratio of 1:15.

Table G-1: Average EDX Results of Water Leaching Residue at Different Solid-Liquid Ratio.

Wt%	**Raw**	**1:5**	**1:10**	**1:15**
OK	32.27	45.15	21.92	44.09
MgK	1.28	0.70	0.58	0.54
AlK	21.90	2.11	1.84	2.15
SiK	34.80	42.12	50.43	43.10
PbM	1.76	6.71	21.75	6.48
SnL	2.10	1.02	0.81	0.94
CsL	1.42	1.18	1.28	1.30
FeK	4.45	1.01	1.38	1.40

Table G-2: Extraction Efficiency of Elements at Different Solid-Liquid Ratio.

η%	**1:5**	**1:10**	**1:15**
O	-	-	-
Mg	45.2	54.6	57.7
Al	90.4	91.6	90.2
Si	-	-	-
Pb	-	-	-
Sn	51.3	61.6	55.5
Cs	17.3	9.8	8.9
Fe	77.4	68.9	68.6

Appendix H: Parameter Studies of Water Leaching Time – EDX

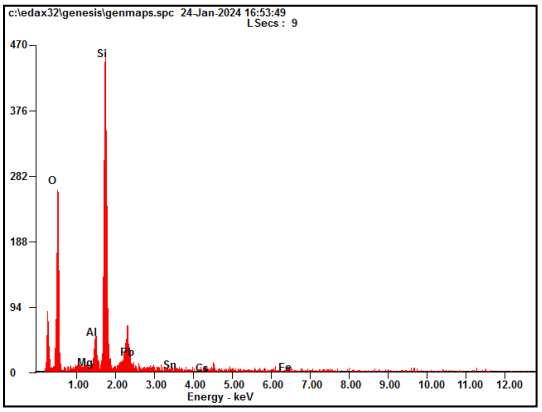

Element	Wt%	At%
OK	42.04	62.93
MgK	00.22	00.22
AlK	03.47	03.08
SiK	36.50	31.12
PbM	13.51	01.56
SnL	01.07	00.22
CsL	01.97	00.35
FeK	01.23	00.53
Matrix	Correction	ZAF

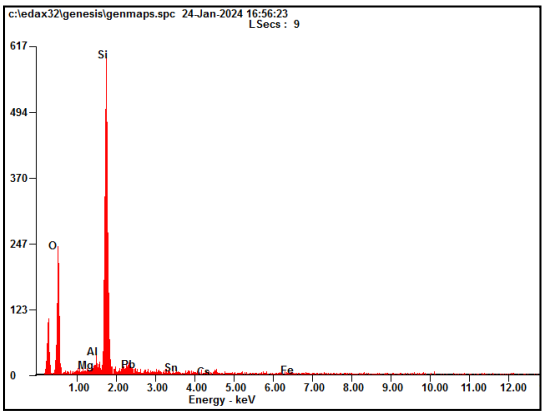

Element	Wt%	At%
OK	40.67	57.59
MgK	00.83	00.77
AlK	01.88	01.58
SiK	48.02	38.73
PbM	06.08	00.66
SnL	00.58	00.11
CsL	00.99	00.17
FeK	00.96	00.39
Matrix	Correction	ZAF

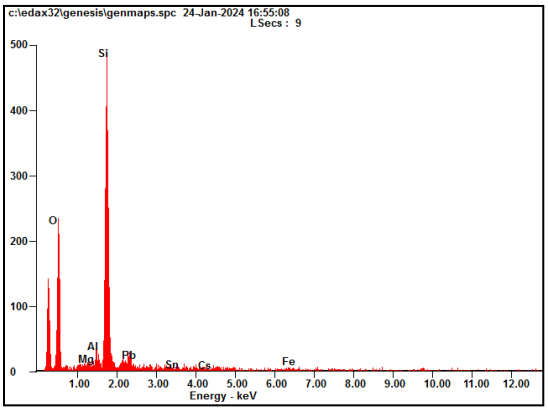

Element	Wt%	At%
OK	45.65	61.82
MgK	00.29	00.26
AlK	01.92	01.54
SiK	46.12	35.57
PbM	05.37	00.56
SnL	00.00	00.00
CsL	00.00	00.00
FeK	00.64	00.25
Matrix	Correction	ZAF

Figure H-1: EDX of Water Leaching Residue from Three Different Locations at 30 Minutes Leaching Time.

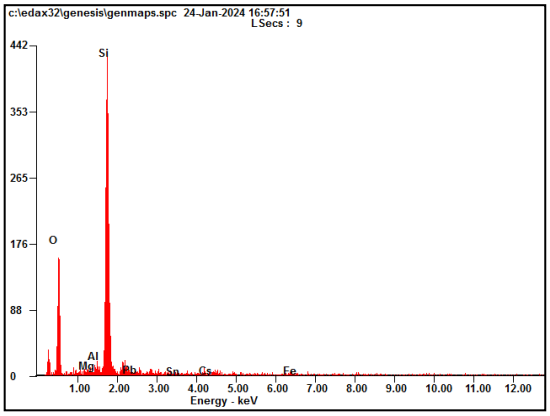

Element	Wt%	At%
OK	41.15	57.00
MgK	00.96	00.88
AlK	01.58	01.30
SiK	50.33	39.71
PbM	02.83	00.30
SnL	01.02	00.19
CsL	00.99	00.16
FeK	01.14	00.45
Matrix	Correction	ZAF

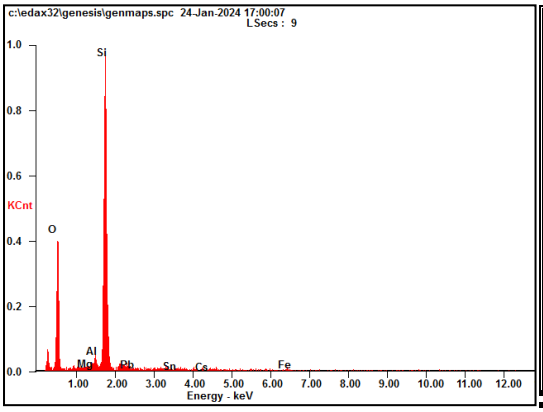

Element	Wt%	At%
OK	42.96	58.64
MgK	00.19	00.17
AlK	01.73	01.40
SiK	49.65	38.61
PbM	01.67	00.18
SnL	00.56	00.10
CsL	01.60	00.26
FeK	01.64	00.64
Matrix	Correction	ZAF

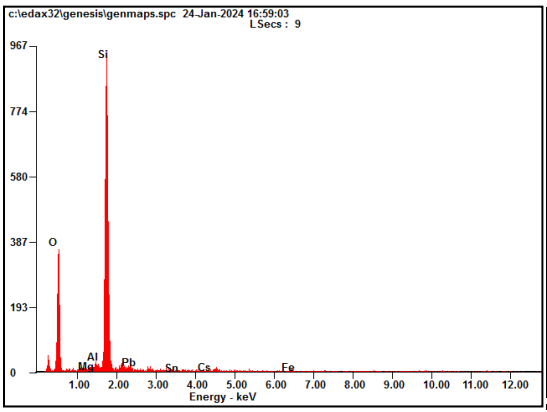

Element	Wt%	At%
OK	42.46	58.20
MgK	00.23	00.21
AlK	01.14	00.93
SiK	50.71	39.60
PbM	02.53	00.27
SnL	00.62	00.12
CsL	00.96	00.16
FeK	01.34	00.53
Matrix	Correction	ZAF

Figure H-2: EDX of Water Leaching Residue from Three Different Locations at 90 Minutes Leaching Time.

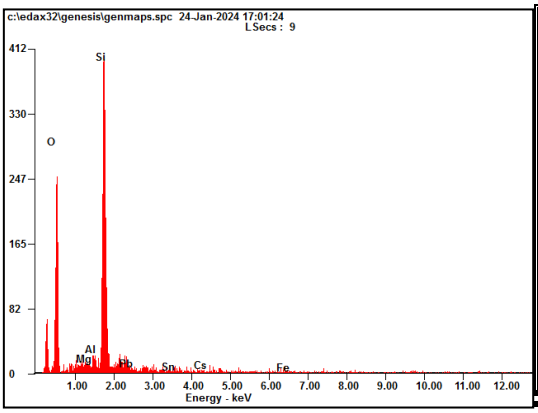

Element	Wt%	At%
OK	50.17	65.99
MgK	00.39	00.34
AlK	01.09	00.85
SiK	42.38	31.76
PbM	03.92	00.40
SnL	00.00	00.00
CsL	00.50	00.08
FeK	01.56	00.59
Matrix	Correction	ZAF

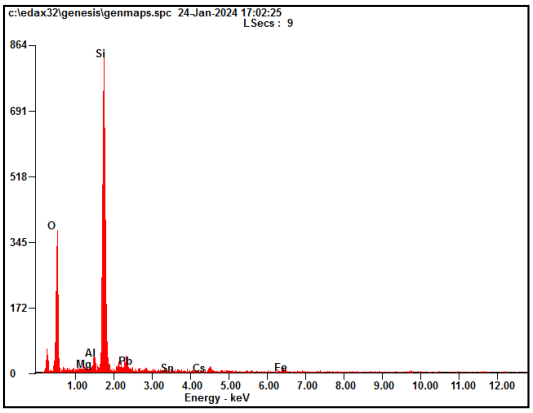

Element	Wt%	At%
OK	42.04	59.70
MgK	00.37	00.35
AlK	01.71	01.44
SiK	45.07	36.46
PbM	06.43	00.71
SnL	01.05	00.20
CsL	00.87	00.15
FeK	02.47	01.00
Matrix	Correction	ZAF

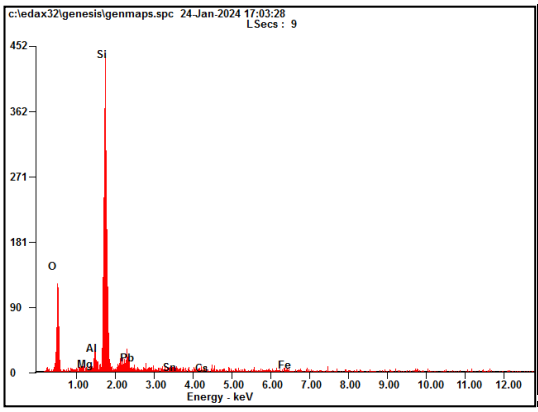

Element	Wt%	At%
OK	35.35	52.34
MgK	00.22	00.21
AlK	02.45	02.15
SiK	51.48	43.42
PbM	06.80	00.78
SnL	01.45	00.29
CsL	00.60	00.11
FeK	01.64	00.70
Matrix	Correction	ZAF

Figure H-3: EDX of Water Leaching Residue from Three Different Locations at 120 Minutes Leaching Time.

Table H-1: Average EDX Results of Water Leaching Residue at Different Water Leaching Time.

Wt%	Raw	30	60	90	120
OK	32.27	42.79	21.92	42.19	42.52
MgK	1.28	0.45	0.58	0.46	0.33
AlK	21.90	2.42	1.84	1.48	1.75
SiK	34.80	43.55	50.43	50.23	46.31
PbM	1.76	8.32	21.75	2.34	5.72
SnL	2.10	0.55	0.81	0.73	0.83
CsL	1.42	0.99	1.28	1.18	0.66
FeK	4.45	0.94	1.38	1.37	1.89

Table H-2: Extraction Efficiency of Elements at Different Water Leaching Time.

η%	30	60	90	120
O	-	-	-	-
Mg	65.0	54.6	64.0	74.4
Al	88.9	91.6	93.2	92.0
Si	-	-	-	-
Pb	-	-	-	-
Sn	73.9	61.6	65.1	60.4
Cs	30.7	9.8	16.9	53.9
Fe	78.8	68.9	69.2	57.6

Appendix I: Gallery of Experiment

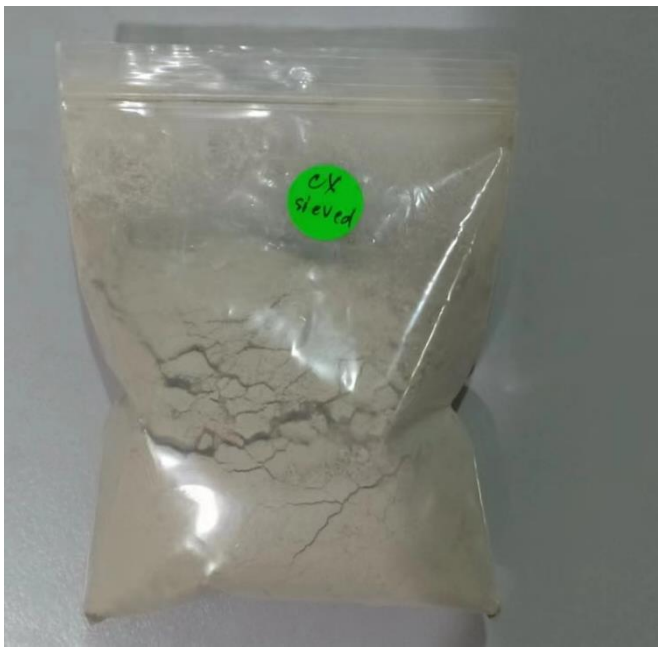

Figure I-1: Dried Raw Coal Mining Sludge.

Figure I-2: Sulfation Roasting in Muffle Furnace.

Figure I-3: Water Leaching with Heating Mantle Under Reflux.

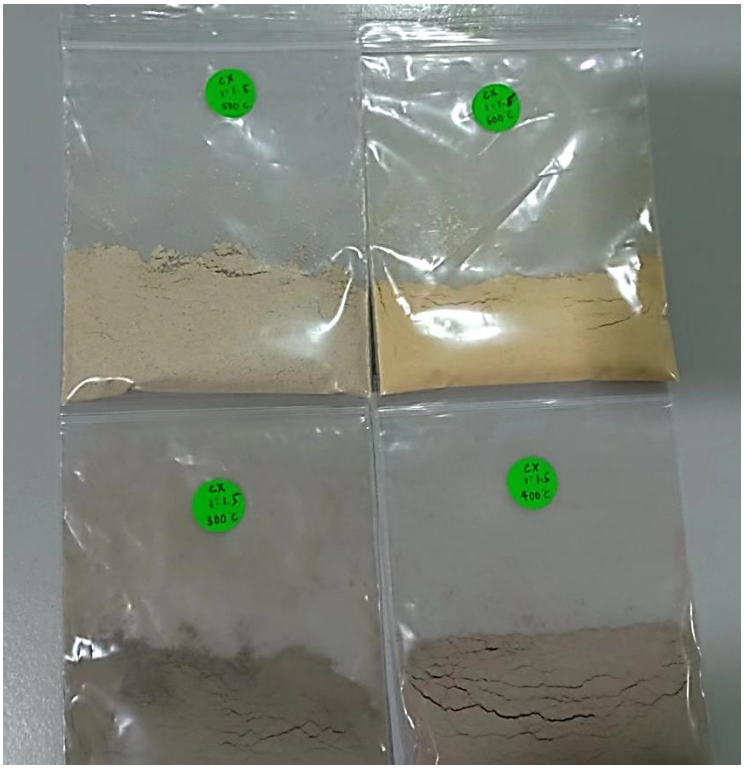

Figure I-4: Treated Coal Mining Sludge at Different Roasting Temperature.

Figure I-5: Treated Coal Mining Sludge at Different Mass Ratio.

Figure I-6: Treated Coal Mining Sludge at Different Roasting Time.

Table I-7: Treated Coal Mining Sludge at Different Leaching Temperature.

Table I-8: Treated Coal Mining Sludge at Different Solid-Liquid Ratio.

Table I-9: Treated Coal Mining Sludge at Different Leaching Time.